

CHALMERS



Verification of virtual sealing process and specification of gluing process requirements

*Master of Science Thesis performed for Volvo Car Corporation,
Sweden*

Quan Li
Meisam Pourghahreman

Department of Product and Production Development
CHALMERS UNIVERSITY OF TECHNOLOGY
Göteborg, Sweden, 2012

Verification of virtual sealing process and specification of gluing process requirements

QUAN LI

MEISAM POURGHAHREMAN

Supervisor at Volvo Cars Corporation:

Andreas Jonsson ajonss32@volvocars.com
Manufacturing Engineering
Volvo Cars Corporation
Dept. 81022/PVÖS 32
SE-405 31Göteborg
Sweden

Examiner at Chalmers University of Technology:

Rolf Berlin rolf.berlin@chalmers.se
Department of product and production development
CHALMERS UNIVERSITY OF TECHNOLOGY
412 96 Göteborg
Sweden

Supervisor at Chalmers University of Technology:

Per Nyqvist per.nyqvist@chalmers.se
Department of product and production development
CHALMERS UNIVERSITY OF TECHNOLOGY
412 96 Göteborg
Sweden

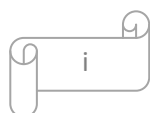
Abstract

Development of virtual software for processes performed in the Body-In-White shop such as spot welding has been carried out for decades, ending up in accurate simulation of process before ramping up the production. On the other hand the situation for continuous process like sealing and gluing needs to be improved further. So far, robot off-line programming to launch a sealing or gluing process for newly introduced cars in production line has been verified based on time and resource consuming experiments and several years of process experience. This highlights the necessity of developing virtual tools to verify continuous processes before initiation of production. Therefore, this thesis was performed at Volvo Cars Corporation to verify the performance of newly developed software named IPS sealing.

Verification of IPS sealing required extracting proper data regarding sealing robot movements from Process Simulate and converting the extracted data to XML format by using the concept of robot kinematics and by means of Matlab. This XML document was used as an initial input for IPS sealing. Another indispensable input for running IPS sealing simulation is an applicator providing sealing material rheology data and brush data and determining how the sealing beads look like. Gathering these data involves studying of sealing material properties as well as robotic sealing process. These two mentioned inputs plus a 3D model of a car were utilized to simulate sealing beads on car body. The simulation result was compared with reality in terms of bead width, thickness, appearance and material consumption to verify IPS sealing. It turned out that IPS sealing results were rather satisfactory for bead width and appearance while for bead thickness and material consumption IPS results were greater than in real situation, meaning that IPS sealing functions well to reflect reality to some extent but it needs to be developed further to better simulate reality. Investigating different influential parameters in robotic sealing suggested that special considerations should be given in finding the real flow in production instead of nominal flow to perfect IPS sealing simulation.

Another purpose of this thesis was to collect required information to implement gluing process into IPS. This part of the thesis was mainly performed by studying literature about application of adhesives in automotive industry and interview with experts in this area. The requirements of virtual gluing process were specified and categorized into gluing bead geometry, gluing material consumption, gluing material requirements and robotic gluing process, which are essential in gluing simulation.

Keywords: Process Simulate, IPS sealing, Robot forward Kinematics, adhesive/sealant material rheology, verification, Robotic sealing and gluing process



Acknowledgments

First we would like to thank our examiner Rolf Berlin who provided continuous guidance along the progress of the project and gave suggestions for the structure and overall quality of the thesis report. Especially thanks are given to our supervisor at VCC Andreas Jonsson, for his supervision of this thesis, continuous assistance of us both technically and non-technically and the kind help of providing tips for the solutions of many problems. But for his help and care, we would not have come so far to complete the thesis so wonderfully.

Many thanks are extended to our academic supervisor in Chalmers Per Nyqvist who showed great interest and passion in our project and provided guidance in attacking robot kinematic problems. We sincerely forward great thanks to Anders Carlsson, the manager of Advanced Engineering & IT methods at VCC. During the thesis period, he showed tremendous interest in this thesis, provided us with many help and shared a lot of his insights as well as lovely stories in VCC. Further thanks are given to Christian Silvesjö at VCC who exerted a large amount of energy helping us to solve technical problems and also gather data needed from production line.

We also want to thank BG Bengtsson at Teamster, Andreas Mark from FCC and Glen Svensson from Revocoat for their kind help in assisting us collecting data and for the sharing of their experience in the specialized field. During the period of carrying out this thesis, we worked at VCC manufacturing department and all the team members from PVÖS showed great welcome for us and the care about the thesis, so many thanks are also given to them.

Quan Li
Master of Production Engineering

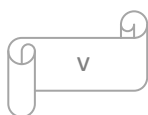
Meisam Pourghahreman
Master of Product Development

Content

1	Introduction	1
1.1	Overview.....	1
1.2	Background.....	1
1.3	Aim	2
1.4	Objective.....	2
1.5	Process Simulate	2
1.6	IPS sealing	3
1.7	XML as the bridge between PS and IPS.....	3
1.8	Methodology	3
1.8.1	Literature study.....	3
1.8.2	Interview	3
1.8.3	Regression analysis	4
1.8.4	Simulation.....	4
1.8.5	Shop-floor investigation	4
2	Theoretical frame work	6
2.1	Robot forward kinematics.....	6
2.1.1	Homogenous transformation of a series of frames.....	6
2.1.2	Denavit-Hartenberg transformation of successive frames.....	7
2.2	Robot ABB IRB 2400.....	9
2.2.1	A 6-axis robot.....	9
2.2.2	Closed kinematic chain.....	10
2.3	Material rheology.....	10
3	Implementation.....	15
3.1	Sealing station st52-11-080	15
3.2	Extracting information related to sealing station from Process simulate	16
3.3	Kinematic modeling of the sealing station.....	16
3.3.1	Frame transformation—from world frame to robot base frame.....	18
3.3.2	Frame transformation—from robot base frame to robot last joint frame.	19
3.3.3	Frame transformation— from robot last joint frame to the sealing nozzle tip	21
3.4	Matlab functions	23

3.4.1	Input arguments	24
3.4.2	Function Body	25
3.4.3	Output	28
3.5	Creating applicator	29
3.5.1	Sealing material at VCC	29
3.5.2	Rheology Calculation	29
3.5.3	Brush Data	30
3.5.4	Applicators created	31
3.6	Identifying important sealing verification parameters	31
4	Verification of virtual sealing software	35
4.1	Applicator selection	35
4.2	Appearance	37
4.2.1	General appearance of six selected areas:	37
4.2.2	Finished surface of sealing beads	44
4.2.3	Conclusion for appearance comparison	45
4.3	Manual measurement	46
4.3.1	Measuring beads on flat plates	46
4.3.2	Measuring beads on real car body	48
4.3.3	Conclusion for manual measurement	53
4.4	Material consumption verification	54
4.4.1	Conclusion for volume verification	56
4.5	Influence of modifying sealing path and mass rate in simulation	57
4.5.1	Modifying sealing path	57
4.5.2	Modifying mass rate	59
4.5.3	Conclusion for Modifying sealing path and mass rate on simulation	61
5	Specification of robotic gluing process requirements	62
5.1	Gluing Process	62
5.2	Typical material used as adhesive in automotive industry	63
5.3	Adhesives application for body in white	64
5.4	Typical property requirements to have an acceptable adhesive	64
5.5	Important parameters in applying adhesives	64
5.6	Requirement specification	66

6	Discussion & Conclusions.....	70
7	Recommendations and future work	73
	Bibliography.....	76



List of Figures

Figure 2-1: Relationship between two coordinate systems	6
Figure 2-2: Transformation between the old frame and last new frame	7
Figure 2-3: DH frame transformation	8
Figure 2-4: Positive directions for rotation	9
Figure 2-5: A CAD drawing of a 6-axis [13]	10
Figure 2-6: Closed chain in the structure of ABB IRB 2400	10
Figure 2-7: Shear rate vs. Shear Stress for Newtonian material.....	11
Figure 2-8 : Viscosity does not change by shear rate in Newtonian material	11
Figure 2-9: shear stress vs. shear rate for shear thinning material	12
Figure 2-10 : Viscosity vs. shear rate for shear thinning fluid.....	12
Figure 2-11 : shear stress vs. shear rate for shear thickening material.....	13
Figure 2-12: Viscosity vs. shear rate for shear thickening fluid.....	13
Figure 2-13: Shear rate vs. Shear Stress for Bingham material	14
Figure 2-14: Viscosity vs. shear rate for Bingham material.....	14
Figure 3-1: Robotic sealing station st52-11-080 at VCC shown in PS	15
Figure 3-2: The seventh joint that facilitates the movement of robot on its track.....	16
Figure 3-3: Frames setting for ABB IRB 2400[10]	17
Figure 3-4: Three steps of transformation from world frame to nozzle tip frame	18
Figure 3-5: Consideration of closed kinematic chain in PS	19
Figure 3-6: Sealing gun used for IRB2400-10(left) and for IRB2400-5(right).....	21
Figure 3-7: Transformation process from the last joint frame to the nozzle tip frame.....	22
Figure 3-8: Schematic of Matlab scripts	23
Figure 3-9: Robot joint values text file	24
Figure 3-10: Relation between shear rate and shear stress.....	30
Figure 3-11: Effect of flow on thickness , width and volume.	33
Figure 3-12: Effect of Speed on thickness, width and volume.....	33
Figure 3-13: Effect of TCP distance on thickness , width and volume.....	34
Figure 4-1: Sealing design for upper corner inside the engine room of V60	38
Figure 4-2: Complicated corner inside the engine room of V60.....	39
Figure 4-3: A corner inside the engine room of V60	40
Figure 4-4: An important corner inside the engine room of V60.....	40
Figure 4-5: Designed sealing bead around spring tower.....	41
Figure 4-6: Sealing around spring tower inside the engine room	41
Figure 4-7: Another view of figure 4.24 b	41
Figure 4-8: Designed sealing beads in front right wheel house of V60	42
Figure 4-9: Crossed sealing beads inside the front wheelhouse.....	42
Figure 4-10: Designed seal underneath the car, the designed bead has two 90 degree rotations	43
Figure 4-11: Sealing beads in an area underneath the car	43
Figure 4-12: Design of sealing beads underneath a car with two cross beads	44
Figure 4-13: Crossed sealing beads underneath the car	44

Figure 4-14: The outer surface of the selected beads	45
Figure 4-15: The outer surface of the selected beads created by simulation.....	45
Figure 4-16: Real beads created by static and flat stream applicator	46
Figure 4-17: Simulated beads created by static flat stream applicator	47
Figure 4-18: Width and thickness measured in experiment and IPS sealing when sealing material are sprayed statically.....	47
Figure 4-19: Bead width comparisons in experiment and simulation with flat stream.....	48
Figure 4-20: Wet film thickness gauge	48
Figure 4-21: Upper left corner inside the engine room of a car model V60	49
Figure 4-22: Width and thickness of bead Y352SB2511.....	49
Figure 4-23: Width and thickness of bead Y352SB2609b.....	50
Figure 4-24: Width and thickness of bead Y352SB6313d.....	50
Figure 4-25: Width and thickness of bead Y352SB9307.....	50
Figure 4-26: Width and thickness of bead Y352SB9602a	51
Figure 4-27: Width and thickness of bead Y352SB6306.....	51
Figure 4-28: Width and thickness of bead Y352SB6121	51
Figure 4-29: Width and thickness of bead Y352SB9102.....	52
Figure 4-30: Width and thickness of bead Y352SB1320.....	52
Figure 4-31: Width and thickness of bead Y352SB2708.....	52
Figure 4-32: Width and thickness of bead Y352SB2404b.....	53
Figure 4-33: Log file for volume consumption during one cycle in the sealing station.....	55
Figure 4-34: Bead Y352SB6313d	58
Figure 4-35: Bead Y352SB9307	58
Figure 4-36: Reference flow and real flow in production for sealing robot r21	60
Figure 5-1: Traditional robotic gluing systems	62
Figure 5-2: The event triggering model	63
Figure 5-3: Not enough adhesive on its designed place.....	66
Figure 5-4: Enough adhesive on its designed place	66
Figure 7-1: Grids that should be counted to gain width and thickness.	74

List of Tables

Table 3-1:DH parameters for IRB 2400-10	20
Table 3-2:DH parameters for IRB 2400-5	20
Table 3-3: Different sets of rheology data.....	31
Table 4-1: Thickness results from the two applicators in fast simulation and from production for bead Y352SB6313d	35
Table 4-2: Width results from the two applicators in fast simulation and from production for bead Y352SB6313d	36
Table 4-3: Bead appearance results for bead Y352SB6313d from the two applicators in fast simulation and from production	36
Table 4-4: Volume and mass results for bead Y352SB6313d from the two applicators both in fast and slow simulation as well as results from production.....	37
Table 4-5: Volume consumption in production, IPS and in theory.....	56
Table 4-6: Comparison between total volumes consumed in theory and in production during one cycle for robot 6421	56
Table 4-7:material consumption with and without via points.....	59
Table 4-8: Volume and mass obtained from modified mass rate, predefined mass rate and production for bead Y352SB6313d	60
Table 5-1: Requirement specifications in terms of geometry	66
Table 5-2: Requirement specifications in terms of material consumption.....	67
Table 5-3: Requirement specifications in terms of material properties	67
Table 5-4: Requirement specifications in terms of process	68
Table 5-5: Requirement specifications in terms of quality	69

Nomenclature

IPS	Industrial Path Solutions (IPS sealing software)
PS	Process Simulate
XML	Extensible Mark-up Language
VCC	Volvo Cars Corporation
DH	Denavit–Hartenberg
TCP	Tool Centre Point
FCC	Fraunhofer Chalmers Centre
V60	the car used in this thesis
ABB IRB 2400	Robot model that is used in VCC sealing station
OEM	Original Equipment Manufacturer
Body-in-White	The stage in automotive manufacturing where car body's sheet metal components have been welded together before installing moving parts such as chassis , motor, windows, etc and also before painting. [1]

1 Introduction

1.1 Overview

With the advent of new technology, the automobile industry has undergone tremendous changes during the last few decades and will continuously be re-shaped in the future. New materials are continuously developed as a result of customer's demand for better performance of cars, such as improved safety, less weight and less energy absorption. As a consequence, different manufacturing processes are provoked to replace the conventional ones to meet production purposes. Given such background, adhesive and sealant technology is gaining wider popularity in automobile industry. It can be used for various applications, including noising reduction, vibration dampening and even for decorative purpose. For sealants, the purpose of its usage is mainly for preventing dirt, dust, water and fumes from getting inside a vehicle [2] [3].

Currently in automotive sector, robots are used frequently for different applications. Generally, sealing robots can replace humans in hazardous or unhealthy working situations, save considerable amount of sealing materials, and improve product quality, which ultimately boost competitiveness of the company [4]. During the manufacturing process of a car, considerable amount of sealants and adhesives are applied on the car body within the 'body-in white' stage, followed by cleaning procedures aiming to remove the oil on the car, then after drying, the car is sent to electro-coat painting process and thereafter to the oven for curing. The common materials used for industrial robot sealing are based on acrylic esters, epoxies and PVC [5]. There exists a trend that many automobile manufacturers are trying to use innovative sealing process as well as better but fewer sealing materials in order to reduce the car weight and achieve better energy-efficiency [6].

1.2 Background

As mentioned previously, the automotive industry has recently undergone huge changes due to the market globalization. To keep and gain market shares it is increasingly important to shorten the time to market with new functional concepts but without failing to meet market demands of high quality, and reasonable price. Simulation and virtual verification are seen as a powerful tool to meet these demands.

For processes in the Body-In-White shop, especially spot welding, the development of virtual tools has been going on for decades meaning that most automotive OEM:s today can verify the process simulation with good certainty. For continuous processes such as sealing and gluing, up until now good quality simulation and robot off-line

programming is achieved based on several years of process experience. This is due to the lack of tools to support the virtual verification of sealing or gluing processes.

Together with AB Volvo, Scania, Saab Automobile, FCC Fraunhofer Chalmers has developed a new software supporting "Virtual Sealing". The research projects are funded by Vinnova through the FFI and MERA programs. The first version of the software IPS "Virtual Paint" was originally developed to support paint simulation to achieve more accurate simulation of paint processes. But IPS is now also extended to support sealing process, and the plan is to develop IPS to simulate gluing process on car body components. For Off-line programming of robots VCC uses Process Simulate and the intention is to have the two software working together meaning that the data exchange between the two(IPS and Process Simulate) should be efficient to support efficiency and simplicity.

1.3 Aim

This thesis aims to help Volvo Car Cooperation shorten time to market and minimize production cost without jeopardizing product quality, which in the short term can boost the productivity and production, and in the long run can increase the competitiveness and expand market share.

1.4 Objective

The main objective of this thesis is to verify the sealing process simulation. Since the virtual sealing simulation is achieved by IPS Virtual Sealing recently, it is important to verify the simulation results against reality to secure product quality. Meanwhile, as gluing process simulation is still not realized, but with the ever increasing expectations from users, developing software for gluing simulation is of significant importance. Therefore, specifying and collecting data for developing IPS gluing is another objective for this thesis.

1.5 Process Simulate

Process Simulate is a simulation tool developed by Siemens to verify the feasibility of an assembly process through its different stages. It performs this feasibility verification by simulating the full assembly sequence in terms of products and required tools by validating reachability, zone allocations and avoidance of interlocks [7] [8]. In this thesis PS is used as a tool to create paths for sealing beads on car body components and provide outputs indicating robots' movements during sealing operation.

1.6 IPS sealing

IPS (Industrial Path Solution) is developed by Fraunhofer Chalmers Centre (FCC) to verify assembly feasibility, motion planning, optimization of multi-robot operations and simulation of key surface treatment processes [9]. It was first successfully implemented for virtual painting simulation, and now it has been modified for virtual sealing simulation. IPS sealing can be run both for single sealing beads, or a couple of beads in sequence or simultaneously. The Simulation results can be checked by naked eyes and also by measuring the profile characteristics of simulated beads, thickness, width, mass of simulated beads, and volume of material used in simulated beads.

1.7 XML as the bridge between PS and IPS

XML language is used to specify data structured in a particular way. It has been investigated for years by both research and industry parties [10]. In this thesis two types of XML documents are used as IPS inputs to run simulation. The first type consists of positions and orientations of discrete points along a robot path and the gun-on/off commands. These XML documents are created by two Matlab scripts developed during this thesis transforming the output of process simulate to XML documents to provide input for IPS Sealing. The other type used to run IPS includes rheological data about sealing material and sealing process properties such as mass rate, and injection velocity of material. Appendix A gives two examples of these two types of XML documents.

1.8 Methodology

Several methods and tools were used throughout this thesis. This section describes these used methods.

1.8.1 Literature study

Literature study was performed to gain knowledge about robotic sealing and gluing processes in automotive industry, sealing and gluing material properties related to these processes, robot kinematics, and the two main software used in this project, Process Simulate and IPS sealing. This information helped to verify IPS sealing and collect information to be used to develop IPS gluing.

1.8.2 Interview

To complement the knowledge gained from literature study and gain more insight from real production situation, it was necessary to interview people dealing with the sealing and gluing process in different companies. Those people were put in four categories, the experts developing IPS sealing software, the experts at VCC using the Process Simulate and IPS in daily basis to run the production line, an expert in a company called

Teamster who has knowledge about robotic sealing and gluing process and an expert from Revocoat company, the sealing material supplier for VCC.

1.8.3 Regression analysis

To find the influence of different parameters on sealing beads during robotic sealing process, linear regression analysis was performed with the result of DOE tests from VCC. The result helped to understand how different parameters in a robotic sealing process affect the sealing results.

1.8.4 Simulation

Since IPS sealing is being developed continuously with more new features added in, continuous testing of this software consisted of a big part of this thesis. In order to run IPS simulation successfully, considerable amount of preparatory work needed to be completed: extracting data from Process Simulate, converting the extracted data into desired data with appropriate format and creating sealing applicator for simulation. During the whole preparation period for running IPS, converting data was the most challenging, time consuming yet fundamental part. Thus extensive literature study about robot forward kinematics was carried out and Matlab software was used in this step to transfer data derived from PS to XML documents which were then read by IPS. Then large amount of simulations were run repetitively in IPS and the results were measured and compared with reality.

1.8.5 Shop-floor investigation

To collect real life data to compare with simulation results it was necessary to carry out intensive investigation on sealing beads on car body components. This investigation was done in three steps to help verify the newly developed virtual sealing software. These three methods are explained following.

1.8.5.1 Manual measurement of width and thickness

To collect valid data about geometry of sealing beads to verify the accuracy of IPS sealing, manual measurements were accomplished. By manual measurement, width and thickness of some carefully selected beads were measured and compared with the simulation results of those selected beads.

1.8.5.2 Appearance comparison

Photos were used to compare the appearance of the sealing beads between reality and simulation results. Also, pictures helped to observe if the sealing beads simulated by IPS sealing are placed on the right location intended by design departments at VCC.

1.8.5.3 Material consumption comparison

To compare the material consumption in simulation and in reality, the amount of material used in production was logged with the help from Teamster, the supplier of VCC for sealing flow system. The material consumption comparison was performed in terms of the volume and the mass of simulated material and sprayed in reality.

2 Theoretical frame work

Different theories used to carry out this thesis are explained in this chapter, including robot kinematics, robot ABB IRB 2400 description and material rheology. To understand this report, readers should get familiar with these theories.

2.1 Robot forward kinematics

Robot forward kinematics refers to the study of the motion and position of the end-effector given the robot joint values. So by forward kinematics, one can always calculate the positions of an end-effector along a moving path [11] [12]. Robot forward kinematics is usually modeled by homogenous transformation and DH convention, which are explained in the following sections.

2.1.1 Homogenous transformation of a series of frames

The relation between two coordinate systems A and B in 3D space is explained by the concept of homogenous transformation. Homogenous transformation allows representing a series of translation and rotation by a matrix operation [11]. Consider two coordinate systems displayed in Figure 2-1.

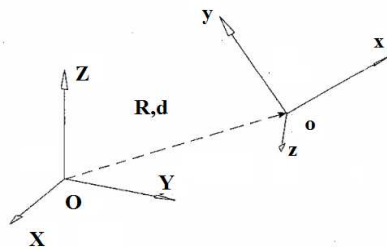


Figure 2-1: Relationship between two coordinate systems

New frame {o x y z} is the result of applying a translation and series of rotation on the old frame {O X Y Z}. These translation and rotations can be shown in a matrix form. By transposition of the result of the translation and rotation the following transformation matrix is obtained [11] [13] [14].

$$T_{old}^{new} = \begin{bmatrix} R_{old}^{new} & d_{old}^{new} \\ 0 & 1 \end{bmatrix} \quad (2.1)$$

Where R_{old}^{new} equals the rotation matrix to derive the new frame from the old frame, and d_{old}^{new} equals the translation matrix to derive the new frame from the old frame. In case there are more than two frames which the last one is resulted from transformation of the

first one, homogenous transformation matrix is obtained in the following order [11] [13] [14].

$$T_{old}^{new} = T_{old}^1 \times T_1^2 \times T_2^3 \dots \times T_{i-1}^{new} \quad (2.2)$$

In equation (2.2) each T represents a transformation matrix between a frame and its previous frame. [11] [13] [14]. Figure 2-2 clarifies the equation 2.2.

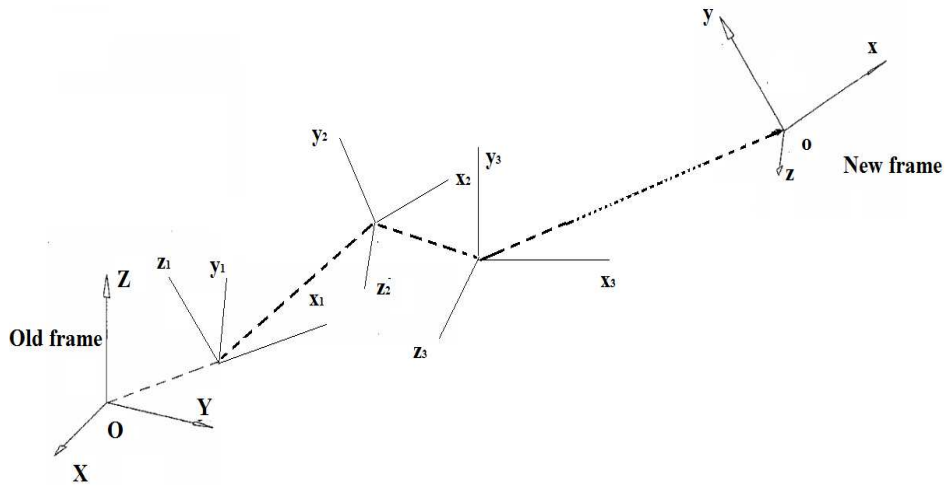


Figure 2-2: Transformation between the old frame and last new frame

2.1.2 Denavit-Hartenberg transformation of successive frames

Denavit-Hartenberg transformation is widely used as a standard approach for selecting frames of reference in robot application because it is fairly systematic and involves only four variables instead of six in homogenous transformation. The DH transformation is conveyed as a product of four successive basic transformations, shown in equation 2.3 [11] [14].

$$A_i = Rot(Z_{i-1}, \theta_i) Trans(Z_{i-1}, d_i) Trans(X_i, a_i) Rot(X_i, \alpha_i) \quad (2.3)$$

The whole transformation process is shown in figure 2-3.

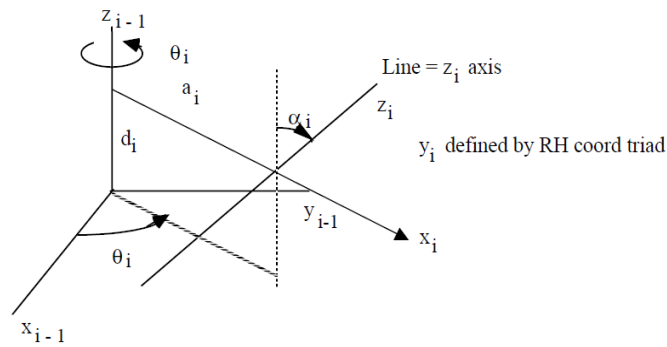


Figure 2-3: DH frame transformation

In this representation, first the frame is rotated around z_{i-1} axis by an angle θ_i , then translated along z_{i-1} axis by distance d_i then translated along x_i axis by distance a_i and finally rotated around x_i axis by angle α_i . Therefore, there are four DH parameters to take into consideration: link rotation θ_i , link length a_i , link offset d_i and link twist α_i . [11] [15].

- Link rotation θ_i : angle between the link length a_{i-1} and a_i axis measured in the plane perpendicular to z_{i-1} axis.
- Link offset d_i : the displacement from the origin of frame i-1 to x_i axis along z_{i-1} axis;
- Link length a_i : the offset displacement between z_{i-1} and z_i axes along x_i axis;
- Link twist α_i : the angle between x_{i-1} and x_i axes about z_{i-1} axis.

Of all the four parameters, three of them are constant while the remaining one is a variable. For prismatic joint, d_i is a variable and for revolute joint, θ_i is a variable [11] [15].

Furthermore, to make a standard framework to find correct DH parameters for each robot, the following principles are considered [11]:

- Right hand frame. Each rotation that is clockwise is considered as a negative rotation and each rotation that is counter-clockwise is considered as a positive rotation. Figure 2-4 can be used to illustrate the rotation [11].

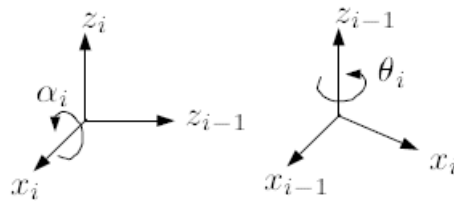


Figure 2-4: Positive directions for rotation

- x_i should be perpendicular to z_{i-1} axis;
- x_i should intersect z_{i-1} axis.

2.2 Robot ABB IRB 2400

The robots installed in VCC sealing station are ABB IRB 2400. These robots are classified as 6-axis robots with closed kinematic chain in their structure. This section first explains the concept of a 6-axis robot and then the meaning of closed kinematic chain structure in a robot body.

2.2.1 A 6-axis robot

A 6-axis robot is made of six joints together by consecutive links. In a 6-axis robot the first axis placed at the robot base, allows the robot to rotate 180 degree from center point to left and right. This motion extends the work area to include the area on either side and behind the arm. Second axis facilitates the extension of lower arm of the robot forward and backward. Third motion extends the vertical reach of robot by allowing the upper arm to raise and descend. Also it enables the upper arm to have better access to parts upper than robot height. Wrist roll or forth axis facilitates the manipulation of the part between vertical and horizontal orientation by rotating the upper arm in a circular motion. To tilt the wrist of the robot arm upward and downward the fifth axis is used. The last axis on the robot, which is the sixth axis, rotates freely in a circular motion clockwise or counterclockwise. It is used to position end effectors and also to manipulate parts. This axis is usually able to rotate more than 360 degree [16]. Figure 2-5 displays a structure of a 6-axis robot.

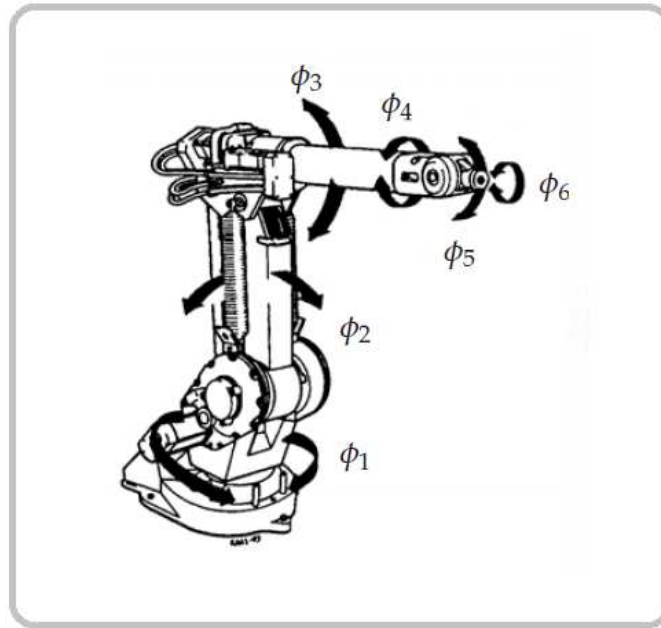


Figure 2-5: A CAD drawing of a 6-axis [14]

2.2.2 Closed kinematic chain

A kinematic chain is the product of robot links. There are two types of Kinematic chain, open and closed. In case every link is connected to the adjacent link by one and only one chain, the structure is called open kinematic chain. But, when two or more than two links form one or more loops, the structure is called closed kinematic chain. ABB IRB 2400 that is investigated in this thesis consists of a closed kinematic chain because of the parallelogram-linkage structure [14] shown in figure 2-6.

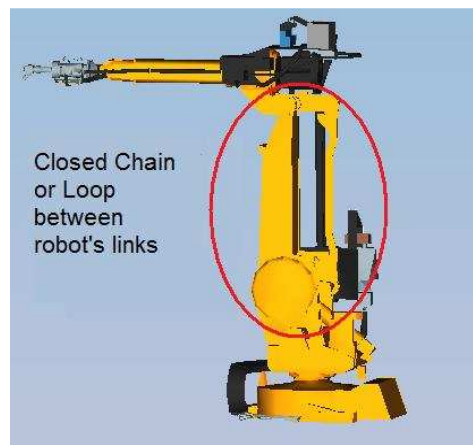


Figure 2-6: Closed chain in the structure of ABB IRB 2400

2.3 Material rheology

This section first introduces Newtonian and Non-Newtonian fluids, and then explains the properties of non-Newtonian fluids related to this thesis.

There are different ways to categorize fluids. One common way is to group fluids as Newtonian and Non-Newtonian fluids. In Newtonian fluids, plot of shear stress versus shear rate at a specified temperature is a straight line that passes through the origin. In other words, this plot is a line with a constant slope, which is equal to fluid viscosity, independent of the shear rate. Mathematically, it can be displayed as $\tau = \eta \left(\frac{d\theta}{dt} \right)$, where τ is shear stress, η is the line slope (constant) and $d\theta/dt$ is shear rate. The fact that the plot passes through the origin indicates that the shear rate is zero when the shear stress is zero. Water, milk, and mineral oil are some examples of Newtonian materials. Figure 2-7 displays the relation between shear rate and shear stress and figure 2-8 shows the relation between shear rate and viscosity in Newtonian material [17] [18].

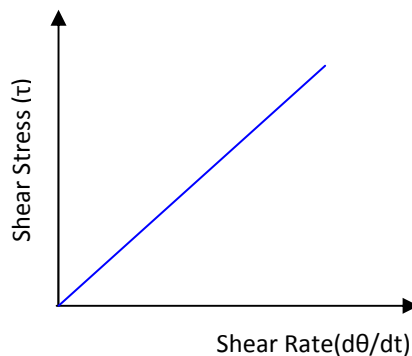


Figure 2-7: Shear rate vs. Shear Stress for Newtonian material

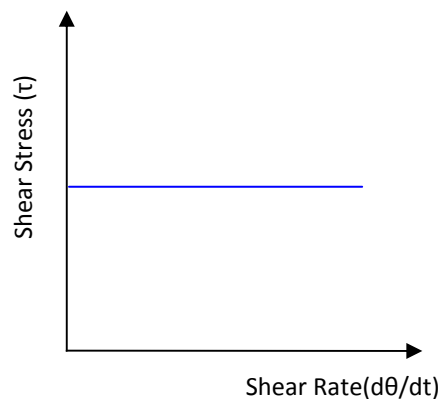


Figure 2-8 : Viscosity does not change by shear rate in Newtonian material

But all materials do not follow the rules of Newtonian materials and they are put in the group of Non-Newtonian materials. For this kind of liquids the viscosity is not a constant value. In other words, the viscosity or the slope of shear stress vs. shear rate curve will change when shear rate changes. These materials include a vast range of fluids with high molecular weight, such as polymeric fluids or liquids with suspended fine particles in their structures [17] [18].

Non-Newtonian materials can further be divided into three subgroups [17] [18]:

- Shear-thinning or Pseudoplastic group: Shear thinning materials are the materials in which the viscosity decreases with increase in shear rate. Mathematically, it can be displayed as $\tau = \eta * (d\theta/dt)^n$, where τ is shear stress, η and n are constants and $d\theta/dt$ is shear rate. For shear-thinning fluid, the exponent $n < 1$. [17] [18]

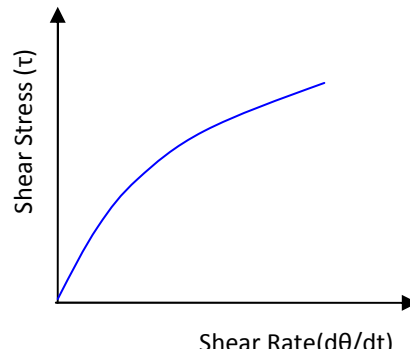


Figure 2-9: shear stress vs. shear rate for shear thinning material

As it is shown in figure 2-10 for shear thinning material the slope of the curve is decreasing with the increase of shear rate.

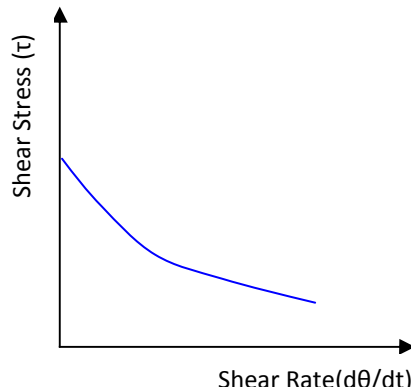


Figure 2-10 : Viscosity vs. shear rate for shear thinning fluid

- Shear-thickening or Dilatant fluids: Shear thickening materials are the materials in which the viscosity increases with increase in shear rate. Like the shear thinning material formula, the mathematic expression is also conveyed as $\tau = \eta * (d\theta/dt)^n$, but in this case, the exponent $n > 1$ [17] [18].

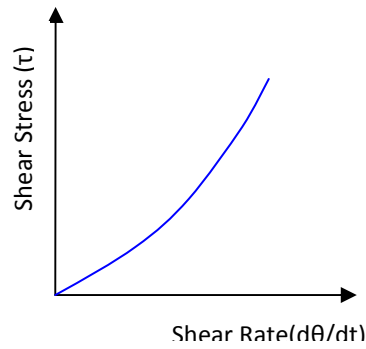


Figure 2-11 : shear stress vs. shear rate for shear thickening material

As it is obvious in figure 2-12, the slope of the curve is increasing with the increase of shear rate.

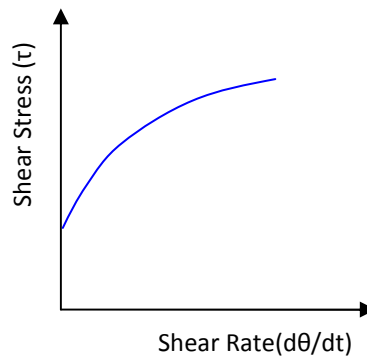


Figure 2-12: Viscosity vs. shear rate for shear thickening fluid

- Viscoplastic fluids: The behavior of viscoplastic fluid is different in a way that viscoplastic materials behave like solid under static conditions; therefore to initiate fluid flow a certain amount of force, known as yield value, should be applied. While the force is less than yield value, no visible change is observed on the material, but as soon as the yield value is exceeded the material starts to flow. When flow begins, plastic fluids may display Newtonian, Shear Thinning or Shear Thickening flow characteristics. There is a special class of viscoplastic fluids known as Bingham plastic fluids. Bingham fluids exhibit a linear behavior of shear stress versus shear rate after it starts to flow. Figure 2-13 reveals how shear stress and shear rate are related in Bingham fluids. Figure 2-14 displays the relation of viscosity and shear rate for such fluids [17] [18].

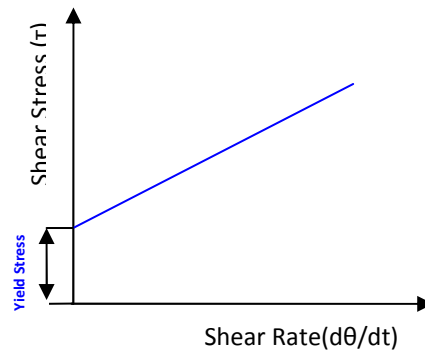


Figure 2-13: Shear rate vs. Shear Stress for Bingham material

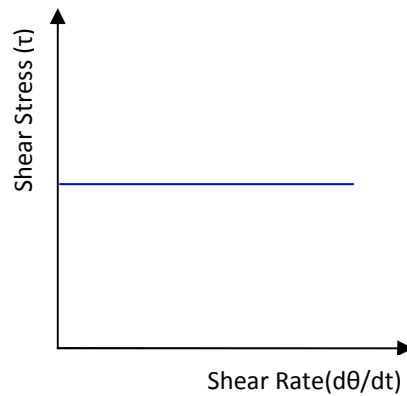


Figure 2-14: Viscosity vs. shear rate for Bingham material

Since the material used for sealing and gluing are amongst Bingham fluids, here, the focus is on non-Newtonian Bingham fluids. The relation between shear stress, viscosity and shear rate is obtained from following formulas:

$$\tau = \tau_0 + \eta \left(\frac{d\theta}{dt} \right) \quad (2.4)$$

Where τ is the amount of shear stress in Pa, τ_0 is the yield stress in Pa, η is viscosity in Pa.s and $d\theta/dt$ is the value of shear rate in 1/s.

3 Implementation

In this section, first the layout of a sealing station at VCC is explained, and then the procedure of making a kinematic model for robots in this station based on information extracted from PS is clarified step by step. A description of Matlab scripts written to facilitate the procedure of the kinematic model is given. Later on, the process of creating a proper applicator, to run IPS sealing, based on material rheological data and sealing process data is described. Moreover, the influential parameters for sealing results are found by performing regression analysis based on DOE test results for sealing process at VCC. Appendix B shows the hierarchical tasks for sealing verification.

3.1 Sealing station st52-11-080

There are five robots installed in the sealing station st52-11-080, which is the sealing station investigated and used in this thesis. These robots are from the family of ABB IRB 2400 robots. The first robot mounted alone at the back of the sealing station is IRB 2400-5. This robot is used to seal the rear part of the car, both inside and outside. The two robots standing on two sides of the sealing station are IRB 2400-10 and mainly spray sealing materials underneath the car body, rear and front wheel houses in two sides of car. The last two robots hanging from two sides of the station are IRB2400-5. These two hanging robots mainly are programmed to spray sealing materials inside the car body. Figure 3-1 shows the layout of the station st52-11-080 in Process Simulate.

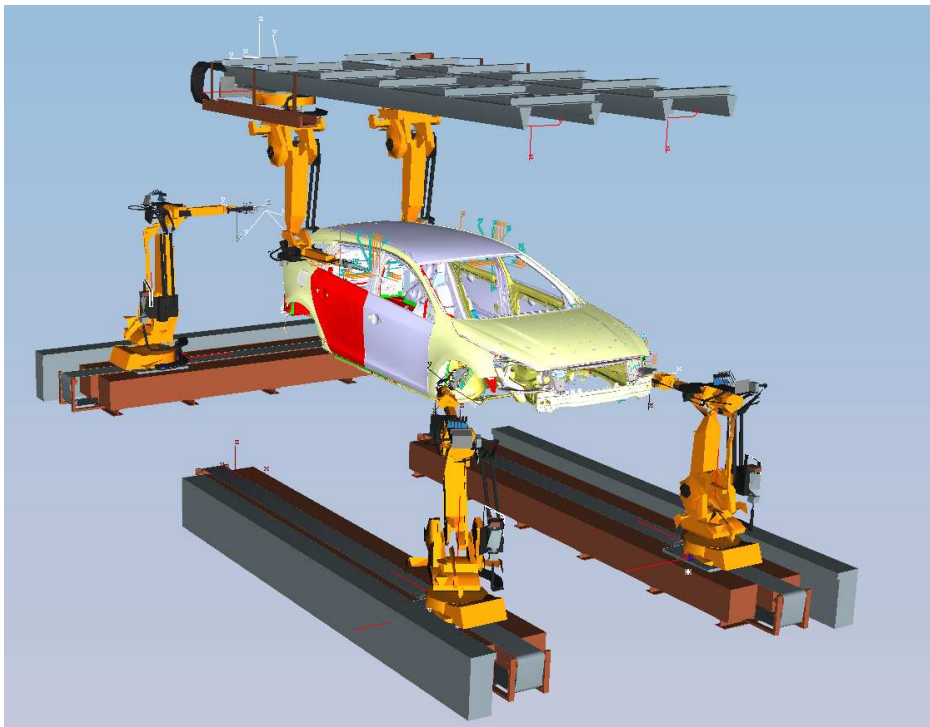


Figure 3-1: Robotic sealing station st52-11-080 at VCC shown in PS

The robots in this station are installed on track motions to allow them better reachability to different parts of a car. The track created an extra degree of freedom for each robot and was treated as the seventh joint of robots when building kinematic model for sealing station. Figure 3-2 shows a model of a robot in sealing station of VCC that can move along a track with assistance of the added external joint, named extdev.

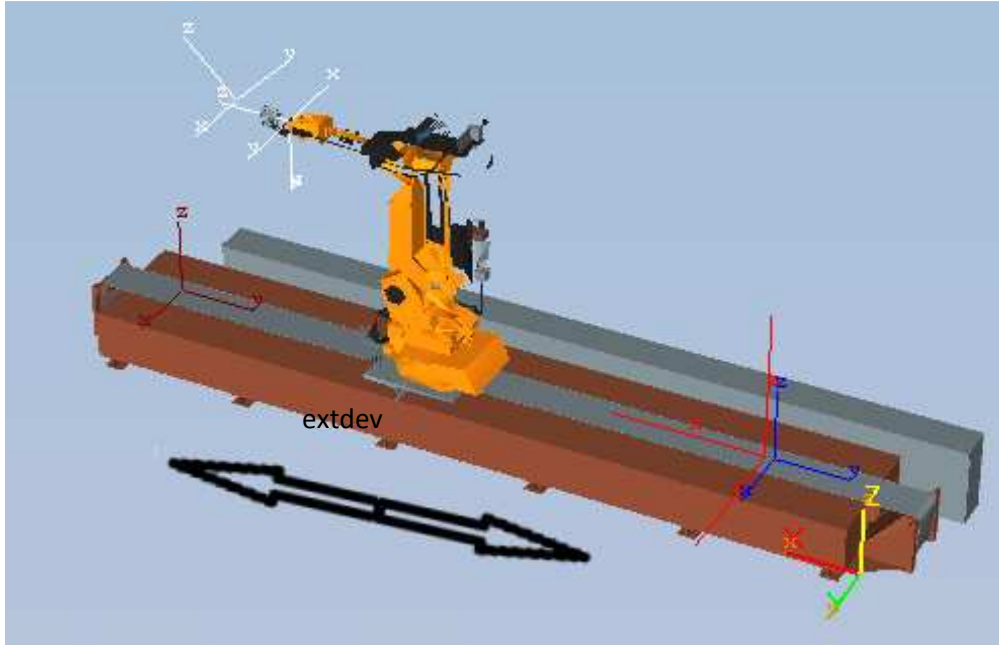


Figure 3-2: The seventh joint that facilitates the movement of robot on its track

3.2 Extracting information related to sealing station from Process simulate

To create a kinematic model from robots installed in the station it was necessary to extract following information form PS:

- Robot joints values at different times along a sealing path. This information was derived from PS as a text file after running the simulation.
- Distance and angle of nozzle installed on each robot from the last joint of the robot: these values were measured from PS.
- Position and orientation of each robot base with respect to the station world frame: these values also were measured from PS.

Using above information as an input for the kinematic model which will be explained in next section would give the position(x, y, z) and the orientation (roll, pitch, yaw) of the nozzle TCP related to the sealing station word frame along a sealing path in a specific time interval.

3.3 Kinematic modeling of the sealing station

In order to make a kinematic model of robots installed at VCC sealing station, the first step was to understand how the robot frames were set in Process Simulate. This assisted in getting the correct orientation for robot joint frames and nozzle tip frames related to world frame of the sealing station resulting in finding correct DH parameters of robots that were basis for this robot kinematic model. Figure 3-3 displays the position of robot joints frame used for ABB IRB 2400.

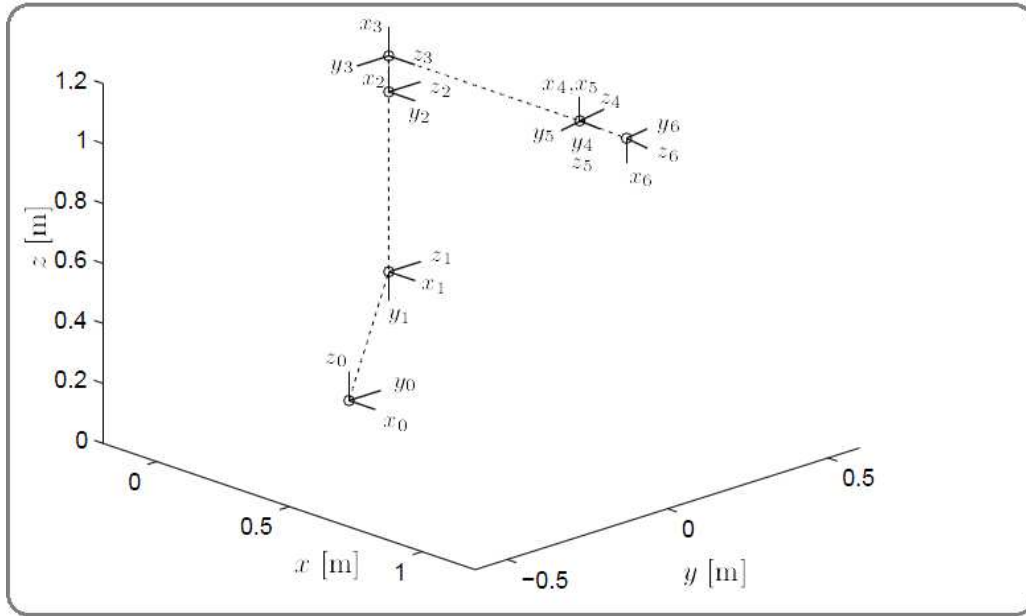


Figure 3-3: Frames setting for ABB IRB 2400[10]

Next step to establish a kinematic model giving the position and orientation of nozzle tip related to world frame was to determine three different following areas in the sealing station:

1. From station's world frame to robot base frame
2. From robot base frame to robot last joint frame
3. From robot last joint frame to the sealing nozzle tip frame

Figure 3-4 shows these three different areas for a robot in a sealing station.

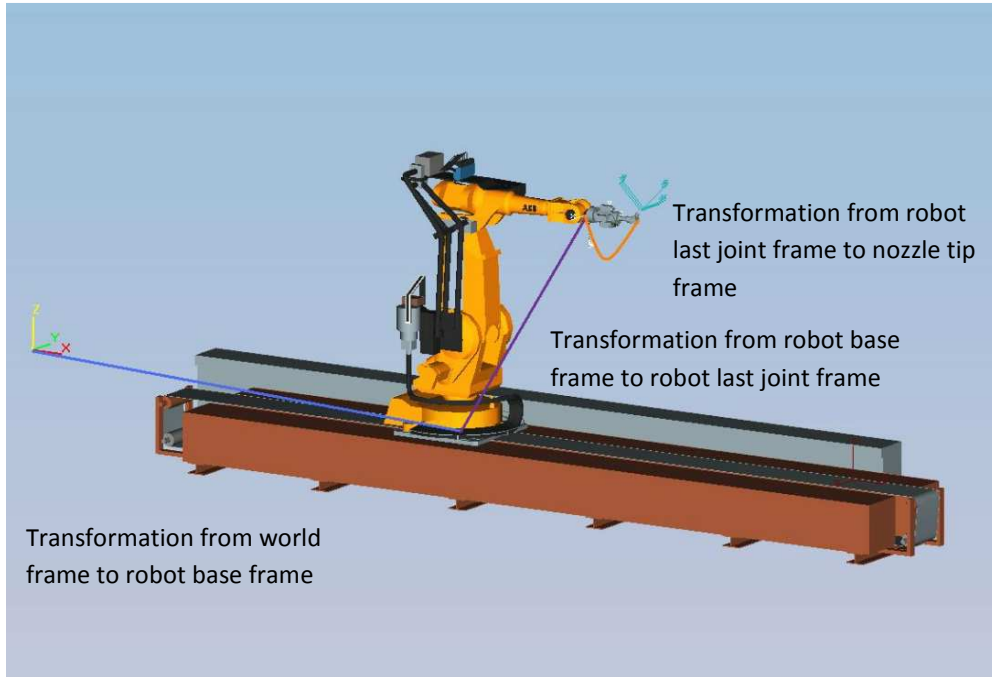


Figure 3-4: Three steps of transformation from world frame to nozzle tip frame

3.3.1 Frame transformation—from world frame to robot base frame.

Since the world frame is unique for a single workstation, decision was taken to use world frame as the origin to calculate the coordinates of the nozzle tip used in IPS sealing simulation. Ascertaining robot base coordinates was not challenging, however the problem relied on the movement of robot. Since each robot moves on a track, more accurately an external axis, it is allowed to move along a certain axis, which further results in the variation of the positions of nozzle tip. For each robot, the movement along one axis is the same as movement along the same or another axis in the world frame, and this was considered when creating transformation matrices. Following is an example of the built transformation matrices in kinematic model.

$$TR1 = \begin{bmatrix} 1 & 0 & 0 & 6427.39 \\ 0 & 1 & 0 & 1736.81 - \text{extdev}(i) \\ 0 & 0 & 1 & 498.09 \\ 0 & 0 & 0 & 1 \end{bmatrix} \times \begin{bmatrix} \cos(-p_i/2) & -\sin(-p_i/2) & 0 & 0 \\ \sin(-p_i/2) & \cos(-p_i/2) & 0 & 0 \\ 0 & 0 & 1 & 0 \\ 0 & 0 & 0 & 1 \end{bmatrix} \quad (3.1)$$

As shown in equation 3.1, in TR1 equation, the base frame has a coordinate (6427.39, 1736.81, 498.09) and a rotation of -90° around Z-axis in the world frame. To end up in the base position, coordinate system has to be translated 6427.39mm, 1736.81mm, 498.09mm along X-axis, Y-axis and Z-axis respectively, followed by a rotation of -90° around Z-axis. In addition, extdev(i) should be added on the Y translation to support the robot movement along Y axis within the world frame.

3.3.2 Frame transformation—from robot base frame to robot last joint frame

The transformation from robot first joint (base frame) to its last joint is also referred as forward robot kinematics. Simply put it, it was a procedure of finding out the position and orientation of the last robot joint. Here the notation of homogenous transformation for robot's frames plus DH notation was used to solve the problem of robot kinematics.

3.3.2.1 Finding DH parameters

Robots used in this thesis have closed kinematic chain in their structure. From Figure 3.6, it is obvious that the joint two and three are linked together by an external link limiting the motion of these two joints in a way that they cannot move freely without considering this constraint. This fact was also considered in process simulate. In Process Simulate, there is a tab called joint jog where all the robot joint values are displayed at a given time during the movement of the robot, as shown in Figure 3-5. The figure shows the movement of joint two and three is connected internally and movement of one of them triggers the movement of the other. When one of the two joints reaches a maximum limit, the other reaches a minimum limit and the vice visa.



Figure 3-5: Consideration of closed kinematic chain in PS

To be able to find the translation matrix from robot base to the last joint it was essential to use the frames as used in process simulate. Using the same frame setting it was possible to find appropriate DH parameters that resulted in correct position and orientation for the last joint. Tables 3-1 and 3-2 display the DH parameters for IRB 2400-10 and IRB 2400-5 respectively.

Table 3-1:DH parameters for IRB 2400-10

Joint i/link i	α_i (radian)	a_i (mm)	θ_i (radian)	d_i (mm)
1	$-p_i/2$	100	q_1	615
2	0	705	$q_2 - p_i/2$	0
3	$-p_i/2$	135	$q_3 - q_2$	0
4	$p_i/2$	0	q_4	755
5	$-p_i/2$	0	q_5	0
6	0	0	$q_6 + p_i$	85

Table 3-2:DH parameters for IRB 2400-5

Joint i/link i	α_i (radian)	a_i (mm)	θ_i (rad)	d_i (mm)
1	$-p_i/2$	100	q_1	615
2	0	855	$q_2 - p_i/2$	0
3	$-p_i/2$	150	$q_3 - q_2$	0
4	$p_i/2$	0	q_4	870
5	$-p_i/2$	0	q_5	0
6	0	0	$q_6 + p_i$	65

In tables 3.1 and 3.2, q_i s are values of joint movements obtained from process simulate. To find θ_i much attention was paid to the concept of closed kinematic chain and the initial positions of robots when they are in home position. Considering these two significant issues, θ_2 equals $q_2 - p_i/2$, θ_3 equals $q_3 - q_2$ and θ_6 equals $q_6 + p_i$. a_i and d_i are given in Product specification IRB 2400 M2000 [14].

After DH parameters were found for the robots, it was possible to build the transformation matrix from the base of the robot to joint six of the robot which will later be used in a chain of translation matrices to find the position and orientation of the sealing nozzles related to world frame.

3.3.2.2 Building DH transformation matrix

As described in section 2.1.1, the transformation matrix between two succeeding frames is expressed as expression 3.2 [14].

$$\begin{aligned}
 A_i &= R_{z,\theta_i} \text{Trans}_{z,d_i} \text{Trans}_{x,a_i} R_{x,\alpha_i} \\
 &= \begin{bmatrix} c_{\theta_i} & -s_{\theta_i} & 0 & 0 \\ s_{\theta_i} & c_{\theta_i} & 0 & 0 \\ 0 & 0 & 1 & 0 \\ 0 & 0 & 0 & 1 \end{bmatrix} \begin{bmatrix} 1 & 0 & 0 & 0 \\ 0 & 1 & 0 & 0 \\ 0 & 0 & 1 & d_i \\ 0 & 0 & 0 & 1 \end{bmatrix} \begin{bmatrix} 1 & 0 & 0 & a_i \\ 0 & 1 & 0 & 0 \\ 0 & 0 & 1 & 0 \\ 0 & 0 & 0 & 1 \end{bmatrix} \begin{bmatrix} 1 & 0 & 0 & 0 \\ 0 & c_{\alpha_i} & -s_{\alpha_i} & 0 \\ 0 & s_{\alpha_i} & c_{\alpha_i} & 0 \\ 0 & 0 & 0 & 1 \end{bmatrix} \\
 &= \begin{bmatrix} c_{\theta_i} & -s_{\theta_i}c_{\alpha_i} & s_{\theta_i}s_{\alpha_i} & a_i c_{\theta_i} \\ s_{\theta_i} & c_{\theta_i}c_{\alpha_i} & -c_{\theta_i}s_{\alpha_i} & a_i s_{\theta_i} \\ 0 & s_{\alpha_i} & c_{\alpha_i} & d_i \\ 0 & 0 & 0 & 1 \end{bmatrix}
 \end{aligned} \tag{3.2}$$

Since the robot used are a 6-joint robot, so the DH transformation matrix for the transformation from the robot base frame to robot last joint frame is $A = A1 \times A2 \times A3 \times A4 \times A5 \times A6$. Since the matrix calculation was done using Matlab, the DH transformation matrix is not expanded to each element in this report. The variable during the transformation is θ_i and whenever it changes, a new frame of the nozzle tip is created, generating a continuous moving path for robot nozzle given θ_i input continuously.

3.3.3 Frame transformation— from robot last joint frame to the sealing nozzle tip

Each of the three floor mounted robots has a two-nozzle gun, nozzle 1 (90°) and nozzle 2 (45°), and the two roof mounted robots each has a three-nozzle gun, nozzle 1 (90°), nozzle 2 (45°) and nozzle 3 (180°). Figure 3-6 demonstrates these two types of guns.

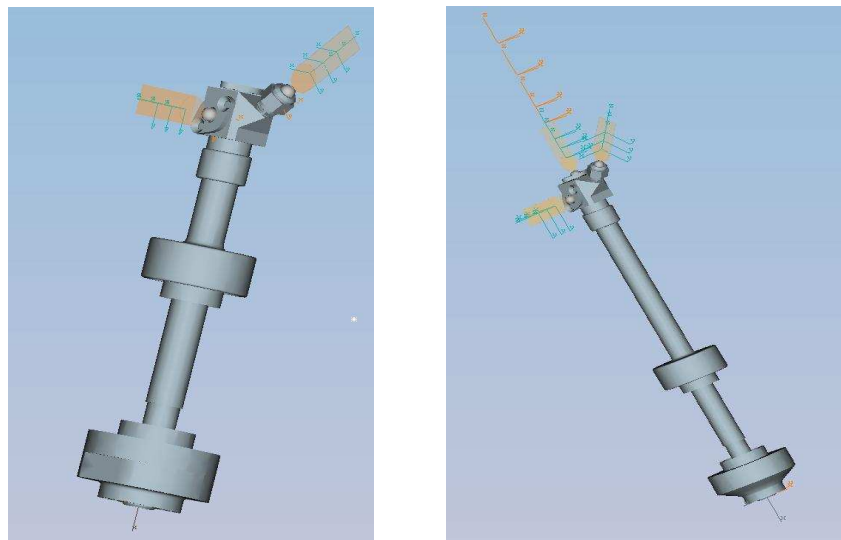


Figure 3-6: Sealing gun used for IRB2400-10(left) and for IRB2400-5(right)

Transformation of the last robot joint frame to the gun tip frame was pretty straightforward for the nozzle 3 since it could be considered as one more translation along Z axis. But for nozzle 1 and 2, the situation was more complex in a sense that the sealing gun is a rigid entity, therefore the movement of the robot last joint can directly and definitely lead to the movement of the nozzle tip. If under the same reference frame, the displacement of robot last joint is the same as the displacement of the nozzle tip, including the positions and orientations. This is different from two consecutive robot joints where one joint movement is independent on the other joint movement (except the closed chain). In closed chain, like joint 2 and 3, the movements are interconnected in a way that when one of them rotates to a greater joint angle, the other one has to rotate to a smaller joint angle, but the two joints do not move with the same pace and same amount of displacement as the same as a rigid body. So the transformation should be different from the transformation between successive robot joints. Investigation of

the sealing gun revealed that the central line of nozzle 1 and 2 intersects with each other at one point (point C as we named it). Then the transformation can be perceived firstly translate the last joint frame to the point C and then rotate at this point along a certain axis (sometimes X-axis, sometimes Y-axis, depending on different gun frame in Process Simulate) to align the Z direction with the Z direction of the final nozzle tip frame, and thereafter translate from the current frame to the nozzle tip frame. Figure 3-7 shows the transformation process.

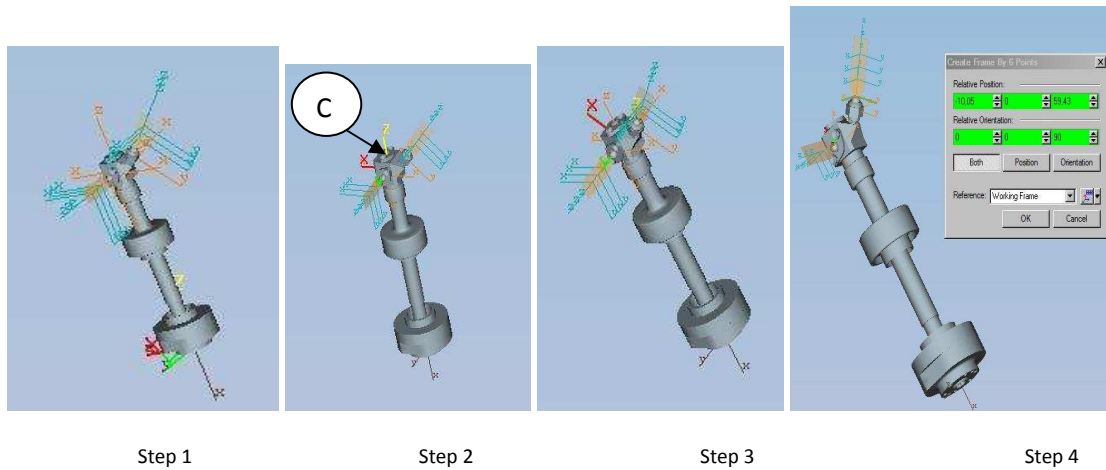


Figure 3-7: Transformation process from the last joint frame to the nozzle tip frame

As shown in Figure 3-7, in step 1 the last joint frame of the robot is defined as working frame, and then in step 2 it is translated around Z axis reaching the nozzle central point C (shown in step2, the position of the working frame) where central line of nozzle 1 and 2 intersect. The frame at point C is then defined as working frame and in subsequent step 3, it rotates -90 degree around Y axis in order to align Z axes of the working frame and the nozzle tip frame. Then in step 4, the positions and orientations of nozzle 2 tip are obtained with respect to the current working frame and a final transformation is accomplished accordingly.

As shown in equation 3.3, the whole transformation procedure starts from the translation along Z axis for 326.9 mm, then rotation 45° around Y-axis to align the Z-axis, then in the frame of the current point (meeting point) translation 10.05 mm and 60.58 mm along X-axis and Z-axis respectively, then rotation around Z-axis for -90° .

Finding the transformation matrix for nozzle 1 has almost the same procedure as for nozzle 2. The only different is that the rotation at the intersection point has a different angle (90° or -90° , instead of 45° or -45°).

$$T_t = \begin{bmatrix} 1 & 0 & 0 & 0 \\ 0 & 1 & 0 & 0 \\ 0 & 0 & 1 & 326.9 \\ 0 & 0 & 0 & 1 \end{bmatrix} \times \begin{bmatrix} \cos\left(\frac{\pi_i}{4}\right) & 0 & \sin\left(\frac{\pi_i}{4}\right) & 0 \\ 0 & 1 & 0 & 0 \\ -\sin\left(\frac{\pi_i}{4}\right) & 0 & \cos\left(\frac{\pi_i}{4}\right) & 0 \\ 0 & 0 & 0 & 1 \end{bmatrix} \times \begin{bmatrix} 1 & 0 & 0 & 10.05 \\ 0 & 1 & 0 & 0 \\ 0 & 0 & 1 & 0 \\ 0 & 0 & 0 & 1 \end{bmatrix} \times \begin{bmatrix} 1 & 0 & 0 & 0 \\ 0 & 1 & 0 & 0 \\ 0 & 0 & 1 & 60.58 \\ 0 & 0 & 0 & 1 \end{bmatrix} \times \begin{bmatrix} \cos\left(-\frac{\pi_i}{2}\right) & -\sin\left(-\frac{\pi_i}{2}\right) & 0 & 0 \\ \sin\left(-\frac{\pi_i}{2}\right) & \cos\left(-\frac{\pi_i}{2}\right) & 0 & 1 \\ 0 & 0 & 1 & 0 \\ 0 & 0 & 0 & 1 \end{bmatrix} \quad (3.3)$$

3.4 Matlab functions

For this thesis two Matlab functions, ps2ips and ps2ipscont, were created to to define coordinates for nozzle tip. These two functions were used when the sealing station described in section 3.1.1 with car V60 was simulated.

The first function was used to calculate coordinates for single bead simulation and was the base of the second one. The second function was used to calculate coordinates for consecutive beads simulation, then by using this function, it can be said if a set of created beads are organized in a proper way or not.

The two functions defined above consist of three main parts. The first part was defined to get input arguments from users. The second part, the main body of the function, performs the main mathematical calculations based on the theory of robot forward kinematics. The last part of the function gives output that is the position and orientation of sealing nozzle tip in a continues path during a defined time interval. These three parts are explained in the following sections. Figure 3-8 displays the schematic relation of these functions.

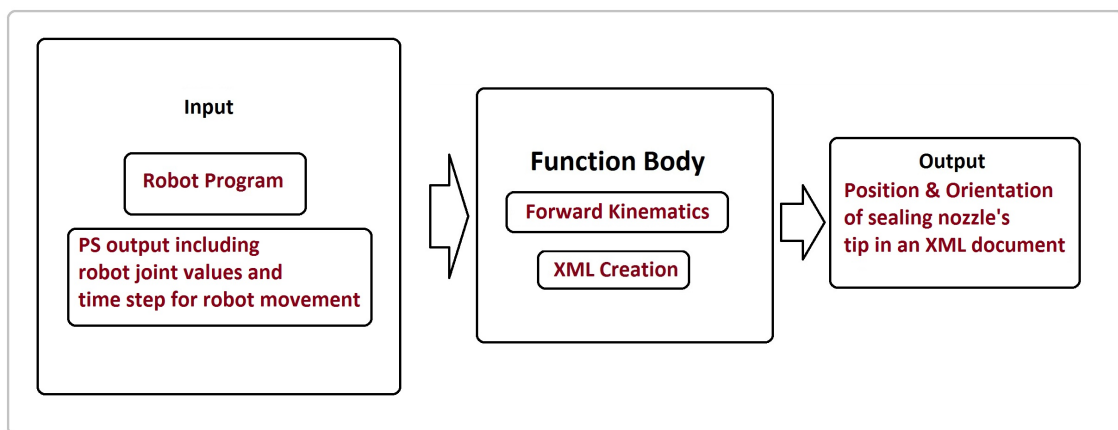


Figure 3-8: Schematic of Matlab scripts

3.4.1 Input arguments

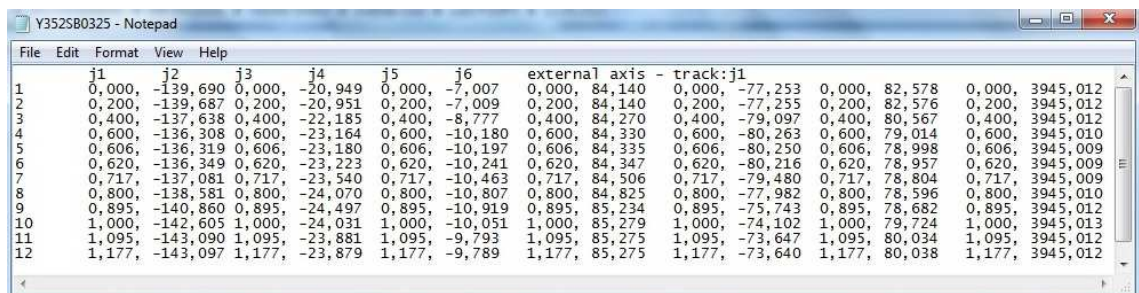
Firstly, the function should take two input arguments. The first argument is the robot program file. The other argument is the joint values text file generated in PS.

The robot program was used to extract information used later in the process of generating output. This information includes:

- Type of the specific robot used for that specific bead
- Nozzle number that is used for that specified sealing bead
- Sealing bead type.

First, robot program defines which robot is used for creating the specific bead. This is important when performing mathematical operation for forward kinematic inside script main body. Then the nozzle used to create the specific bead is read from robot program. This nozzle bead affects the using the mathematical operation, because each nozzle has its own angle and distance from robot base and word frame in station, and these angles and distances are decisive parameters when performing robot forward kinematic operations. Besides that, the robot program is used to extract bead data from the robot program that was created in advance. By bead data, it is defined what kind of bead is used for robotic sealing process, such as material flow, robot moving speed etc. The bead data used for programming sealing robot is shown in Appendix C.

The other input argument is the robot joint values text files created in PS. This text file records robot joint values along the robot path with a given time step specified in PS. In the text files, the joint values are recorded for seven columns, with each column corresponding to a robot joint (shown in Figure 3-9), for example the first column means the values for the robot first joint, the second column means the second joint and so on. The seventh joint is the track that is added to robot to enable its movement on the track along the sealing station. As it was mentioned, this text file also includes time detail in a way that it shows the position of robot joints in a specific time from the initial movement of a robot to put sealant on its place to the last point of the sealing path.



	j1	j2	j3	j4	j5	j6	external axis	track:jl
1	0,000	-139,690	0,000	-20,949	0,000	-7,007	0,000, 84,140	0,000, -77,253
2	0,200	-139,687	0,200	-20,951	0,200	-7,009	0,200, 84,140	0,200, -77,255
3	0,400	-137,638	0,400	-22,185	0,400	-8,777	0,400, 84,270	0,400, -79,097
4	0,600	-136,308	0,600	-23,164	0,600	-10,180	0,600, 84,330	0,600, -80,263
5	0,606	-136,319	0,606	-23,180	0,606	-10,197	0,606, 84,335	0,606, -80,250
6	0,620	-136,349	0,620	-23,223	0,620	-10,241	0,620, 84,347	0,620, -80,216
7	0,717	-137,081	0,717	-23,540	0,717	-10,463	0,717, 84,506	0,717, -79,480
8	0,800	-138,581	0,800	-24,070	0,800	-10,807	0,800, 84,825	0,800, -77,982
9	0,895	-140,860	0,895	-24,497	0,895	-10,919	0,895, 85,234	0,895, -75,743
10	1,000	-142,605	1,000	-24,031	1,000	-10,051	1,000, 85,279	1,000, -74,102
11	1,095	-143,090	1,095	-23,881	1,095	-9,793	1,095, 85,275	1,095, -73,647
12	1,177	-143,097	1,177	-23,879	1,177	-9,789	1,177, 85,275	1,177, -73,640

Figure 3-9: Robot joint values text file

Information about time and joint movements were used later in main body of Matlab script to calculate robot continuous kinematics and create final output.

3.4.2 Function Body

In this section, it is explained how Matlab functions used input arguments to create XML files including the position and orientation of sealing nozzle tip.

After defining the robot program as an input of the Matlab function, the corresponding DH parameters are recognized. As mentioned in section 3.1.1 there are five robots in the station, two of them are ABB IRB 2400-10 and three of them are ABB IRB 2400-5. These two different types of robots have different DH parameters, as written below.

DH parameters for ABB IRB 2400-10:

$$\alpha = \left[-\frac{p_i}{2}, 0, -\frac{p_i}{2}, \frac{p_i}{2}, -\frac{p_i}{2}, 0 \right]$$

$$\theta = [q_1(i), q_2(i) - 90, q_3(i) - q_2(i), q_4(i), q_5(i), q_6(i) + 180] \times p_i/180$$

$$a = [100, 705, 135, 0, 0, 0]$$

$$d = [615, 0, 0, 755, 0, 85]$$

DH parameters for ABB IRB 2400-5:

$$\alpha = \left[-\frac{p_i}{2}, 0, -\frac{p_i}{2}, \frac{p_i}{2}, -\frac{p_i}{2}, 0 \right]$$

$$\theta = [q_1(i), q_2(i) - 90, q_3(i) - q_2(i), q_4(i), q_5(i), q_6(i) + 180] \times p_i/180$$

$$a = [100, 855, 150, 0, 0, 0]$$

$$d = [615, 0, 0, 870, 0, 65]$$

α , θ , a and d was defined in section 3.1.3.

In next step, Matlab function extracts the information about nozzle from robot program. Currently, there are three different nozzles used in the sealing station. So the fact that which nozzle is used is also important to perform the kinematic calculations.

After defining the robot, its DH parameters and the nozzle inside the function, Matlab starts to calculate the position and orientation of the nozzle's tip in four steps.

First step is using DH parameters to find the situation of the last joint of a robot related to base of the robot. This was done by creating 6 joint-by-joint translation matrices using equation 3.4.

$$A = \begin{bmatrix} \cos \theta_j & -\sin \theta_j \cos \alpha_j & \sin \theta_j \sin \alpha_j & a_j \cos \theta_j \\ \sin \theta_j & \cos \theta_j \cos \alpha_j & -\cos \theta_j \sin \alpha_j & a_j \sin \theta_j \\ 0 & \sin \alpha_j & \cos \alpha_j & d_j \\ 0 & 0 & 0 & 1 \end{bmatrix} \quad (3.4)$$

Then by multiplication of all six translation matrixes, the total translation matrix, T, from robot base to robot sixth joint is gained (equation 3.5).

$$T = A1 \times A2 \times A3 \times A4 \times A5 \times A6 \quad (3.5)$$

The second step is to define a transformation matrix from world frame in sealing station to base frame of each robot. In Matlab functions, 5 transformation matrices were predefined for the sealing station of VCC. So depending on which robot is selected, the relevant transformation matrix is also selected. To create this five transformation matrices the movement of all five robots was also taken to account. So even if robots move on their 7th joint, this movement was observed and considered in calculation. This was done by creating a variable called “extdev” and is defined when Matlab functions read the joint values text file as an input argument. For one example, the transformation matrix for the last robot is written below.

$$TR5 = \begin{bmatrix} 1 & 0 & 0 & 5286.59 - extdev(i) \\ 0 & 1 & 0 & -719.47 \\ 0 & 0 & 1 & 3495.55 \\ 0 & 0 & 0 & 1 \end{bmatrix}$$

How the numbers and values inside the transformation matrixes are obtained was explained in section 3.1.

Finally twelve various matrixes that can consider the transformation from each robot’s last joint to its relevant nozzle tip are created. The reason that there are twelve different matrixes is that three of five robots have two nozzles installed on their last joint and two of them have three nozzles installed. So there is a need to create twelve different matrixes to cover all 12 different nozzles available in the station.

Also it should be considered that each nozzle on one robot is different from the other one because of their angle related to the last robot joint. The different nozzle angles used are 45, 90, and 180 degrees. Here the translation matrixes installed on the last robot are shown as an example.

Nozzle 1, 90 degree

$$T_t = \begin{bmatrix} 1 & 0 & 0 & 0 \\ 0 & 1 & 0 & 0 \\ 0 & 0 & 1 & 476.89 \\ 0 & 0 & 0 & 1 \end{bmatrix} \times \begin{bmatrix} 1 & 0 & 0 & 0 \\ 0 & \cos(p_i/2) & -\sin(p_i/2) & 0 \\ 0 & \sin(p_i/2) & \cos(p_i/2) & 0 \\ 0 & 0 & 0 & 1 \end{bmatrix} \\ \times \begin{bmatrix} 1 & 0 & 0 & 0 \\ 0 & 1 & 0 & 0 \\ 0 & 0 & 1 & 34.46 \\ 0 & 0 & 0 & 1 \end{bmatrix} \times \begin{bmatrix} \cos p_i & -\sin p_i & 0 & 0 \\ \sin p_i & \cos p_i & 0 & 1 \\ 0 & 0 & 1 & 0 \\ 0 & 0 & 0 & 1 \end{bmatrix}$$

Nozzle 2, 45 degree

$$T_t = \begin{bmatrix} 1 & 0 & 0 & 0 \\ 0 & 1 & 0 & 0 \\ 0 & 0 & 1 & 476.89 \\ 0 & 0 & 0 & 1 \end{bmatrix} \times \begin{bmatrix} \cos(p_i/4) & 0 & \sin(p_i/4) & 0 \\ 0 & 1 & 0 & 0 \\ -\sin(p_i/4) & 0 & \cos(p_i/4) & 0 \\ 0 & 0 & 0 & 1 \end{bmatrix} \\ \times \begin{bmatrix} 1 & 0 & 0 & 10.06 \\ 0 & 1 & 0 & 0 \\ 0 & 0 & 1 & 0 \\ 0 & 0 & 0 & 1 \end{bmatrix} \times \begin{bmatrix} 1 & 0 & 0 & 0 \\ 0 & 1 & 0 & 1 \\ 0 & 0 & 1 & 59.43 \\ 0 & 0 & 0 & 1 \end{bmatrix} \\ \times \begin{bmatrix} \cos(-p_i/2) & -\sin(-p_i/2) & 0 & 0 \\ \sin(-p_i/2) & \cos(-p_i/2) & 0 & 0 \\ 0 & 0 & 1 & 0 \\ 0 & 0 & 0 & 1 \end{bmatrix}$$

Nozzle 3, 180 degree

$$T_t = \begin{bmatrix} 1 & 0 & 0 & 0 \\ 0 & 1 & 0 & 0 \\ 0 & 0 & 1 & 510.74 \\ 0 & 0 & 0 & 1 \end{bmatrix}$$

How these matrixes were obtained was described in section 3.1. After creating three transformation matrixes, it was time to find the product of these three matrixes to obtain the position and orientation of the nozzle tips. This product is obtained by following equations for each of five robots:

$$T_1 = TR_1 \times T \times T_t$$

$$T_2 = TR_2 \times T \times T_t$$

$$T_3 = TR_3 \times T \times T_t$$

$$T_4 = TR_4 \times T \times T_t$$

$$T_5 = TR_5 \times T \times T_t$$

From these T1 to T5, the position and orientation of the each nozzle tip is gained. For example if it is intended to find out the position and orientation of nozzle tip of the last robot, it is obtained by following formulas in Matlab function:

$$\begin{aligned}
x(i) &= T5(1,4) \\
y(i) &= T5(2,4) \\
z(i) &= T5(3,4)
\end{aligned}$$

$$pitch(i) = (atan2(-T5(3,1), \sqrt{T5(1,1)^2 + T5(2,1)^2})) \times 180/p_i$$

$$\begin{aligned}
& \text{if } abs(pitch) = \frac{p_i}{2} \\
& \quad roll(i) = (pitch(i)/abs(pitch(i))) \times atan2(T5(1,2), T5(2,2)) \times 180/p_i \\
& \quad yaw(i) = 0 \\
& \text{else} \\
& \quad roll(i) = atan2(T5(3,2), T5(3,3)) \times 180/p_i \\
& \quad yaw(i) = atan2(T5(2,1), T5(1,1)) \times 180/p_i \\
& \text{end}
\end{aligned}$$

Here ,x(i),y(i),z(i),pitch(i),yaw(i), and roll(i) are the position and orientation for each time step along the sealing bead.

The last step is to write the output data from the Matlab Function in a XML document format that is read by IPS sealing. After an intensive investigation it was understood that the order IPS sealing understand roll, pitch and yaw is different from the order it is created in Process simulate, and to achieve desired results values of roll and yaw should be changed, while pitch remains the same. The new roll, pitch yaw that is used to create final script output is:

$$pitch(i) = (atan2(-T5(3,1), \sqrt{T5(1,1)^2 + T5(2,1)^2})) \times 180/p_i$$

$$\begin{aligned}
& \text{if } abs(pitch) = \frac{p_i}{2} \\
& \quad yaw(i) = (pitch(i)/abs(pitch(i))) \times atan2(T5(1,2), T5(2,2)) \times 180/p_i \\
& \quad roll(i) = 0 \\
& \text{else} \\
& \quad yaw(i) = atan2(T5(3,2), T5(3,3)) \times 180/p_i \\
& \quad roll(i) = atan2(T5(2,1), T5(1,1)) \times 180/p_i \\
& \text{end}
\end{aligned}$$

3.4.3 Output

The output of Matlab functions is a XML document with time, x(i), y(i), z(i), pitch(i), yaw(i), roll(i) and bead data information as elements of the document. An Example of XML output of Matlab function is given in appendix A.1.

Creating a Matlab script to derive position and orientation of a sealing applicator tips during applying bead material for one bead was a successful process but still needed improvement in a way that a path with more sealing beads can be included in one XML document. Therefore, it was needed to improve Matlab function ps2ips. It is done by creating another script named ps2ipscont based on the first script.

The only difference between the two functions is that the function output is an XML document that includes information about position and orientation of nozzle tip for more than one bead. Therefore, there is more than one 'On' command (like B68) and more than one 'Off' command in script output.

3.5 Creating applicator

Another input to run IPS is named applicator which is also a kind of XML document. The applicator includes information about material rheology data and sealing brush data. This set of information determines how the simulated sealing beads will look like.

3.5.1 Sealing material at VCC

Material rheology refers to the flow properties of the material, normally in a liquid state. As concerned in this thesis, it contains four parameters: density of the material whether it is Bingham or not, plastic viscosity and yield stress.

The material used for seam sealing in VCC is EP2009FL, which is a yellow colored paste like chemical. It contains mainly three substances: PVC, which determines the material mechanical property, Plasticizer, which softens the material and provides more flexibility, and Filler, which is used purposely to reduce cost since it is cheap. The more filler are used, the higher hardness the material gets.

3.5.2 Rheology Calculation

Of all the rheology parameters, density is a constant and can be obtained from different sources and the sealing material used at VCC is Bingham material. In order to obtain the viscosity and yield stress of the sealing material, an experiment was done previously at VCC according to their standard [19]. The experiment was composed of 19 steps, with shear rate varying from step one 1/s to the maximum 450 /s in step ten and then to the final 1/s again. Shear stress and viscosity were measured for each step. In order to get more accurate measuring data each step was repeated 36 times, with a certain time interval of 5 seconds. Appendix D shows the result of the visometric tests performed at VCC.

Rheology calculation started with taking average values of the 36 runs for both the controlled parameter shear rate and measured parameters shear stress and viscosity in each step. Thereafter the relation between shear rate and shear stress were plot out using Matlab, as shown in figure 3-10.

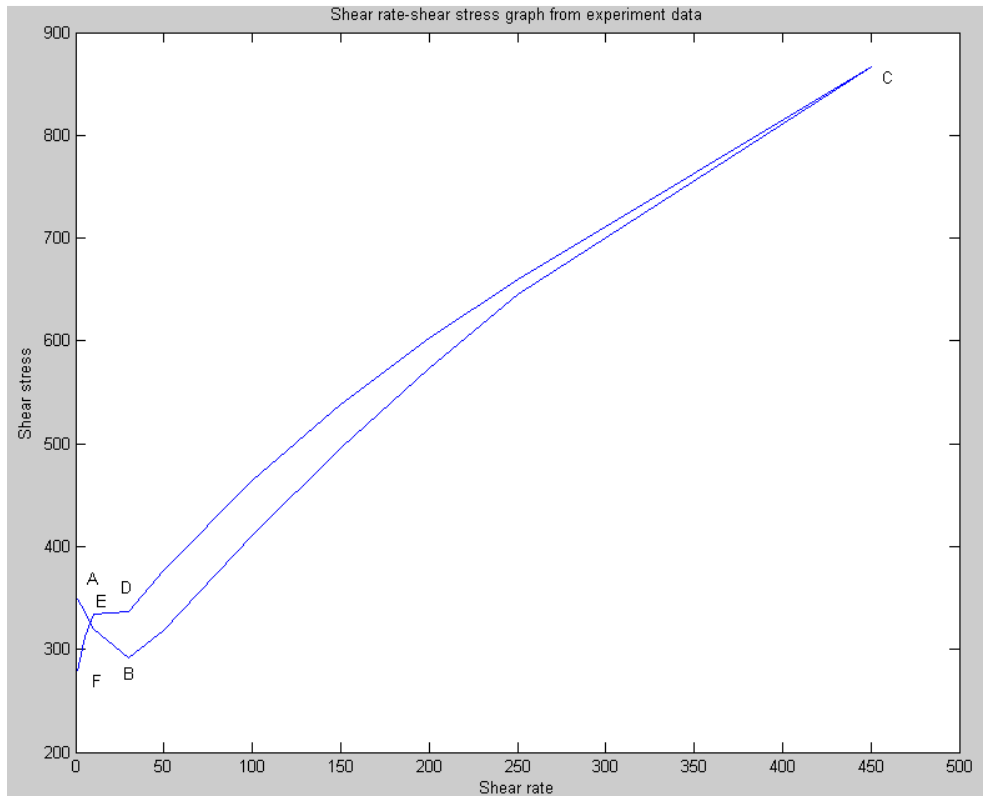


Figure 3-10: Relation between shear rate and shear stress

As specified in the VCC standard, the viscosity is taken as the ratio between the shear stress at the maximum shear rate after the material is broken down and the maximum shear rate. Mathematically, $\eta = \tau / D_{max}$. As can be seen from figure 3-10, the material was not broken down during the experiment, so the shear stress τ was taken when shear rate reached to its maximum. The calculated viscosity was 1.92 p_a.s , which is reasonable given the range of 1.9-2.6 according to VCC standard. To get yield stress, a line interpolation based on curve CD should be deployed and the interception on the shear stress axis was taken as yield stress. The calculated value for yield stress was 299.14 p_a, which is also reasonable given the range of 210-330 according to the VCC standard [19] [20].

It should be noticed that the production temperature at Volvo is around 35 degrees, but the rheology data gathered was for 23 degree, which could lead to some discrepancies to the parameter values.

3.5.3 Brush Data

A sealing applicator contains many sealing brushes and how many brushes an applicator has depends on how many types of sealing beads are defined. At VCC, there are 27 types defined ranging from bead 52 to bead 78(Appendix C). Therefore there should be 27 sets of brush data. Each brush data contains the following parameters:

- Predefined brushes ID, there are 27 brushes, from B52 to B78.

- Bead type, 'flat' for sealing process
- Width, each maximum width is specified in VCC standards.
- Mass rate, the rate of material ejected from the nozzle. It is calculated by following formula

$$Mass\ rate = flow \times density / 10^6 \quad (3.6)$$

Where flow defined by VCC experts is the material flow from sealing nozzle for each bead and has the unit of ml/s, density is the density of sealing material with unit kg/m³ and Mass rate has the unit of kg/s.

- Injection velocity, the velocity of material sprayed from the nozzle tip. This is calculated by following expression:

$$Injection\ velocity = flow \times nozzle\ area \quad (3.7)$$

Where flow has the unit of ml/s and nozzle area is the area of nozzles used in sealing application with unit mm². Injection velocity, therefore, has the unit of m/s.

3.5.4 Applicators created

As mentioned earlier, besides the path motion, another indispensable input parameter for IPS simulation is applicator. The applicator data includes material rheology data and the brush data. In total, there are two sets of rheology data gathered for this thesis: one from VCC material supplier, and one calculated for this thesis. They are displayed table 3.3. All the two sets of data were used for creating applicators for IPS simulation.

Table 3-3: Different sets of rheology data

	Material supplier (applicator1)	Thesis (applicator2)	Reference value	Unit
Material Density	1122	1122	1070-1130	Kg/m ³
Viscosity	2.16	1.92	1.90-2.06	Pa s
yield stress	260	299.14	210-330	Pa

3.6 Identifying important sealing verification parameters

Potential important sealing parameters were investigated for the purpose of evaluating sealing result. Considering viewpoints from experts in sealing area, it was suggested that sealing width and thickness are two important and popularly accepted criteria to evaluate sealing result. In order to identify which input parameter has the most influence on the sealing result, 12 runs of DOE tests concerning flow, speed and TCP distance as

input and width, thickness and volume as output have been completed at VCC in collaboration with Teamster(See Appendix E). The explanation of these parameters is given below:

- Flow refers to bead flow, in the unit of ml/s
- Speed (mm/s) is short for robots TCP moving speed.
- TCP distance (mm) means the distance between the nozzle tip and the target area to spray sealing material on the car
- Width (mm), thickness (mm) and volume (ml) refer to the width, thickness and volume of the sealing bead respectively.

The DOE test was done under the temperature of 35 degree, which is the production temperature. In each run, the flow, speed and TCP were controlled at a given value and bead width, thickness and volume were measured on two kinds of beads: 200mm length beads and 300 mm length beads. Between the runs, the inputs varied from each other and after all the 12 runs were completed; there was a repetition for the whole process to get a more accurate experimental value.

Dealing with the data involved first order liner regression analysis. Since there were three inputs, flow, speed and TCP distance, and three outputs, width, thickness and volume, there were nine possible relations between the inputs and the outputs. The following figures 3-11 to 3-13 reveal all the possible relations.

The slope of the line exhibits the degree of the correlation between a single input and a single output. The greater the absolute value of the line slope means the bigger change of the output value based on the change of the input parameter, thus meaning the more correlations between the single input and single output. If the line is horizontal, it means that the output is independent of the input parameter.

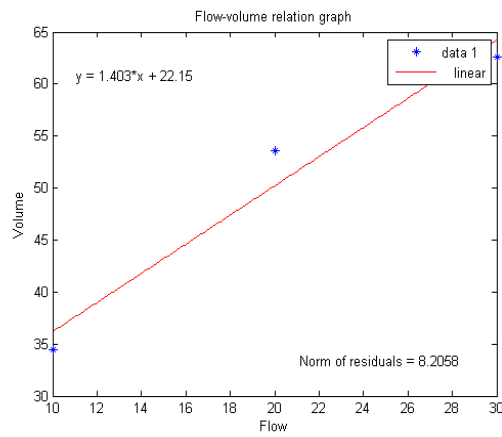
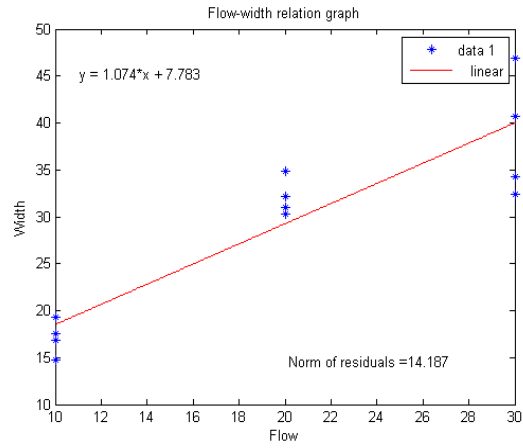
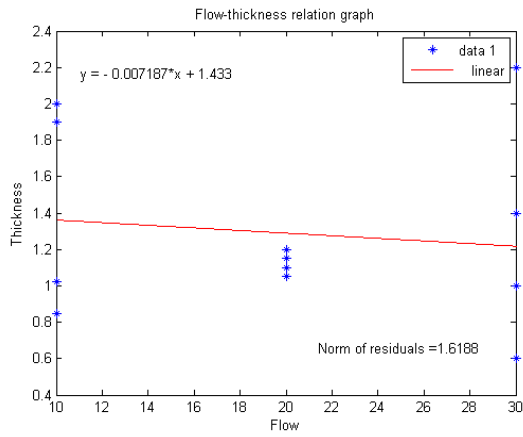


Figure 3-11: Effect of flow on thickness, width and volume.

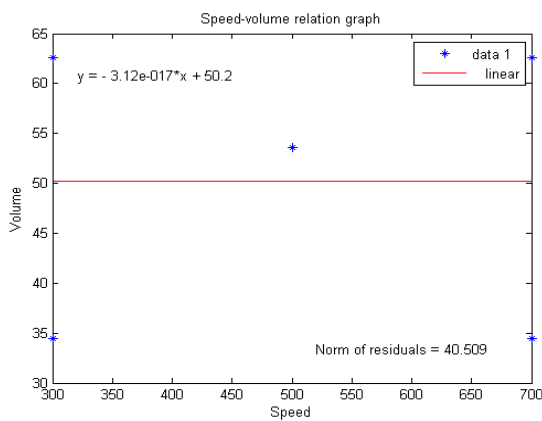
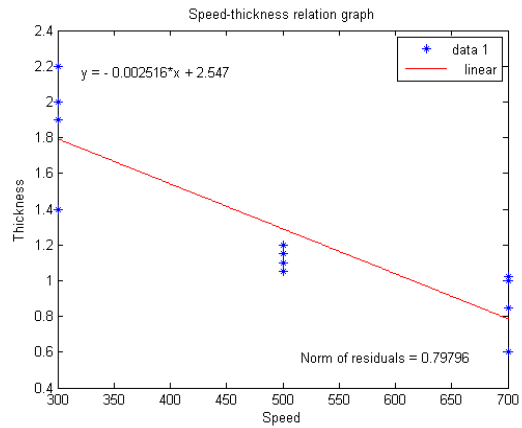
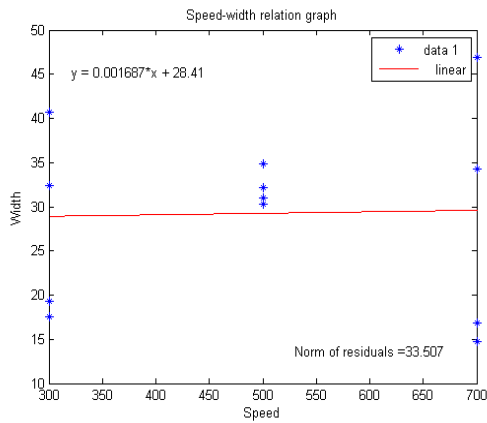


Figure 3-12: Effect of Speed on thickness, width and volume.



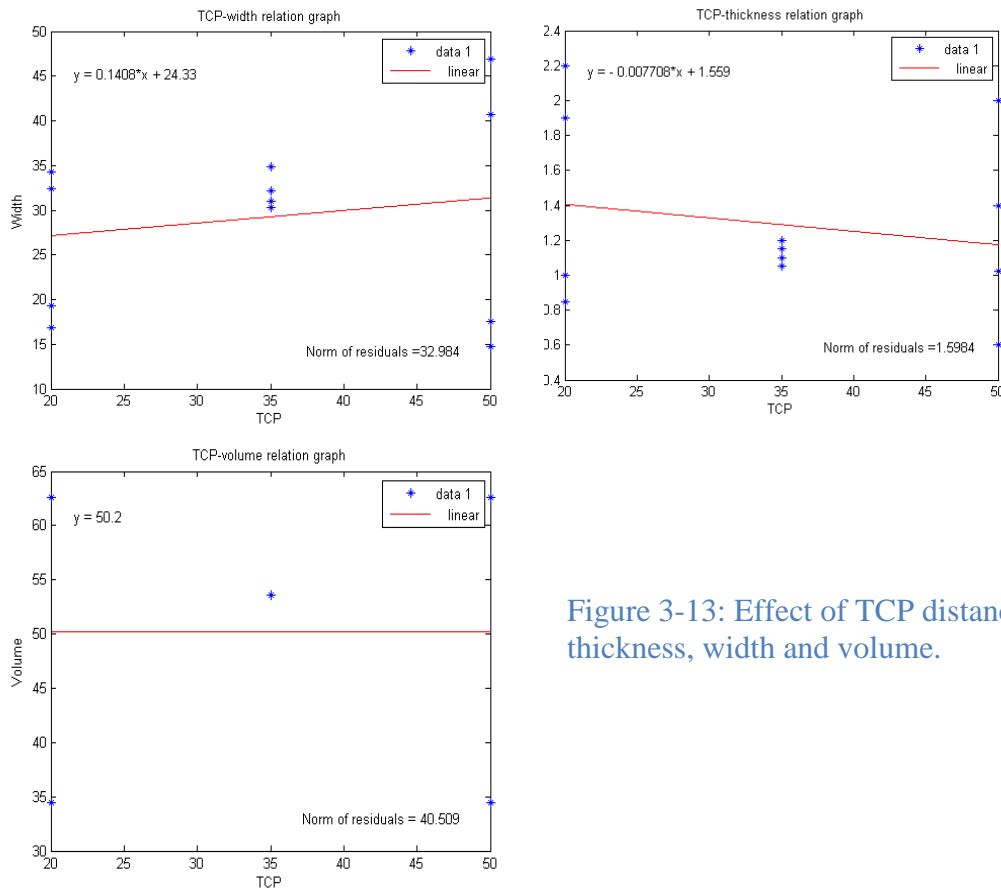


Figure 3-13: Effect of TCP distance on thickness, width and volume.

As indicated in the above figures, the width and volume consumption changes very much with the change of flow (Figure 3-11) while the thickness varies greatly with the variation of TCP moving speed (Figure 3-12). Width changes somehow with the change of speed and TCP distance (Figures 3-12 and 3-13) while thickness changes to a certain degree with the change of flow and TCP distance (Figures 3-11 and 3-13). The volume consumption is not changing with the change of TCP moving speed and TCP distance (Figure 3-12 and 3-13).

In conclusion, flow has a very obvious influence on bead width as well as volume consumption and speed has a big impact on bead thickness. Width has some relations with speed and TCP distance while thickness has some connections with flow and TCP distance. The volume consumption is independent of TCP moving speed and TCP distance.

4 Verification of virtual sealing software

The verification process started with the selection of the better applicator from the two applicators created already. During the selection applicator procedure and later the whole verification period, the following three methods were used for evaluating the sealing result.

- Performing comparison between width and thickness of selected simulated beads and width and thickness of real sealing beads measured manually in production line
- Comparing the appearance and placement of simulated beads with the appearance and placement of those selected beads in reality
- Comparing the material consumption in virtual sealing environment and real material consumption

All the three methods were used to verify the IPS sealing, but the measuring method might vary from bead to bead, depending on the geometry of the places where beads were located on, the number of beads on a place, and the nature of designed beads itself. For example, if a straight bead was located on a reachable place on the car body for a measuring tool, performing manual measurement to find the width and height of the bead seemed an adequate method for the purpose of verification. On the other hand when beads were located in a corner that is difficult to perform manual measurement, appearance comparison and material consumption comparison was a feasible way to verify the simulation result. The final verification was done based on the result of all three methods performed on sealing beads in production line and in virtual environment.

4.1 Applicator selection

As outlined previously, there were two applicators created, so the first step of verification was to check which applicator gave better simulation results, results closer to reality. A series of simulation was completed for the two applicators and the results were demonstrated below in table 4.1, 4.2 and 4.3.

Table 4-1: Thickness results from the two applicators in fast simulation and from production for bead Y352SB6313d

	Thickness in IPS(mm)				Thickness in production(mm)			
	t=0.5s	t=1s	T=1.5s	Average thickness	t=0.5s	t=1s	t=1.5s	Average thickness
Applicator1	3	2.8	3.7	3.17	1.7	1.6	1.6	1.63
Applicator2	3.1	3.2	3.6	3.3				

Table 4-2: Width results from the two applicators in fast simulation and from production for bead Y352SB6313d

	Width in IPS(mm)				Width in production(mm)			
	t=0.5s	t=1s	T=1.5s	Average thickness	t=0.5s	t=1s	t=1.5s	Average thickness
Applicator1	34.1	32.8	35.8	34.23				
Applicator2	33.2	32.8	36	34	29	29	32	30

Table 4-3: Bead appearance results for bead Y352SB6313d from the two applicators in fast simulation and from production

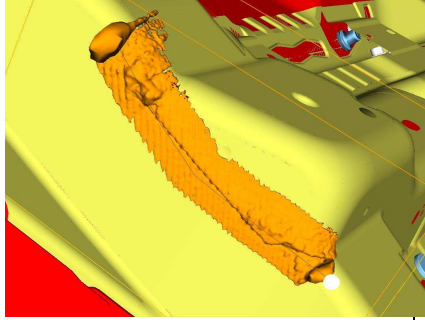
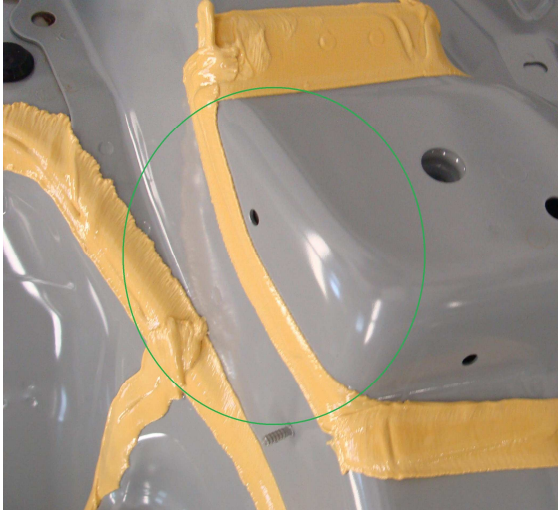
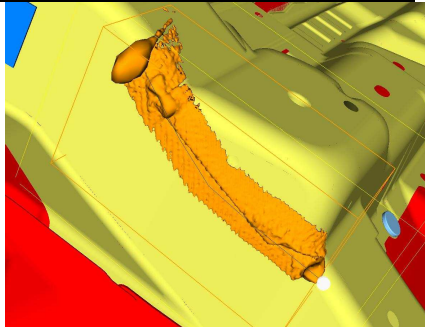
	Picture in IPS	Picture in production
Applicator 1		
Applicator 2		

Table 4-4: Volume and mass results for bead Y352SB6313d from the two applicators both in fast and slow simulation as well as results from production

	Volume in IPS(mm3)	Volume in production(mm3)	Mass in IPS(g)	Mass in production(g)
App1_fast simulation	12434,32	6756,90	13,95	7,58
App1_slow simulation	13472,61	6756,90	15,12	7,58
App2_fast simulation	12434,32	6756,90	13,95	7,58
App2_slow simulation	13472,61	6756,90	15,12	7,58

Table 4.1 and 4.2 reveal that the thickness, width and bead appearance from both applicator 1 and applicator 2 are almost the same, indicating the two applicators are nearly equivalent and exchangeable to each other in IPS simulation. From table 4.3, one can easily perceive that the two applicators, applicator 1 and 2 lead to the exact same simulation results in terms of volume and mass consumption. Since the two applicators differ from other only in the rheology data but not in brush data, the conclusion can be drawn that rheology data does not affect the simulation results. Under such circumstance, one can choose either one of the two applicators for IPS sealing simulation.

4.2 Appearance

Another way to verify if the sealing simulation results corresponded to the designed sealing beads and real sealing beads in production line was to compare the appearance of real sealing beads and the appearance of simulated beads created by IPS sealing. To do this comparison two methods were used:

- Comparing general appearance of six carefully selected areas covered by sealing beads in design, reality and fast simulation;
- Comparing the finished surface of sealing beads in reality with the surface of beads created by fine high resolution simulation.

4.2.1 General appearance of six selected areas:

For such judgment, six important areas covered with sealing beads were selected and it is explained why those areas were selected. By means of pictures from designed sealing beads, real beads and simulated beads comparisons were made between design, reality and simulation appearance of sealing beads. Following this comparisons were explained.

Figure 4-1 shows sealing design for a complicated geometrical area in a corner inside the engine room of V60. Figure 4-2a displays the real situation of this area after applying sealing material. Here, more than five metal components constitute a complicated corner that is not easy to reach for robots. As it is obvious, the presence of many sealing beads plus the fact that robots do not move fast when sealing this corner, ends up in accumulation of sealing material here. It is not important to have beautiful appearance here, while it is more important to cover all the seams intended to be sealed since water and dirt can intrude the engine room easily if the seams and gaps are not sealed completely. Also, it is not that easy to make any kind of manual measurement for sealing beads on this complex geometry. Therefore, when designed beads are created by design experts at VCC want to make sure that sealing beads on this area are applied on their right places to perform their sealing function as it is intended in design stage. Then, it is important that the simulation has the same result as real situation for beads created on this complicated geometry.

Figure 4-2b shows the simulation picture resulted from IPS sealing software. As it is shown in this picture, simulation result is close to what is visible in reality. Sealants are put on the targeted seams and the coverage is done perfectly. Due to presence of more than one sealing bead and slower robot movements in this area there is a bunch of material in this corner. Thus, it can be said that the general appearance of the simulation is compatible with the appearance of the real sealing beads.

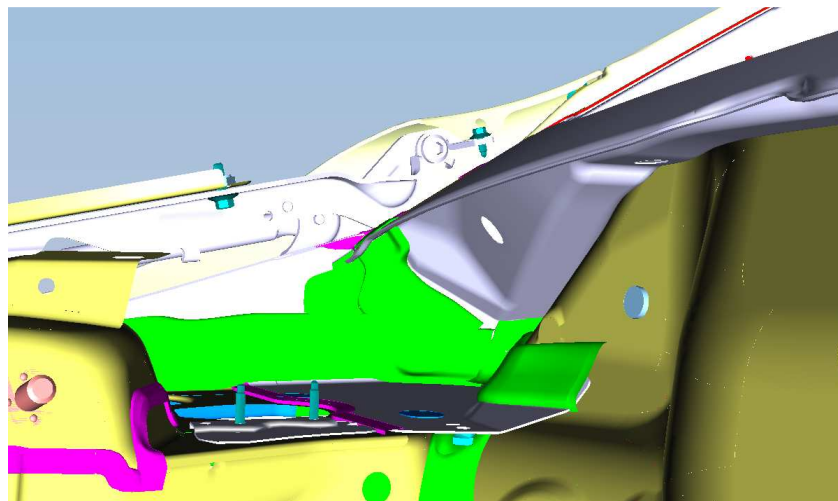
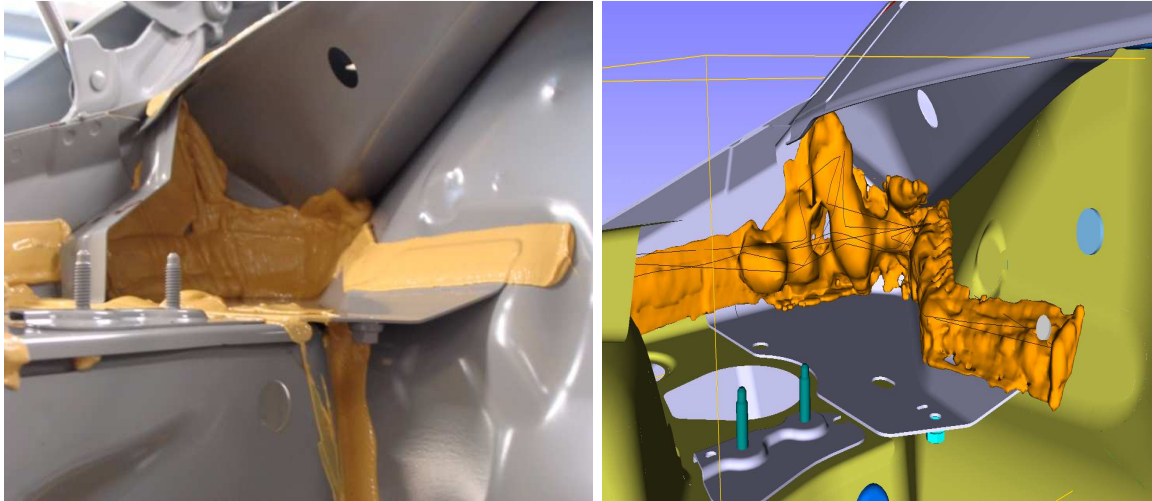


Figure 4-1: Sealing design for upper corner inside the engine room of V60



a: Sealing beads on one complicated corner inside the engine room b: The simulation result for the mentioned area inside the engine room

Figure 4-2: Complicated corner inside the engine room of V60

Figure 4-3 demonstrates how another corner inside the engine room of V60 should be sealed based on design criteria. Figure 4-4a displays how this corner looks in reality after applying sealing material on it. Here, there is enough space for robot movements compared to Figure 4-2a, while there is still more than one bead sprayed in the area and met in one location that makes a cross area for sealants. These beads intend to prevent water and dirt entry to the engine room. Therefore, based on geometry of this location and beads application, it is interesting to know how designed beads are located on their places before initiation of real production.

The simulation result from IPS sealing shown in figure 4-4b implies that in the beginning parts of the upper bead a complete coverage area on the intended seam is not created. This can happen because the created sealing path by Process Simulate is not accurate. In such cases, previously corrective actions were taken in production line before initiating ramp up production, but now the defect is known early in creating paths and is corrected simultaneously while creating sealing path. Other portion of this sealing bead and also the other two beads shown in figure 4-4b, created by simulation, match the real situation in production. Especially in the place three beads meet together the accumulation of material has a general similar appearance compared with reality.

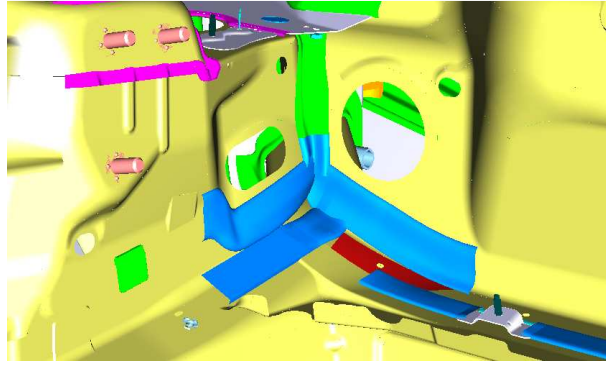
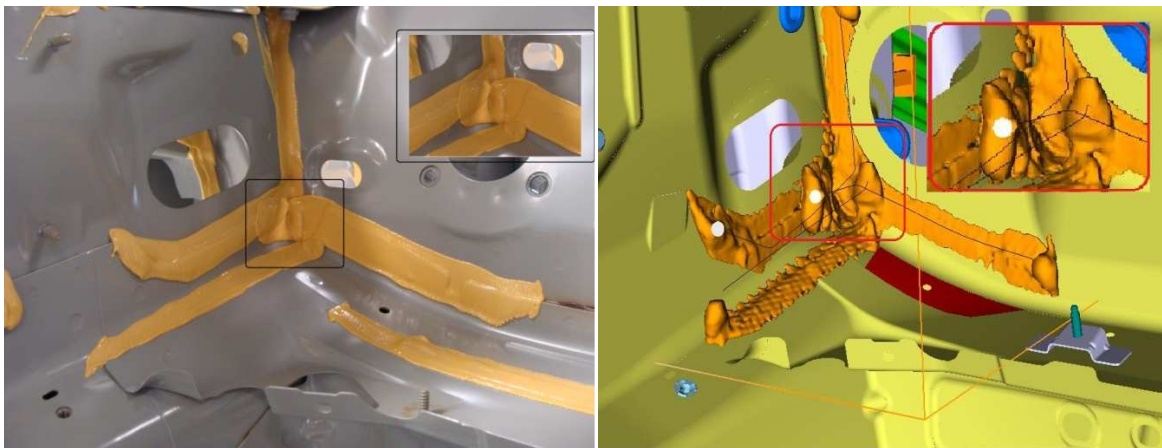


Figure 4-3: A corner inside the engine room of V60



a : Sealing beads on one corner inside the engine room b: Simulation result for the mentioned area

Figure 4-4: An important corner inside the engine room of V60

Figure 4-5 represents designed sealing beads around the spring tower. Here the geometry of car body is not as complicated as the two previous cases. But it is still important to put sealing materials on their right place because they also prevent water and dirt from entering into the engine room. As it is shown in figures 4-6a, sealing beads are wide and thick enough to cover all intended seams. Figure 4-6b shows the simulated result for sealing beads in the area described in figure 4-6a. As it is shown in these simulation picture, the appearance of the simulated beads comply the reality and covers all intended seams with the same curves and appearance in real situation, while there are still places that are not covered completely with sealing materials. Figure 4-7 shows another view of these simulated sealing beads.

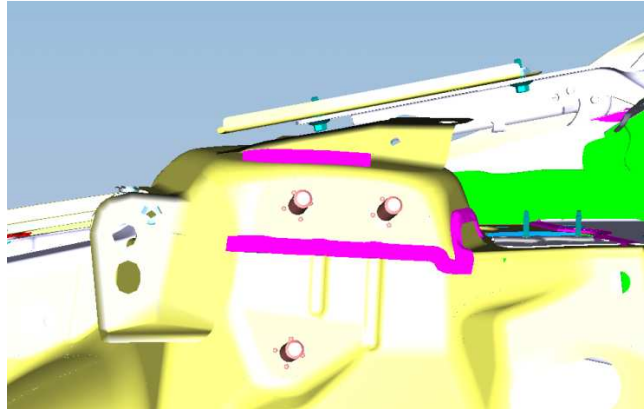
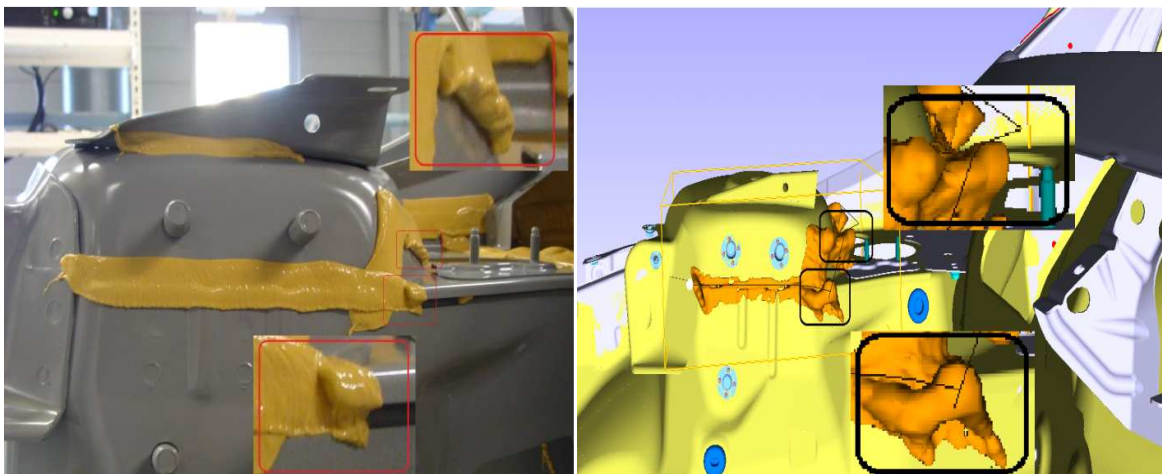


Figure 4-5: Designed sealing bead around spring tower



a : Sealing beads in reality

b : Sealing beads in simulation

Figure 4-6: Sealing around spring tower inside the engine room

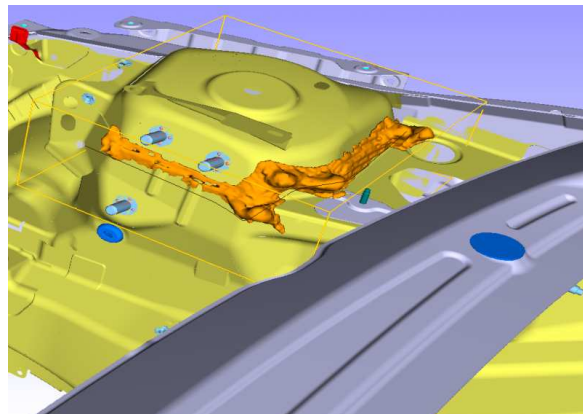


Figure 4-7: Another view of figure 4.24 b

Figure 4-8 represents another geometrical complicated area in the front wheelhouse of a V60 car. Three beads present on this area from which two meet on a corner and one follow a curve in that corner. It is also not important how beautiful the beads are in this place while the application is much more important. Sealants are intended to prevent

water and dirt entry from wheelhouse to engine room and inside the car as well. So it should be considered that sealing beads cover all intended gaps and seams properly and correctly. Figure 4-9a demonstrates how this place exists in reality.

Figure 4-9b demonstrates the result of simulation for this complex geometrical corner located in front wheelhouse of V60. The three intended beads cover seams and gaps compatible with the reality and there is an accumulation of sealant material on the cross point of three beads also. Thus, in general it can be said that appearance of the simulation is compatible with the appearance of the real sealing beads.

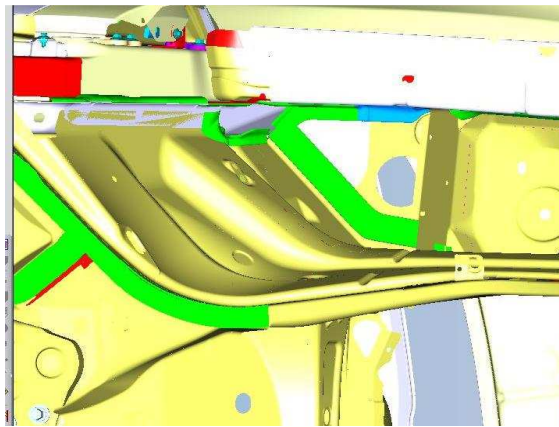
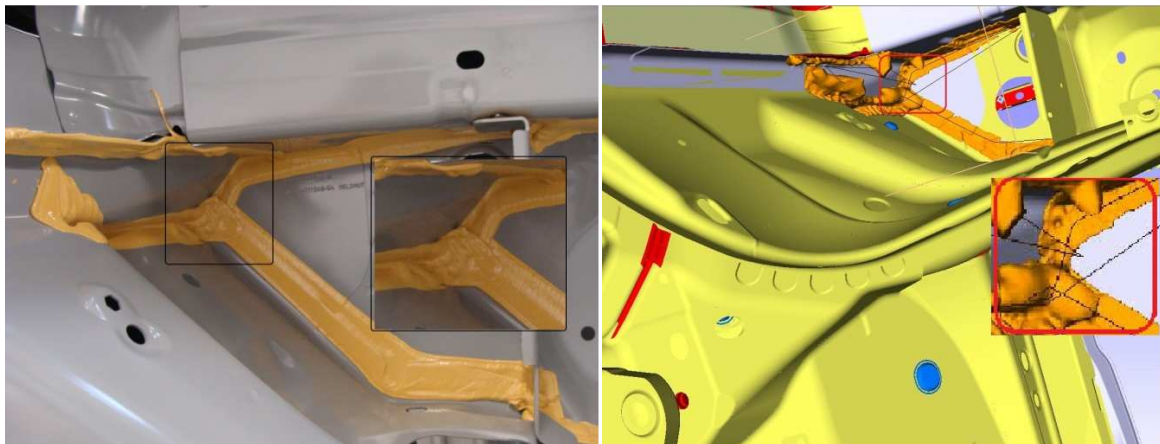


Figure 4-8: Designed sealing beads in front right wheel house of V60



a: crossed sealing beads inside the front wheelhouse in reality

b: crossed sealing beads inside the front wheelhouse in simulation

Figure 4-9: Crossed sealing beads inside the front wheelhouse

Figure 4-10 shows an area underneath the car body. This area is selected because there are two rotation about 90 degree in this sealing bead, which makes the flat stream gun rotate 90 degree when reaching the corners. Figure 4-11a shows the real sealing beads on the mentioned area.

Figure 4-11b displays the simulation result for the targeted area. The simulation result is compatible with the real situation and covers all the intended seam length in that target area.

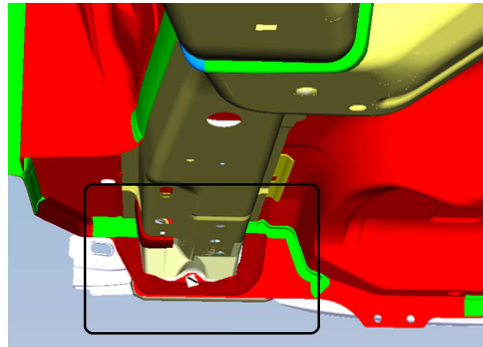
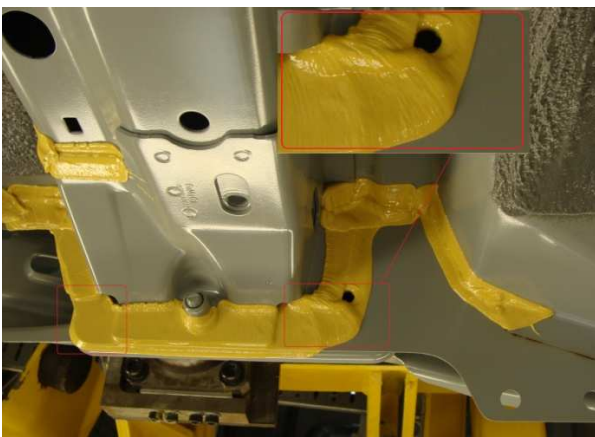
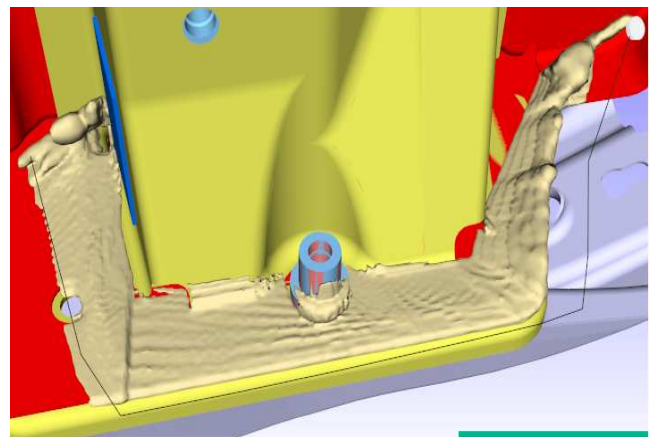


Figure 4-10: Designed seal underneath the car, the designed bead has two 90 degree rotations



a: sealing beads underneath the car in reality



b: sealing beads underneath the car in simulation with last version of IPS sealing

Figure 4-11: Sealing beads in an area underneath the car

Figure 4-12 shows a location with more than one cross area of sealing underneath the car body. The geometry of this area is not complicated and beads are quite straight. On the other hand this is the lowest part of car body and when it is raining outside or when the car is passing a hole full of water, this area is the first area to meet water. Therefore sealing materials are applied underneath the car to prevent water entry into car room in such situation and this is too important that they cover the right area. Thus, experts in manufacturing department of VCC want to know if the sealing path created by Process simulate is accurate enough to cover all intended gaps and seams or not before going to production. Figure 4-13a displays the real situation of this area after applying sealing material.

Figure 4-13b displays the simulation results taken from IPS sealing software. As it is shown in figures 4-13b the general appearance of simulated beads on selected area is the same as the general appearance of selected beads on reality. There are more materials on two shown cross beads on simulation and also reality. But it is obvious that the material pile created by simulation seems more than what it is in reality. The straight parts of beads that do not cross are generally similar to reality and follow the geometry of the plates beads are located on. In general it can be said that the result of fast simulation is compatible with the reality and can be trusted.

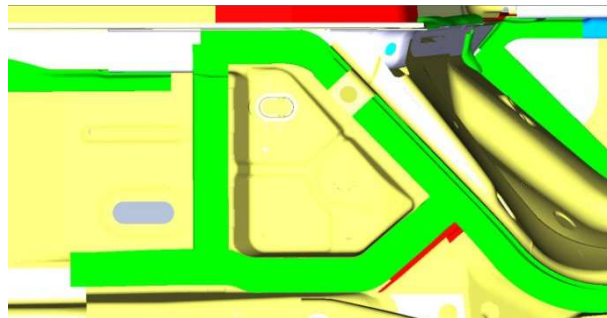
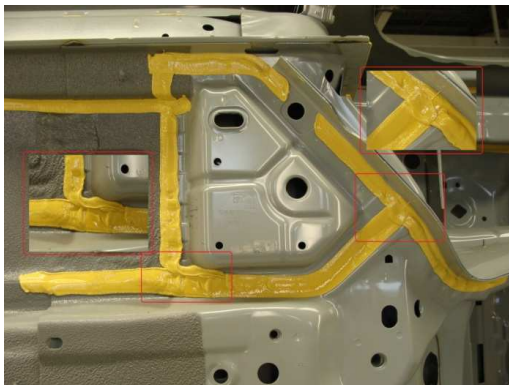


Figure 4-12: Design of sealing beads underneath a car with two cross beads



a: sealing beads underneath the car in reality

a: sealing beads underneath the car in simulation

Figure 4-13: Crossed sealing beads underneath the car

4.2.2 Finished surface of sealing beads

To compare the finished surface of beads from closer view one simulation with better and finer resolution for shorter beads was performed. The surface of simulated bead was compared with a close view of surfaces of a bead on production line. Using fine resolution to carry out a long simulation might be time consuming, so this was just done for one small sealing path for the purpose of verifying how IPS sealing makes the final surface of sealing beads.

Figure 4-14 displays a real sealing bead from closer view. This bead is created by flat stream applicator on V60.



Figure 4-14: The outer surface of the selected beads

Figure 4-15 shows the outer surface of the selected beads created by simulation.

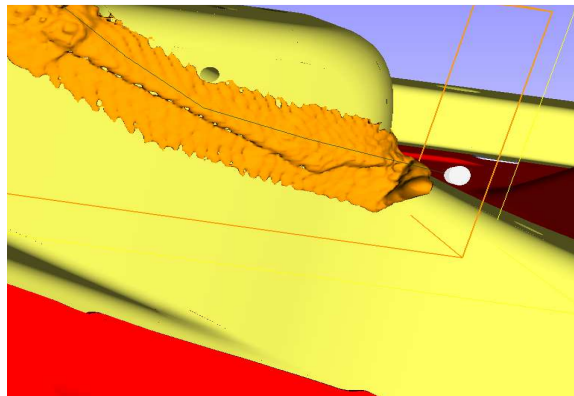


Figure 4-15: The outer surface of the selected beads created by simulation

As it is obvious from figures 4-1 4 and 4-15 the final appearance of beads created by IPs for a short bead by setting finer resolution for simulation can be said compatible with the final appearance of real beads. While this fact should be considered that the software for virtual simulation, IPS sealing, is still under development. Therefore in final versions the final surface created by IPS for beads should be the same while the simulation is done under any circumstances.

4.2.3 Conclusion for appearance comparison

Based on what is mentioned in section 4.3.1 and 4.3.2, the general appearance of a sealing bead simulated with IPS sealing is compatible with the real situation. Sealing material is put on the right place and covers the gaps and seams if the path for creating beads is generated correctly. When there is material accumulation in reality, it also exists in simulation environment, for example the cross beads have similar shape when comparing pictures from production line and pictures from simulation environment. The closer view of sealing beads in reality and simulation shown also prove that virtual simulation software are able to create fine surface like the real surfaces in production line. But it is needed to adjust the setting and resolution of simulation before running it.

In short, the investigation to verify the appearance of simulated sealing beads shows that IPS sealing software works well in this stage.

4.3 Manual measurement

One way to verify the result of virtual sealing software, IPS sealing, is to make manual measurements regarding the width and thickness of sealing beads in reality and compare them with the simulation result from IPS sealing. Two types of measurements were carried out.

- Measuring beads on flat plates: This was done by collaboration of Volvo Cars and FCC experts and result of this experiment was also used in this thesis for the purpose of verification.
- Measuring beads on real car body: That was done by measuring width and thickness of beads on real car body after sealing stations.

4.3.1 Measuring beads on flat plates

Even the most straight sealing beads on car body are not really straight and are under the effect of car body geometry and noise and unwanted impacts in production line. Therefore carrying out an experiment of applying beads on flat plates is a very trustable method to compare the width and thickness of sealing beads created by robots in reality and created by virtual simulation software. For this purpose a series of experiment were carried out in collaboration with VCC and FCC experts. Results of these experiments were explained below.

First, the width and thickness of beads applied by flat stream applicator on a plate when the applicator is static are measured at different times. Figures 4-16 and 4-17 show the beads created in reality and by IPS sealing software under mentioned circumstances. Figures 4-18a and 4-18b shows respectively width and thickness measurement against time for those beads.



Figure 4-16: Real beads created by static and flat stream applicator

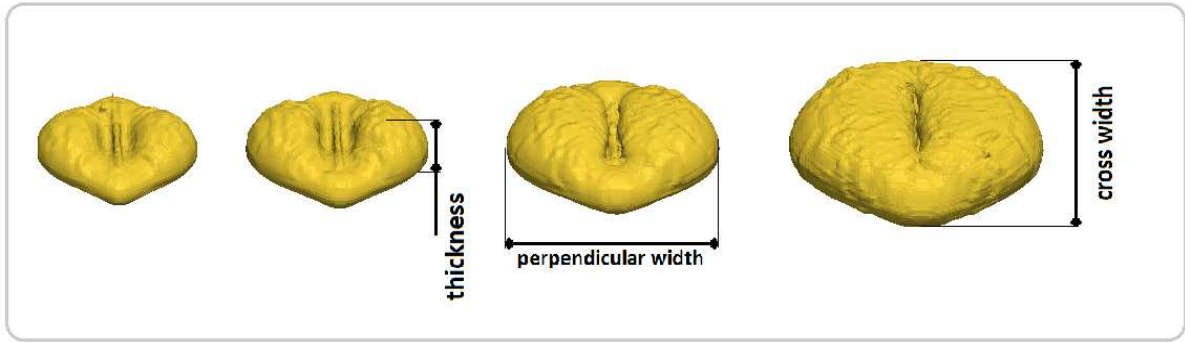


Figure 4-17: Simulated beads created by static flat stream applicator

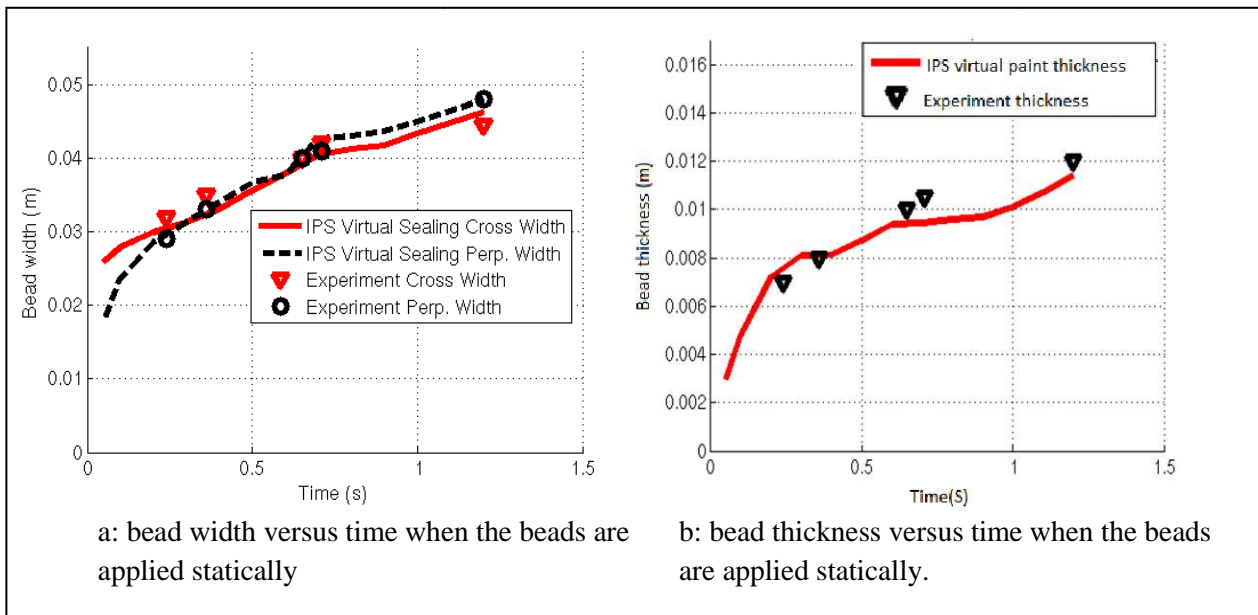


Figure 4-18: Width and thickness measured in experiment and IPS sealing when sealing material are sprayed statically.

Width of beads were measured in two different directions, one was the same direction in parallel with the direction of sealing nozzle tip, and it is called cross width, and the other direction was perpendicular to the nozzle tip, and it is called perpendicular width (Figure 4-17). Figure 4-18a shows that width of beads increases both in reality and in simulation with the time passage. As it is evident, the measured width of simulated beads both in cross direction and perpendicular direction has very slight differences with experimental result that in most cases can be considered negligible. Also the thickness of the beads was measured in experiment and IPS sealing simulation as the time passed. The result is shown in figure 4-18 b. The graph depicted in figure 4-18 b displays that the thickness of beads is also increasing when time passes. The value of measured thickness for simulated beads and the experimental width has very slight differences and like what was mentioned for width the difference can be neglected.

Another set of experiment was also performed for moving nozzles applying sealing material on a plate, with flat stream. The width of created beads were measured and compared with the result of simulation. Figure 4-19 displays the result of measurement for experimental and simulated beads.

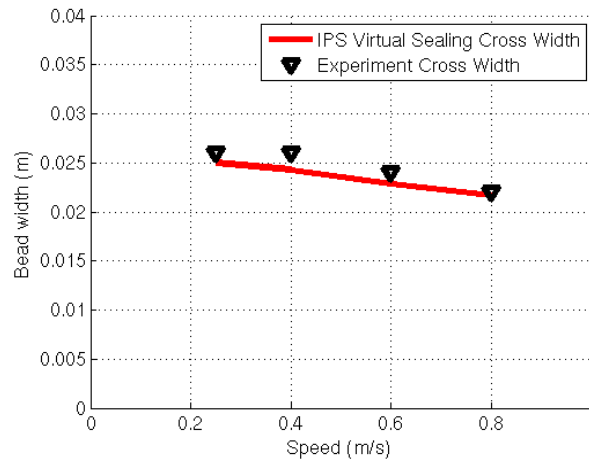


Figure 4-19: Bead width comparisons in experiment and simulation with flat stream

As it is obvious in figure 4-19, there is almost no difference between the width of beads simulated by IPS sealing and the width of beads created by experiment. In figure 4-19, when nozzle moving speed increases from 0.2 m/s to 0.8 m/s the width of bead decreases both in experiment and in simulation. The difference between widths created in experiment and simulation is negligible.

4.3.2 Measuring beads on real car body

In this section, width and thickness of simulated beads with IPS sealing were compared with the same beads created in production line. The result of measurements is shown in appendix F. To measure the width and thickness of real beads on car body two measuring equipments were used. A simple ruler was used to measure the width of sealing beads and a wet film thickness gauge was used to measure the thickness of selected beads. Figure 4-20 shows a wet film thickness gauge.



Figure 4-20: Wet film thickness gauge

When two or more sealing beads crosses at the same area, because of accumulation of material, manual measurement is not a proper method for verification purpose. A worse scenario occurs when twisted beads meet in a place that located in a corner. An example of such places is shown in figure 4-21, while in this case, bead appearance and volume are used as criteria to evaluate the sealing result. To make the manual measurement more accurate, measuring is done in three points on a sealing bead, in the beginning, in the middle and at the end of each selected bead.



Figure 4-21: Upper left corner inside the engine room of a car model V60

Figures 4-22 to 4-32 plot the value of width and thickness of sealing beads measured in production line and also from IPS sealing software in three different area of sealing bead, beginning, middle and end, where measurement is possible.

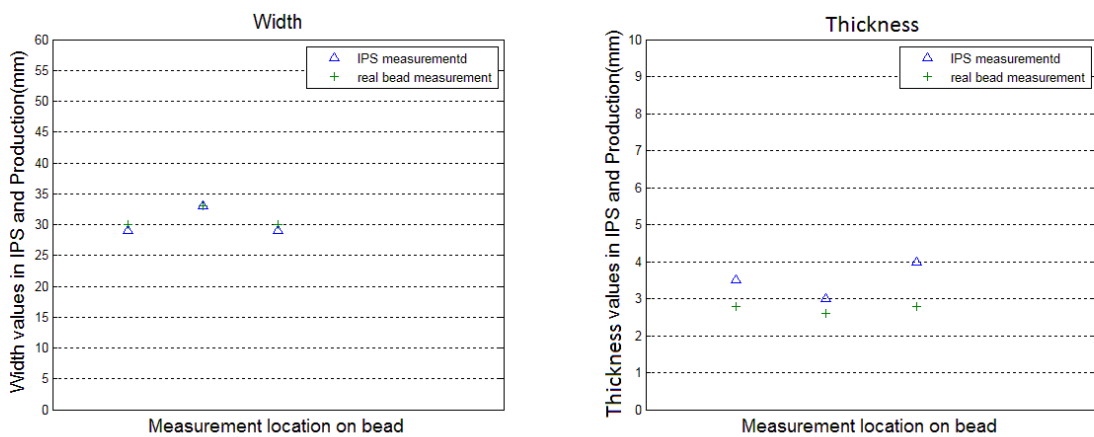


Figure 4-22: Width and thickness of bead Y352SB2511

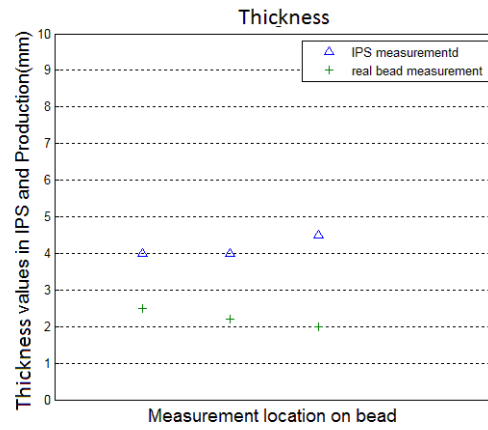
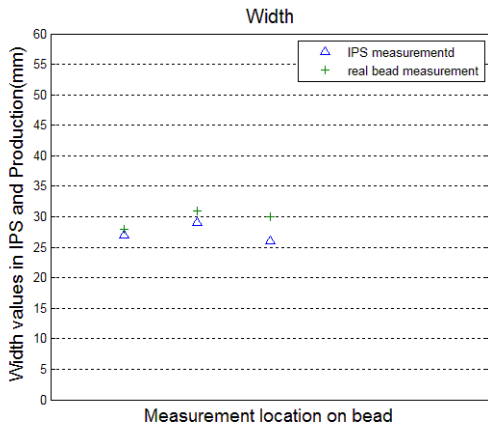


Figure 4-23: Width and thickness of bead Y352SB2609b

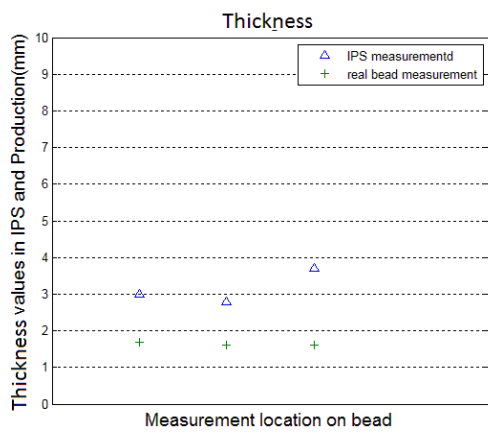
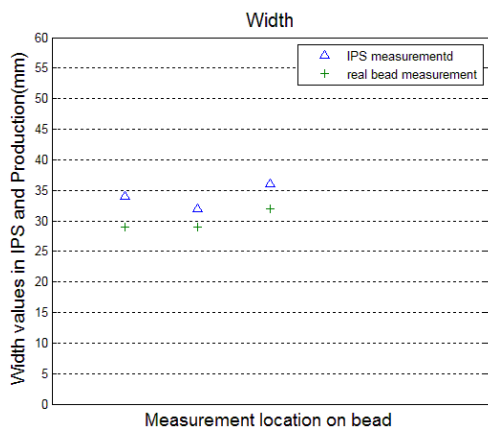


Figure 4-24: Width and thickness of bead Y352SB6313d

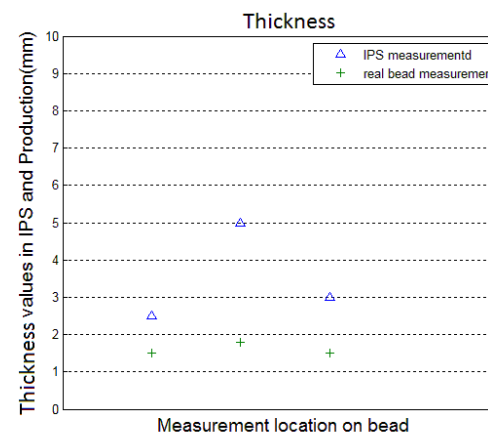
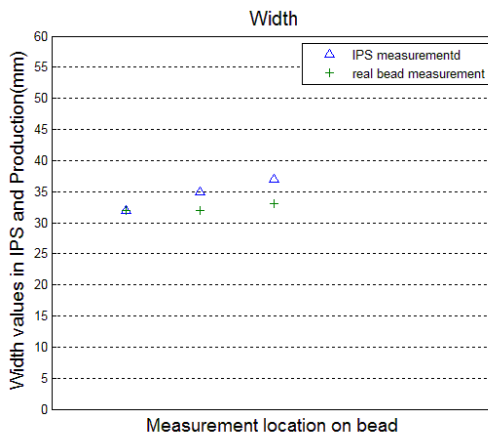


Figure 4-25: Width and thickness of bead Y352SB9307

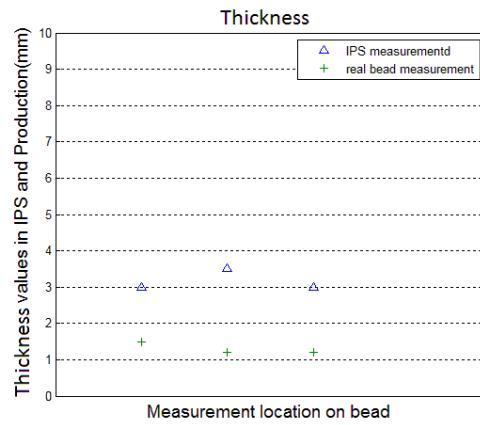
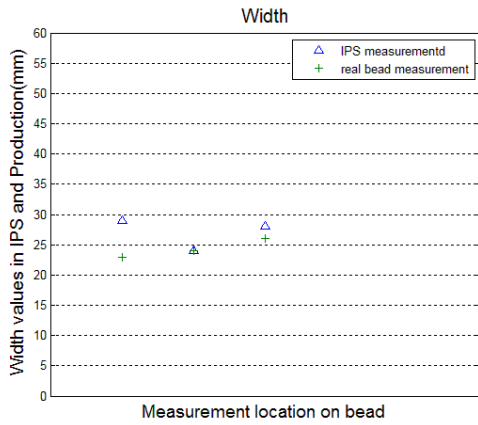


Figure 4-26: Width and thickness of bead Y352SB9602a

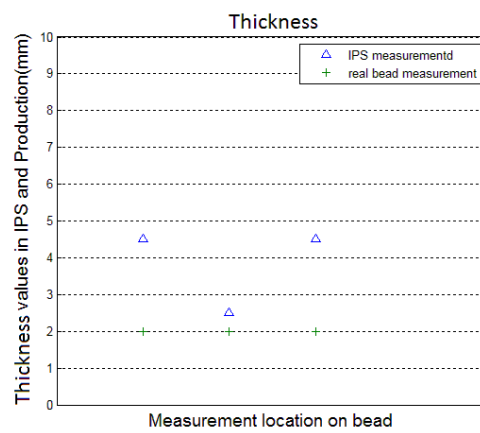
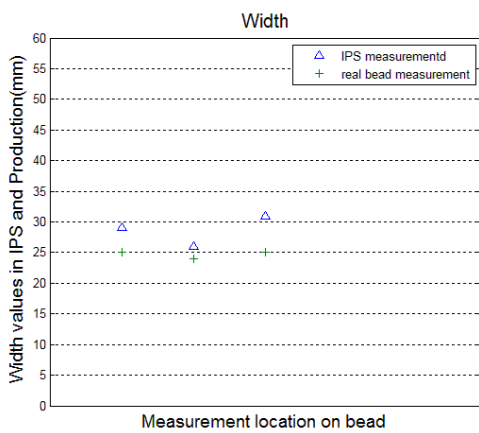


Figure 4-27: Width and thickness of bead Y352SB6306

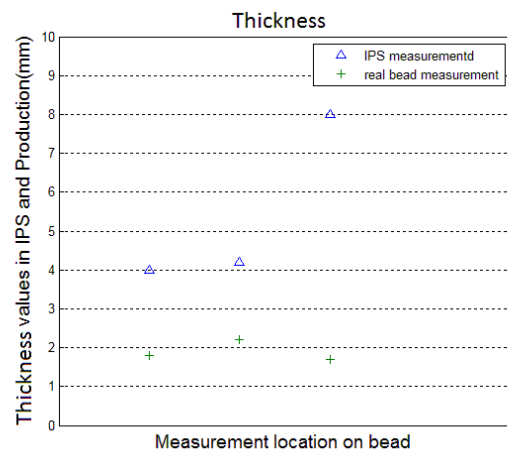
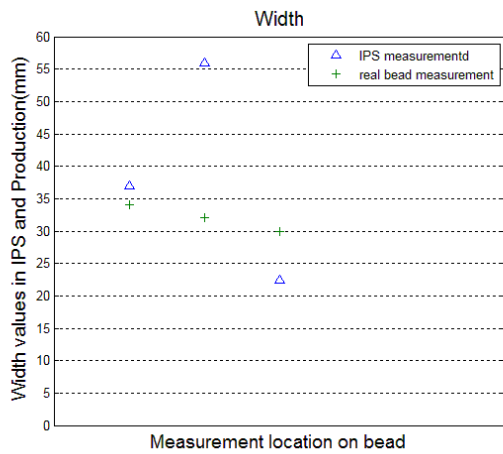


Figure 4-28: Width and thickness of bead Y352SB6121

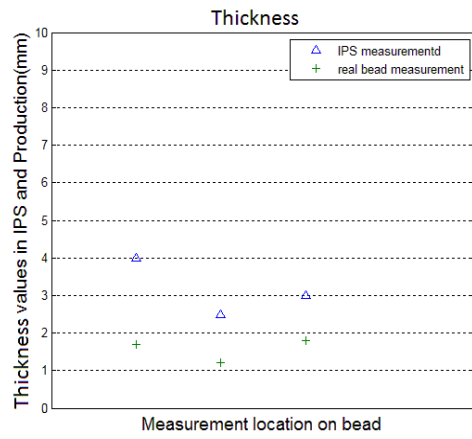
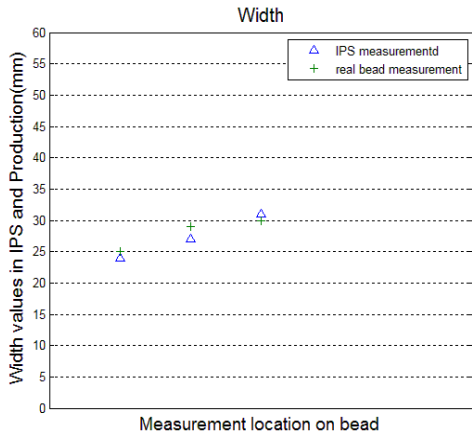


Figure 4-29: Width and thickness of bead Y352SB9102

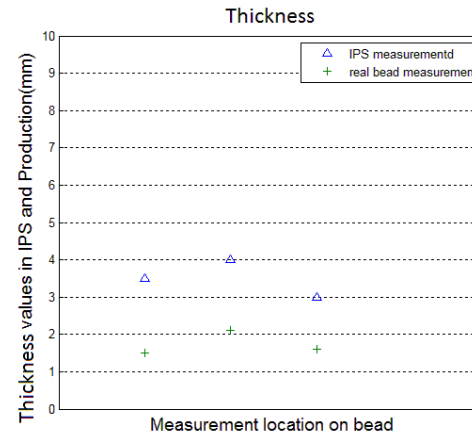
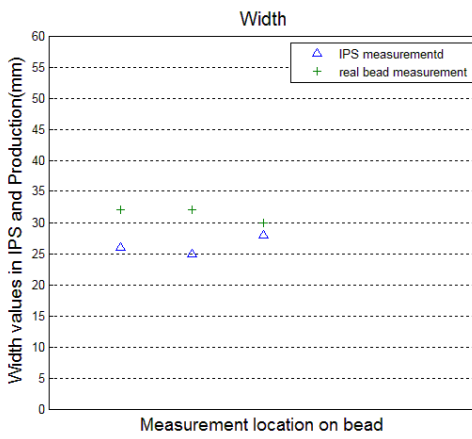


Figure 4-30: Width and thickness of bead Y352SB1320

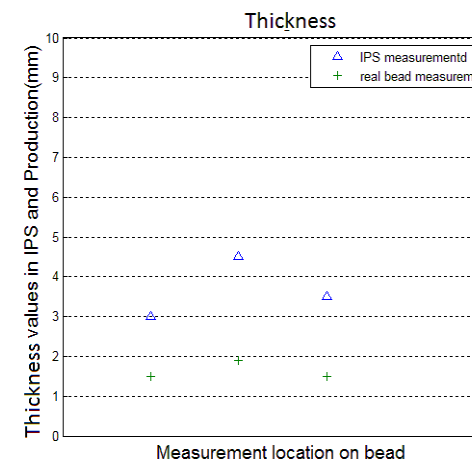
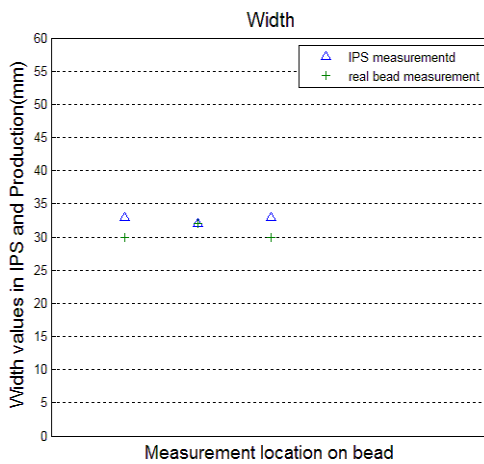


Figure 4-31: Width and thickness of bead Y352SB2708

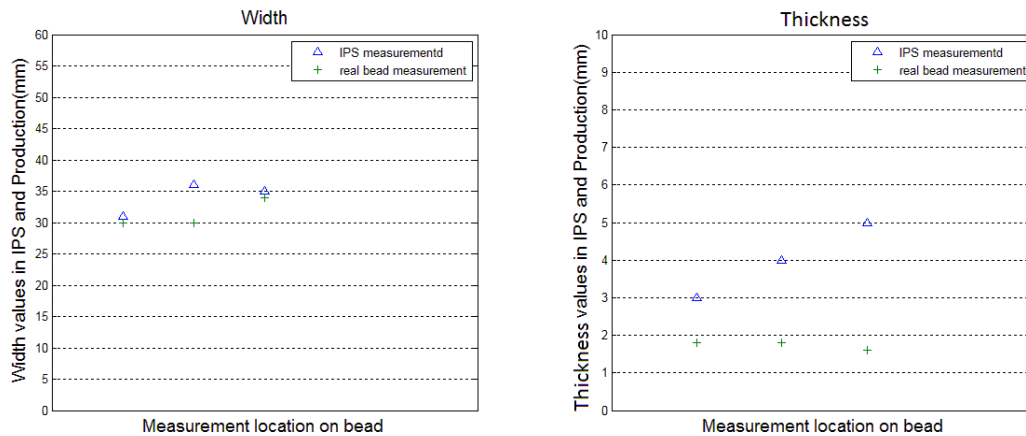


Figure 4-32: Width and thickness of bead Y352SB2404b

Investigating the twelve selected beads on V60 and comparing reality and simulation result for width and thickness of beads shows that the width of beads are almost the same or if there is any difference, in most cases this difference is slight. On the other hand when measuring thickness of beads it is evident that the thickness of each beads in three different selected points, in the beginning and middle and end of the seal beads are greater in IPS sealing compared to real sealing beads on car body.

4.3.3 Conclusion for manual measurement

In this section a short conclusion regarding the findings of comparison between thickness and width of simulated beads and real beads created in experiment and in production line is given.

As mentioned in section 4.2.1 when sealing materials are spraying statically on a plate, the result of sealing in terms of bead width and thickness are similar in simulation and real beads. Also, when robots are moving on a straight path, the result of measuring width in simulation and experiment are alike. However, for this experiment, no measurement regarding thickness of sealing beads were performed, so it is impossible to conclude about the situation regarding thickness of sealing beads when spraying sealing material in this experiment.

Comparison between selected beads on car body and simulation result of those beads in section 4.2.2 reveals that width of simulated beads are almost the same both in simulation and on real car body. The difference occurs for the thickness of simulated beads. The thickness of simulated beads is in most cases greater than the thickness of sealing beds on car body. It means that when simulating sealing beads the bead volume is higher than real bead volume. This difference can be originated from the fact that the system controlling material flow during robotic sealing adjusts this flow with the speed of robots. In other words, the flow of material is not independent from robots speed.

Finding this the relation between flow and speed is beyond the scope of this thesis and should be investigated in next projects in collaboration with VCC, FCC and Teamster.

4.4 Material consumption verification

As the information regarding the sealing verification in VCC indicates that the actual verification way, normally the most effective way in the factory at VCC, is using watertight test. Watertight test is a test during which high pressure water is ejected on the sealing beads situated on important parts of a car such as the wheel house, the engine room with the purpose of checking if there is a leakage on those parts. Since there is not a virtual watertight test simulation supported by any software, we believe that in order to seal a car component, two requirements have to be fulfilled:

1. The correct and accurate path of the sealing applicator which complies with the position of the seam or hole on a component.
2. Enough sealing material ejected to the target areas.

The first requirement is a prerequisite of a successful sealing process and it is solved by creating XML files offering the accurate positions and orientations of the seal points along the path.

The second requirement is for checking the sealing quality. Since some geometrical complex beads are very irregular and cannot be described simply by width and thickness and using appearance is sometimes not a quantified criterion and may vary from person to person, volume consumption was adopted as another criterion for sealing verification. If the simulation reflects that robot ejects the comparable amount of material at the target area in simulation as that in reality, then we can on a certain degree conform the virtual sealing result. Furthermore, given all the bead volumes figured out, we can calculate the mass for each bead and therefore the total material mass consumed for a car.

The volume consumption comparison is executed between the IPS simulation, production and the theoretical calculation. The volume consumption of sealing material in the factory was logged by experts from Teamster and the result is displayed in Figure 4-33.

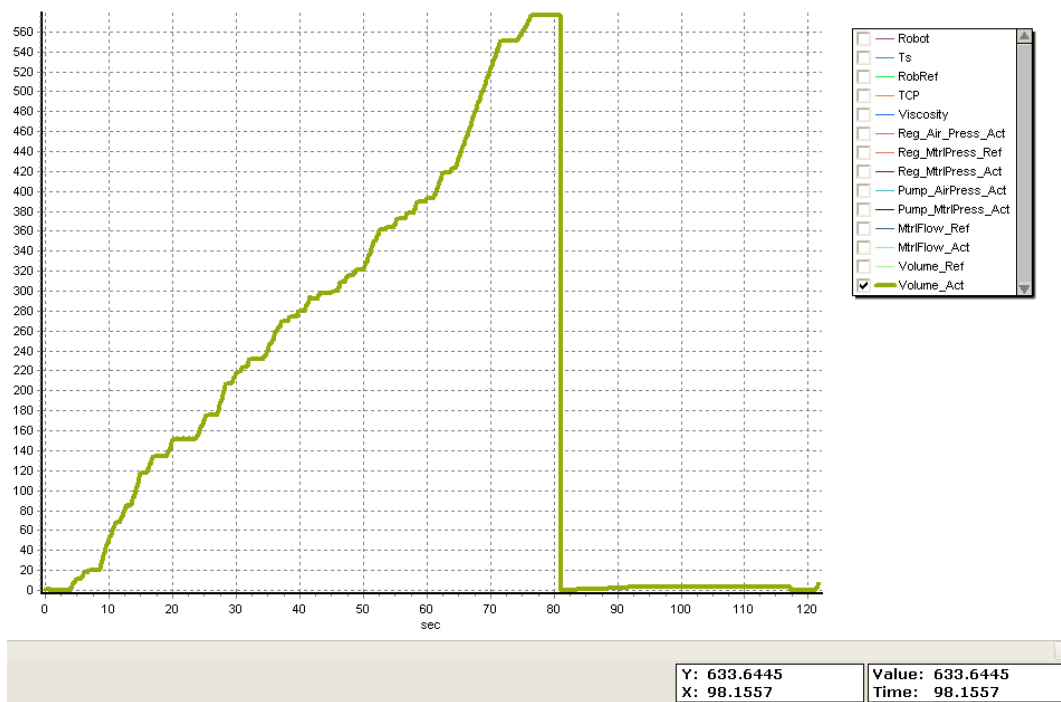


Figure 4-33: Log file for volume consumption during one cycle in the sealing station

This log file records detailed accumulative volume consumption with the passage of time during each cycle. Wherever there is a climb-up, there is a sealing bead applied in reality. The coordinates of all the turning points can be found out on the graph. Therefore, volume consumed for each bead as well as for a whole cycle of the sealing robot can be found out by simple calculations.

Besides that, the theoretical volume consumption can be calculated as a product of duration for each bead and the flow for that bead: $\text{volume (ml)} = \text{duration(s)} \times \text{flow(ml/s)}$

- The duration of each bead is extracted from Process Simulate after running the simulation.
- The flow of all kinds of beads are predefined and can be found in Appendix C

In IPS, the volume of sealing materials ejected can be measured directly after the simulation using an embedded function and the results of all the three sets of data are documented in table 4.4. The total volume consumed in reality and theory is compared in table 4.5.

Table 4-5: Volume consumption in production, IPS and in theory

Bead number	Volume consumption in production(mm3)	Volume consumption measured in IPS(mm3)	Volume consumption calculated theoretically (mm3)
Y352SB6313d	6756.91	12434.32	13335.00
Y352SB9307	16253.13	79088.63	79335.00
Y352SB9602a	6026.50	14603.47	15793.00
Y352SB6306	3287.22	41232.02	41232.00

Table 4-6: Comparison between total volumes consumed in theory and in production during one cycle for robot 6421

	Theoretical value (mm3)	In Production(mm3)
Total volume consumption for one cycle for robot 6421	913830.57	571065.49

As can be seen from the table 4.4 above that the volume consumption measured in IPS is more or less the same as the volume calculated theoretically while the volume consumed in reality is much less than that in IPS and the theoretical value. Table 4.5 shows that the total volume consumption in production is also much less than the amount of volume in theory.

4.4.1 Conclusion for volume verification

As it is mentioned in section 4.4, IPS sealing beads have much higher amount of materials than materials used for the same beads in production line. A similar situation also was revealed when measuring the thickness of simulated beads on car body component in section 4.3.2. This difference in material consumption has two different reasons. The first reason has the same origin as the difference in thickness of beads in simulation and reality. As mentioned in section 4.3.3 there is an adjustment between flows of sealing material sprayed on car body and robot speeds that is taken care by flow system controlling robots in sealing stations. The second reason is that so far the sealing path created for sealing beads did not consider delay for on and off command for initiating and ending a sealing process. Chapter 4.5 shows the effect of considering this delay time and modifying mass rate on simulation result in term of material consumption.

4.5 Influence of modifying sealing path and mass rate in simulation

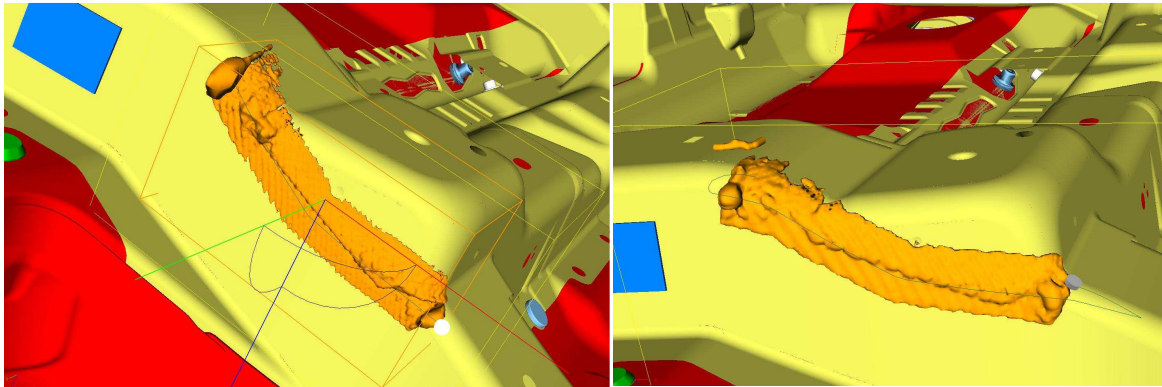
Investigating current situation regarding simulation and reality, two types of modification can be done while running simulation to have a situation close to what it is in production line. First one is creating sealing paths including via points before and after a sealing path itself. Second one is manipulating the mass rate in sealing applicator to have it as close as possible to real mass rate in production line. Both modifications are done in this thesis and the result is mentioned in this section.

4.5.1 Modifying sealing path

In real production line, when a sealing robot is programmed to reach a target point to spray sealants on its intended place, the nozzle tip passes some points before and some points after the sealing path without spraying material. These points are known as Via points and are created to give a smooth movement for robots to reach targeted areas. Another application of these Via points before the initial points of a sealing path is considering delay times before reaching the path. Delay time for spraying material on the beginning of a path is the time from when “On” signal is sent by flow controller and the time that material are sprayed from nozzle tips, when it is in the beginning of a sealing path. The same principle also applies to “Off” command at the end of a sealing bead. Therefore, considering Via points in sealing simulation can affect the simulation result. This is explained in this section.

To identify Via points effect on simulation results, bead Y352SB6313d and bead Y352SBSB9307 were selected to go under simulation. Adding Via points to the simulation paths for these two beads affect simulation results in two way.

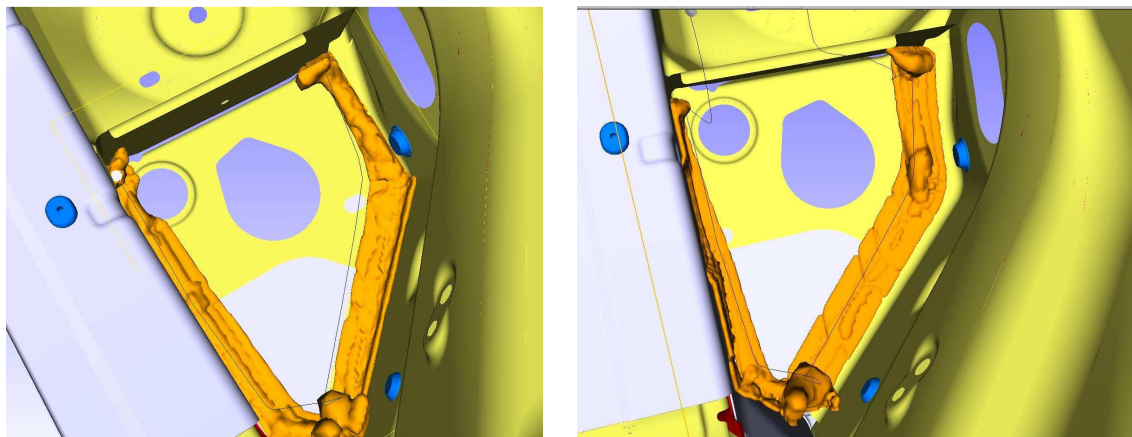
First, the appearance of simulated beads became better in the beginning and end of simulated beads. Simulating without considering these via points create a big pile of material in the initial point as well as the end point of a simulated bead, while adding via points to the sealing path ends up in a smaller material pile on the beginning and end of the simulated bead. Figure 4-34, and 4- 35 compare the two simulated sealing beads with and without considering the Via points for sealing paths.



Simulation without Via points

Simulation with Via points

Figure 4-34: Bead Y352SB6313d



Simulation without Via points

Simulation with Via points

Figure 4-35: Bead Y352SB9307

The other effect of using Via points in bead simulation is on the amount of material used for creating simulated beads. It is true that there is a slight difference in material consumption when using Via points. In other words, using Via points reduces the amount of simulated material used but this reduction still is not enough to reach the actual material consumption in reality. Table 4-4 shows the difference in material consumption when simulation is done with Via points and without Via points. As it is evident in table 4-4, the material consumption after using via points is still more than material consumption in real sealing beads.

Table 4-7:material consumption with and without via points

	Material consumption				Material consumption in production	
	Without Via points		With Via points			
Bead Number	Volume(ml)	Mass(gr)	Volume(ml)	Mass(gr)	Volume(ml)	Mass(gr)
Y352SB 6313d	12.43	13.95	10.73	12.04	9.13	10.24
Y352 SB9307	79.09	88.74	75.37	84.57	48.50	54.42

Based on what is mentioned in this section, using Via points has an effect on the appearance of sealing bead and simulated material consumption. The effect of Via points on the appearance of sealing bead is that there is a smaller pile on the initial point and the end point of sealing beads in comparison with the simulation without Via points. On the other hand, the effect of adding Via points to the sealing path is not satisfactory and the material consumption is still more than material consumption in reality.

4.5.2 Modifying mass rate

In real production line, when robots spray material on the car body material flow is not fixed and varies because of different parameters, such as the mechanical equipment of the flow system itself [21], and speed of robot movement. Since flow of material has direct effect on mass rate of sprayed material on the car body, change in flow varies mass rate. The result of simulation will be closer to reality if the real flow and mass rate in production is used to run the simulation. Figure 4-36 shows how the real flow in production varies in time compared to pre-defined reference flow. Green curve in Figure 4-36 display the real flow of material and blue curve demonstrate the reference flow.

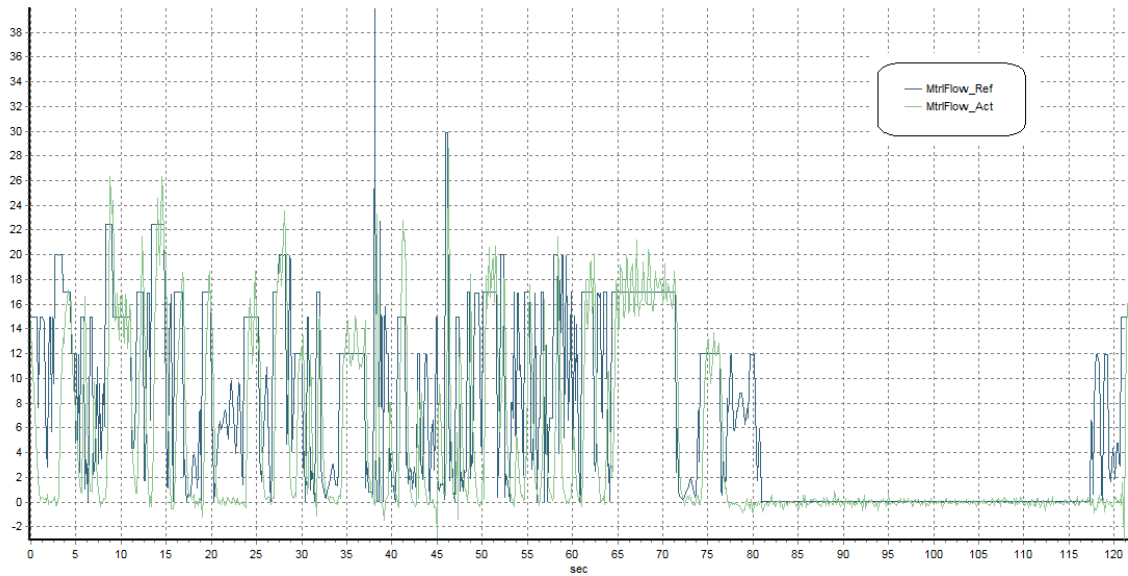


Figure 4-36: Reference flow and real flow in production for sealing robot r21

Finding the exact relationship between actual flow and reference flows and therefore mass rate of sprayed material is beyond the scope of this thesis. On the other hand, it was interesting to estimate an approximate number for flow and mass rate for one bead to see how using this approximate number can change the simulation result. For this purpose bead number Y352SB6313d was selected and the average real flow for this bead was calculated using picture 4-37. the average flow for this bead is $19.36l/sec$. Therefore the average mass rate for this bead is $21.72gr/sec$ calculated by equation number (4.1) here the density of sealing material is $1122 kg/m^3$

$$average\ mass\ rate\ in\ production = average\ flow\ in\ production \times density \quad (4.1)$$

Also, from section 4.5.1 the real path with via points are derived from bead Y352SB6313d. Therefore, to have a simulation close to reality, it is decided to use the modified path with Via points and modified mass rate for this bead. The focus of this simulation is on finding the simulated amount of material and to compare it with real material consumption. The result is shown in table 4-5.

Table 4-8: Volume and mass obtained from modified mass rate, predefined mass rate and production for bead Y352SB6313d .

	Simulation with		Production
	Modified mass rate	Pre defined mass rate	
Volume(ml)	3.851	10.734	6.769
Mass(gr)	4.3209	12.0441	7.581

As it is evident from table 4-5, the amount of volume and mass of material produced in simulation varies with change in mass rate used for simulation. Using modified mass rate with the real sealing path including Via points ends up in almost half material consumption in simulation compared with reality. It proves that using a simple average amount for flow and mass rate for one bead is not enough to obtain a satisfactory simulation, and the real relation between flow in production, and reference flow should be found and applied in simulation to get satisfactory results.

4.5.3 Conclusion for Modifying sealing path and mass rate on simulation

In section 4.5.1 two sealing beads were created by using Via points before and after sealing beads paths. The simulation result for these two sealing beads proves that the surface of simulated bead in initial and end points are better than when there is no Via points in sealing paths. In other words, less material is piled in the beginning and end of simulated beads. Decreasing the size of initial pile for sealing beads ends up in decreasing material sprayed for simulation. But it is evident that the material consumption is still higher than the value of material consumption read from flow system (table 4-4).

In section 4.5.2 the real mass rate for one sealing bead were estimated by calculating the average amount mass rate for one selected bead by investigating the log file in picture 4.37. This number was replaced in sealing applicator to perform simulation. Also, simulation was done by a bead with Via points to simulate the real situation in production line. Table 4.5 reveals that even after this modification, the simulation result regarding material consumption is not satisfactory yet. It means using simple average of flow and mass rate for a sealing bead is not enough and more investigation should be performed to find the real mass rate during production.

5 Specification of robotic gluing process requirements

Today's trend to produce automobiles lighter than what it was previously lead car manufacturers to use new materials and methods from design to production of their final products. Therefore, using new structural components in car body such as aluminum sheets instead of stainless steel sheets is gaining a large popularity amongst car manufacturers all around the world. New structural components need new production methods that are compatible with properties of those new structural materials. Also it should be considered that those new production methods should still keep the production price in a reasonable range and also do not affect the quality of the final product [2] [3] [22].

Among new production method, using adhesive for different purposes in automotive industry is gaining a huge amount of popularity. Using adhesive bonding to join components of car body is proved suitable regarding lightness, tensional stiffness and strength issues. Using adhesives to join body components results in a fault-free external surface. On the other hand, the process of applying adhesives to join car body components should be under careful control to end up in a perfect surface [23].

This section of thesis work gives a brief insight about robotic gluing process, typical materials used as adhesives, adhesive applications, and requirements to have a good quality adhesive after application, and important parameters in robotic adhesive application, all regarded to automotive industry. Finally, table 5.1 gives requirement specifications for robotic gluing process considering all mentioned area above.

5.1 Gluing Process

Traditional robotic gluing systems consist of two parts: a robot which guides the gluing applicator to the correct position and the flow system which provides gluing materials (Figure 5-1). [24]

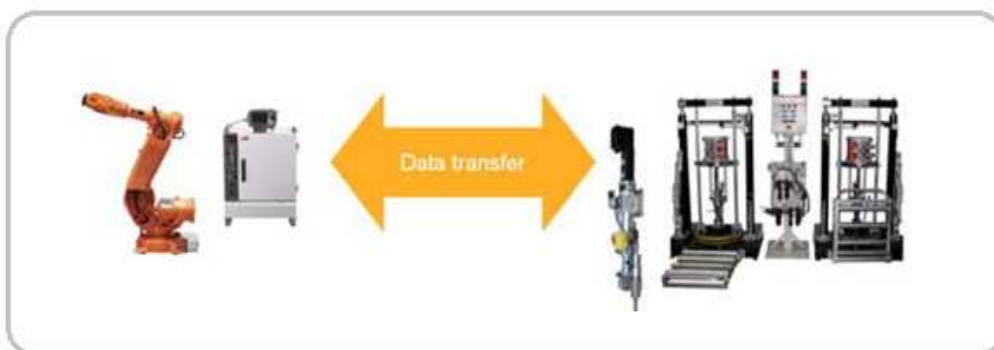


Figure 5-1: Traditional robotic gluing systems

Since these two parts are separate in nature, in order to run a successful gluing process, they should be coordinated and synchronized in production. However, this type of

gluing process is criticized for several reasons: too complex system, time consuming due to data transferring, insufficient gluing accuracy and high gluing material consumption. One great substitute is deploying a newly developed integrated robotic gluing system. In this system, the control of the flow system is embedded in the robot controller using the extra unused capacity of the processor. The time is calculated for every point on the moving path and an event triggering model is used to control the material flow (figure 5-2) so that accurate amount of material can be ejected at the right time at the right place [24].

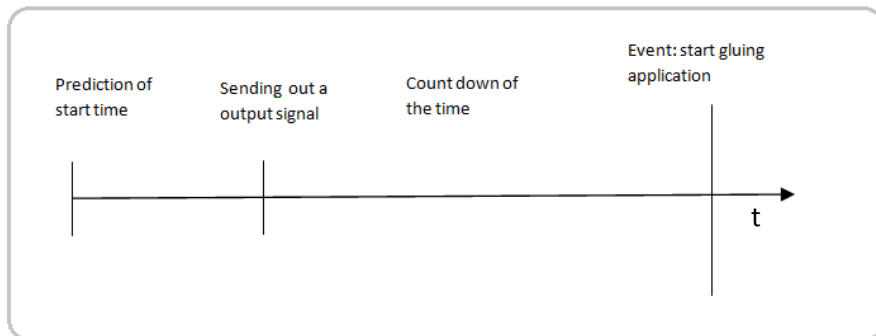


Figure 5-2: The event triggering model

As seen from Figure 5.2, if the material application is planned to happen at time t , then the applicator sends out an output signal commanding the gluing material application starts at time t and the control begins to count down. After time t , the nozzle opens and the material is ejected out. By using this integrated robotic gluing system, the goal of improving gluing quality, saving gluing material and reducing gluing cycle time is achieved [24].

5.2 Typical material used as adhesive in automotive industry

Adhesives based on acrylic esters, epoxies, polybutadienes, polyurethanes and PVC/epoxy blends are the most used types of adhesives currently used in body in white. Some suppliers recently introduced new developed adhesives known as Elastosols. These newly developed adhesives are PVC and Epoxy free materials. Elastosols show better properties during different tests including hot, humid atmosphere and salt spray test, so they become more popular amongst car manufacturer [5].

At VCC the material used for gluing is BM5096 which contains three substances: the structural gluing substance to absorb energy and avoid crash, the stiffening substance to reinforce the body structure and fatigue-preventive substance applied on the joints to prevent the car from fatigue damage. BM 5096 meets the general requirements demanded in automobile industry and is strong enough to withstand the wash-off process in final steps of production [22].

5.3 Adhesives application for body in white

There are different applications for adhesives in automotive industry, but the main applications of adhesive in body in white can be grouped into three main categories.

- Preventing vibration: to prevent fluttering low module adhesives are placed between sheet metals and panels [5].
- Contribution in structure of car body: high module adhesives are vastly used in structure of car body to contribute to the tensional stiffness and also improve the impact resistance of car body components [5].
- Sealing joints between spotwelds: before going to the procedure of spot welding, some material is applied to panels to perform the role of sealant of spotweld joints [5].

5.4 Typical property requirements to have an acceptable adhesive

Rheological properties of adhesives used to produce car body components should be suitable. It means that the gluing material used to join car body components should be selected in compatibility with the material used to produce that component [5]. After curing the component that has gone under application of adhesives, the final product should meet the physical requirements designed. To make sure that the final product meets these requirements they go under test procedures. Test procedures, for instance, can include lap shear and peel strength test under a set temperature. Typical test temperatures used vastly in automotive industry are -30° , $+20^{\circ}$ and $+90^{\circ}$. Besides that final product should stand a series of aging tests depending on the design requirements and customer requirements. These aging tests include salt spray tests, cycling tests and humid cataplasme test. These tests are performed under intensive situations and make sure that applied adhesives on car body components meet the required demands [5].

5.5 Important parameters in applying adhesives

There are two methods to apply adhesives on car body components. First method is applying adhesive material manually on work pieces. The second method is applying adhesives at body in white by means of robots. The aim of this thesis work is to deal with the important parameters for automated robotic adhesive application. These important parameters would be explained through following paragraphs. The result of this section would provide amount of requirements that is going to be used to develop a virtual test environment for adhesive application on car body components.

One of the important issues when applying adhesives on car body is finding the rheological properties of adhesives under working condition. Also it should be considered that when applying adhesives on car body the adhesive materials are under high pressure, so adhesive liquid becomes hydraulic. This phenomena can affects

material properties, for instance adhesive reaches its maximum density per unit volume [23]. This ends up in the fact that when measuring the adhesive density to prepare a simulation model, this should be a density under application pressure. Similar condition is also valid for plastic viscosity of adhesion material and yield stress.

Since adhesives are designed to join car body components, to reach the purposes of desired final surface which are tensional stiffness and strength two parameters gain high level of importance. The first parameter is path accuracy that should be followed for each component and the second parameter is the exact delivery of material to the target points that adhesives are intended to put on [21] [23].

To reach the accurate path and exact amount of material intended in design process the absolute speed of applicator motion and the relation between the applicator motion speed and injection velocity play important roles. The first mentioned issue is the absolute speed of robot's applicator. As it is obvious the application speed of gluing is higher than the application speed during welding procedure. Therefore the path accuracy of the robot can face significant problems; specially using six axes robots to put adhesive materials on the edges of a working piece can be impacted seriously when the speed is getting higher. Solving the accuracy problem demands more attention when creating robot paths for gluing procedure to have more accurate path. The second mentioned parameter is the relational speed between the robot moving speed and the injection speed of the robot's applicator to spray material on work piece. Here it is important to find a proper relation between these two speeds, but in general the robot motion speed should be lower than the speed of material injection on work piece, otherwise the amount of adhesion material on work piece and the created contact surface between glue bead and work piece would not be proper. Considering the fact that the surface is still oiled and not washed, there will be a risk for glue beads to slide away from its intended places. Figure 5-3 shows a situation under which there is not enough material on the work piece. Also the contact surface is smaller than what it is decide to be in design step. Because the robot motion is faster than material injection speed this phenomenon may happen leading to adhesive material slide away from the intended place. On the other hand when the robot motion speed is adjusted based on injection speed, there would be enough amount of material on intended surface and the risk of material sliding away will be eliminated. Figure 5-4 shows a schematic section of a glue bead seated properly on its intended place [21].

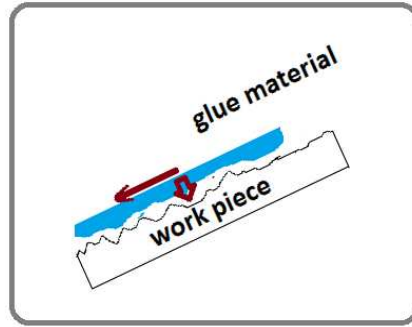


Figure 5-3: Not enough adhesive on its designed place

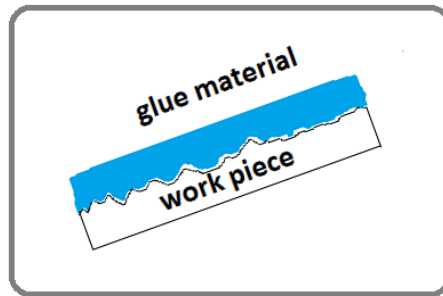


Figure 5-4: Enough adhesive on its designed place

During the robotic gluing process, there are also other parameters that can affect the gluing process, such as interaction of Non-Newtonian fluids and production equipments such as pumps and valves. Investigation of these parameters is beyond the purpose of this thesis work and needs to apply advanced CFD method. This investigation is a current project undergoing at IFAM [21].

5.6 Requirement specification

After considerable amount of research and study of industrial gluing, along with effective communication with professionals in this field, virtual gluing requirements are put forward and summarized in the tables 5-1 to 5-5.

Table 5-1: Requirement specifications in terms of geometry

Requirements	Solution/recommendation
<ul style="list-style-type: none"> Width measurement 	Tools in IPS to measure the width of a glue bead
<ul style="list-style-type: none"> Height measurement 	Tools in IPS to measure the height of glue beads
<ul style="list-style-type: none"> Length measurement 	Tools in IPS to measure the exact length of glue bead
<ul style="list-style-type: none"> Accepted tolerance 	How much is accepted tolerance for each bead misplacement from design requirements
<ul style="list-style-type: none"> Profile of glue beads on cross sections 	Tools in IPS to show cross section profile

Table 5-2: Requirement specifications in terms of material consumption

Requirements	Solution/recommendation
The exact amount of adhesive material according to the design parameters	
<ul style="list-style-type: none"> Volume measurement 	Tools in IPS to measure the volume of glue material used in simulation
<ul style="list-style-type: none"> Mass measurement 	Tools in IPS to measure the mass of glue material used in simulation

Table 5-3: Requirement specifications in terms of material properties

Requirements	Solution/recommendation
What kind of material are used	Material properties should be obtained from test or provided by material supplier and be considered in gluing simulation. Depending on the input of gluing simulation software, some of these properties are not direct input for IPS gluing, while they affect other properties that are direct input for simulation. For example gluing temperature and gluing humidity can affect the density and viscosity and gel time can put effect on speed of robotic processes.
Density under application pressure	
Plastic viscosity under application process	
Yield stress under application process	
Gel time	
Electrical conductivity	
Adhesion strength	
Gluing temperature	
Gluing humidity	

Table 5-4: Requirement specifications in terms of process

Requirements	Solution/recommendation
<i>Movement</i>	
<ul style="list-style-type: none"> • If gluing applicator moves and the car body components are fixed in the station 	It is similar to IPS sealing and paint
<ul style="list-style-type: none"> ○ the speed of applicator 	Considering the speed of robot motion and material flow
<ul style="list-style-type: none"> ○ the speed of applying adhesive material (injection velocity) 	
<ul style="list-style-type: none"> • If the car body components moves and the applicator is fixed in the station 	Considering fixed path and moving work piece
<ul style="list-style-type: none"> ○ the speed of work piece 	Considering the speed of work piece's motion and material flow
<ul style="list-style-type: none"> ○ the speed of applying adhesive material (injection velocity) 	
<i>Position of the work piece</i>	
<ul style="list-style-type: none"> • Position of work piece related to the ground 	slope of work piece related to ground
<ul style="list-style-type: none"> • The position of work piece related to applicator's tip 	slope of applicator's tip and work piece
<i>Working condition</i>	
<ul style="list-style-type: none"> • Masking, grinding, cleaning and priming 	pre-work on metal plates to consider the contact surface between adhesives and work piece
<ul style="list-style-type: none"> • Contact between the gluing materials and substrate 	depend on pre-work
<ul style="list-style-type: none"> • Air entrapment during injection of gluing material 	the real process may include air entrapment , so it can be a concern when developing simulation
<i>Material flow</i>	
<ul style="list-style-type: none"> • The flow of adhesive material in each bead type 	Flow of material when spraying adhesive on work piece should be considered as an input for simulation software
<ul style="list-style-type: none"> • The mass rate of adhesive material in each bead type 	Related to material flow
<i>Glue Bead type</i>	
<ul style="list-style-type: none"> • Is it a hollow cone or a flat stream bead 	the nozzle type should be defined

Table 5-5: Requirement specifications in terms of quality

Quality	
Sliding away of glue beads	It should be investigated regarding Geometry and Material consumption mentioned above.

6 Discussion & Conclusions

Sealant and adhesive materials have been gone under remarkable changes for decades. Beside the application of sealants on car body, different materials are used. The most applicable types of adhesives/sealant used in body in white are based on acrylic esters, epoxies, polybutadienes, polyurethanes and PVC/epoxy blends. On the other hand there is a recent favorable trend amongst supplier to introduce PVC and Epoxy free materials that are mostly known as Elastosols. These materials demonstrate better properties during different tests including hot, humid atmosphere and salt spray test, so they become more popular amongst car manufacturer [5]

The material for sealing car body components in VCC are also different based on their applications. The material that is used as sealing material to create the simulation applicator to verify virtual sealing process in VCC is EP2009FL, which is a yellow colored paste like chemical. It contains mainly three substances: PVC, specifying the material mechanical property, Plasticizer, softening the material mixture to provide more flexibility, and Filler, used purposely to reduce cost. Amongst all material properties, density, plastic viscosity and yield stress are used as input of simulation in the format of applicator. Therefore applying necessary calculation based on information collected from VCC material supplier and tests done at VCC was performed during this thesis. There are different ways of doing such rheological calculations and in this thesis we have just used the method specified in VCC standard VCS 1024, 65659. It should be considered that especially for viscosity, it is difficult to capture an absolutely accurate value because it is quite 'sensitive', meaning that it is dependent on many factors such as the visco-metric testing method, the equipment used for the testing, the geometry of the cylinder, the temperature, time, etc. In order to search the viscosity of the sealing material, the testing environment has to be as close to the real production environment as possible. One thing should be noticed is that at VCC the production temperature is 35degree while the viscosity data obtained is for 23 degree, which could lead to some discrepancies to the parameter values.

Like sealant material, there is also a wide range of adhesives material used in automotive industry depending on their application on car structure. General requirement of the gluing material is that it should have high viscosity and sticky enough on the metal to withstand the wash-off process [22]. The gluing material currently used at VCC fulfills these requirements.

To reach the accurate path and exact amount of material intended in design process the absolute speed of applicator motion and the relation between the applicator motion speed and injection velocity play important roles to have a sealing or gluing path

covered properly by sealant or adhesive materials, the correct TCP speed should be selected by test [21]. Also the injection velocity and robot TCP speed should be adjusted in a way that the material injection velocity is higher than robot movement speed [21]. But the ratio should be found by running tests before going to production. A good combination between these two speeds depends on the process that is performed and each company should run its own test to find that. To find the influential parameters on robotic sealing process at VCC, DOE tests that were performed previously were investigated by applying simple regression analysis to understand how different parameters affect the robotic sealing process. It is concluded that flow is an influential parameter on bead width and volume consumption. On the other hand bead thickness is affected by speed change, and has some relation with flow and TCP distance. But width and volume consumption is not seriously affected by speed and TCP distance. There are some obvious shortages in DOE tests performed at VCC. The DOE test done in VCC did not consider other parameters such as injection velocity, temperature, the drag angle, material viscosity and yield stress, which possibly have effect on the sealing result. Also another conspicuous flaw is that the DOE test is not randomized, which makes the test result less persuasive in the sense that some 'noise' cannot be ruled out, meaning that if the DOE is carried out in a certain sequence without randomization, there is possibility that the result for the current run is caused by factors in the previous run instead of the factor in the current run. Furthermore, based on the DOE data, there are three values for flow, three values for speed, and three values for TCP, so theoretically there should be $27(3 \times 3 \times 3)$ runs of experiments. To achieve a more accurate understanding of the relation between inputs and output of sealing process, complete runs of DOE test with all possible inputs should be done.

The main purpose of this thesis was to verify the newly developed software for virtual sealing simulation, IPS sealing. To perform the verification, first a proper applicator including material rheology properties and robotic process characteristics were created and simulation were performed by means of the created applicator, sealing path extracted from PS and V60 Catia model obtained from R&D department of VCC.

The sealing verification process conducted with IPS provides the result that the width and appearance of the sealing beads in simulation are quite close to the reality, with acceptable difference. This is true not only for simple straight beads but also for the sealing corners, turnings and the geometrical complex places on the car body where there is accumulation of materials due to the meeting of different beads or the slowdown of robot speed at those places. Also running a fine simulation gives better result in terms of bead appearance. But the thickness and the volume consumption are obviously bigger in IPS as opposed to reality. Investigation of this issue reveals that in production at VCC, the material flow has been changed thus differing from the value predefined in the design stage. As the $\text{Volume} = \text{flow} \times \text{duration}$, the amount of change in flow is proportional to the change of volume. So when the flow is changed, the volume is also changed as a consequence, which could fit the situation fairly well. Besides the

simulation result, one other thing should be given adequate attention is that in IPS, the principle of creating the simulation in IPS differs from the philosophy used in VCC for the sealing model design. Specifically, in IPS the width is used as an input as it should be specified in the applicator, but the sealing model designed in VCC specifies material flow, robot speed instead. As claimed from VCC, a bead with a certain width can be achieved by rotating the flat bead from perpendicular to the sealing path to a certain angle from the sealing path. So if FCC uses the same principle as used in VCC for the sealing modeling, a more realistic result can be expected.

In summary, the IPS current version works well for the bead width and appearance, but for thickness and volume, more work should be done to make it more realistic. Furthermore, in order to develop IPS sealing for better reflecting the reality, it is better to adjust the design principle in FCC to comply with the principle used in VCC.

7 Recommendations and future work

In this section the recommendation for future works to make more effective sealing bead simulation is given.

Process Simulate is applicable software that facilitates the process of off-line programming for robots for different usage. This software has different types of output for different robot applications, for example it gives a direct XML document for painting process. This XML document can be immediately used as the input for IPS paint. Unlike painting application, there is no direct XML output from process simulate when a sealing operation is applied. Therefore, it is needed to use a middle tool, such as Matlab, to create proper document as IPS sealing input. So, it is recommended that PS developer remove this weakness and facilitate the process of getting direct XML output for continues operation such as sealing ad gluing. This will benefit Process Simulate and IPS users in a way that the process of simulation would be much faster because there is no need to use a middle data extraction and translation operation.

In this thesis, Matlab is used as a middle facilitator to extract information from PS and generates a readable document for IPS sealing. It cause user dependency on Matlab software, and the person who is going to use Process Simulation and IPS sealing simultaneously must also use the third software that is Matlab. So it is recommended to use one of the programming languages such as C, C++, or java to create an independent bridge between processes simulate and IPS sealing. Therefore, there is no need to install and use Matlab to transform information from Process Simulate to IPS.

Currently, when creating a sealing path by Matlab scripts, if operator intends to simulate the Via points before and after sealing path, some manual work should be done to put the “On” and “Off” commands in XML documents. Investigation on robot program file, log file that records different times when running Process Simulate and the text file including joint values and times of joint movements did not help to find the time for “On” and “Off” commands automatically. Therefore, it is suggested to find a way to obtain those times automatically from Process Simulate. It can be done by investigating other outputs of PS, if any, or by having a direct XML output for continuous operations from Process Simulate.

Currently, IPS sealing’s input is in format of XML documents and PS does not create any XML document for sealing process, therefore there is need to transfer information from PS text output to XML document. It can decrease the accuracy of simulation during data translation. So In case IPS sealing can use the current output of PS such as robot program or joint values text file directly without any mediator, the simulation

result can be of more accuracy while it is faster because there is no need to a middle step to translate data.

When running IPS sealing, some parameters should be set manually, and for all simulation those parameters are the same, such as volume fraction or color of sealing beads. Therefore it would be a good idea if those parameters are fixed automatically. This removes the necessity of setting those parameters every time simulation is being configured.

To measure the width and height of sealing beads in different sections, currently small grids should be counted. It is not a user friendly way to find the information about sealing bead sections. So it is a good idea if this width and thickness are counted automatically. Figure 7.1 shows the current situation and the grids that should be counted to gain width and thickness.

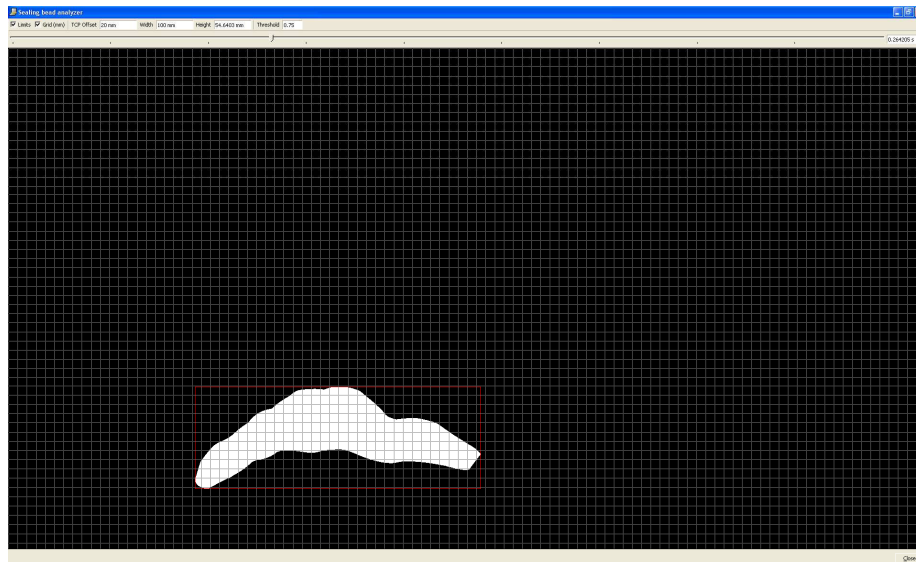


Figure 7-1: Grids that should be counted to gain width and thickness.

In simulation result, the bead sections can be seen based on the time they are created, while in reality, on car body component, when operator is going to measure the width and thickness of sealing beads, they do not know in which time those bead sections were created, while it is easy to understand the distance of each section from the initial point of sealing bead. Therefore, if IPS sealing can provide such tool to give the distance of each section of a sealing bead from the initial point of bead, the verification would be more accurate.

To verify the simulation results three methods were used. The first method was measuring selected beads by means of simple equipment such as ruler and gauge as it mentioned in implementation section, this is not a suitable method for all beads especially for twisted beads on the corners and gaps of car body. The other method used

is taking photo of selected beads and making comparison between the appearance of beads in production line and beads created by IPS sealing. While appearance may not be a good indicator since inside the inner surface of beads are not visible. If one can apply another tool such as a flexible portable measurement arm, more accurate data will be gained to compare with result from IPS sealing. By such machines the previously unreachable sealing beads in corners should be reached easier to find the dimensions of beads.

Bibliography

- [1] "Wikipedia," [Online]. Available: http://en.wikipedia.org/wiki/Body_in_white. [Accessed 12 06 2012].
- [2] R. Harries, "The Role of Sealants and Adhesives in the Automotive Industries," *Journal of Elastomers and Plastics*, p. 7, 1970.
- [3] D. Pullen, "Developments in the use of adhesives in industrial applications," *Assembly Automation*, vol. 25, no. 2, pp, p. 2, 2005.
- [4] P. Cutean, "robotic sealing auotmation," Auburn Hills, MI, 2010.
- [5] M. Lavery, "sealants in the automative industry," *international journal of adhesion and adhesives*, vol. 22, p. 3, 02 07 2002.
- [6] C. L. Grahl, "DRIVING ADVANCES in Adhesives & Sealants," *Adhesives & Sealants Industry*, vol. 14, p. 4, Oct 2007.
- [7] A. Larsson and H. Nilsson, "Visualize an event-based simulation model made in Process Simulate," CHALMERS UNIVERSITY OF TECHNOLOGY, Göteborg, 2011.
- [8] "Process Simulate, Manufacturing process verification in powerful 3D environment," 2011 Siemens Product Lifecycle Management Software Inc..
- [9] "Industrial Path Solutions," [Online]. Available: <http://www.industrialpathsolutions.com>. [Accessed 02 2012].
- [10] M. M. Moro, V. Braganholo, C. F. Dorneles, D. Duarte, R. Galante and R. S. Mello, "XML: Some Papers in a Haystack," *SIGMOD record*, vol. 38, p. 6, June 2009.
- [11] M. Norrlöf, "Modeling of industrial robots," Linköping, 1999.
- [12] A. Verma and V. A. Deshpande, "End-effector Position Analysis of SCORBOT-ER Vplus Robot," *International Journal of Advanced Science and Technology*, vol. 29, 2011.
- [13] D. Ristić-Durrant, *Robotics I, lecture notes*, 2009.
- [14] J. Wallén, "On Kinematic Modelling and Iterative Learning Control of Industrial Robots," Linköping University, Linköping, 2008.

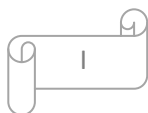
- [15] E. Red, "Lecture Notes in Robot kinematics".
- [16] "six axis robots,6 axes," Robot worx, [Online]. Available: <http://www.robots.com/faq/28/what-are-six-axis-robots>. [Accessed 02 2012].
- [17] "Rheology," Saint Joseph's university, Philadelphia, Pennsylvania 19131, USA, [Online]. Available: <http://www.sju.edu/~phabdas/physics/rheo.html>. [Accessed 03 2012].
- [18] R. Chhabra and J. Richardson, Non-Newtonian Flow and Applied Rheology - Engineering Applications, 2nd ed., Elsevier Ltd., 2008.
- [19] *Certificate of Analysis*, Göteborg, Västra Götland, 2012.
- [20] G. Strannhage, *Volvo Standard*, Göteborg: VCC, 2006-2007.
- [21] M. Peschka, Interviewee, [Interview]. 7 Mars 2012.
- [22] S. Odham, Interviewee, *Gluing process at VCC*. [Interview]. 09 05 2012.
- [23] J. Mortimer, "Adhesive bonding of car body parts by industrial robot," *Industrial Robot: An International Journal*, vol. 31, p. 6, 2004.
- [24] T. Wagner, "Integrated robotic gluing system," in *41st International Symposium on Robotics and 6th German Conference on Robotics*, Munich, 2010.
- [25] *Product Specification, IRB 2400*, Västerås: ABB Robotics AB.

Appendix A

Examples of XML document

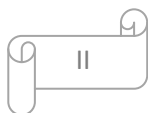
A.1 XML document for sealing path

```
<?xml version="1.0" encoding="UTF-8"?>
-<Motion type="absolute">
  <Offset z="0.0" y="0.0" x="0.0"/>
  -<Frame>
    <Time t="0"/>
    <Translation z="1568.1917749114214" y="723.20980787693838" x="2158.5823139191625"/>
    <RPY yaw="-164.85384357489295" roll="-94.764078631674778"
    pitch="37.208239987331432"/> <Trigger type="B60"/>
  </Frame>
  -<Frame>
    <Time t="0.2"/>
    <Translation z="1568.1936624359957" y="722.94797002722612" x="2158.6376495177451"/>
    <RPY yaw="-164.88421355556292" roll="-94.757724594434094"
    pitch="37.146239551664102"/>
  </Frame>
  -<Frame>
    <Time t="0.4"/>
    <Translation z="1566.6840941587661" y="693.6946561538125" x="2164.4530125741085"/>
    <RPY yaw="-168.51600522023989" roll="-93.706983475578213"
    pitch="29.815751411118409"/>
  </Frame>
  -<Frame>
    <Time t="0.407"/>
    <Translation z="1566.5469876289706" y="691.70382021411581"
    x="2164.8001393361337"/> <RPY yaw="-168.77518785931858" roll="-
    93.627684599883551" pitch="29.320606474895598"/>
  </Frame>
  -<Frame>
    <Time t="0.6"/>
    <Translation z="1562.814866346014" y="650.0484950340533" x="2171.7630133716088"/>
    <RPY yaw="-174.4542601196481" roll="-91.537451066550162"
    pitch="18.985280085907512"/>
    <Trigger type="Off"/>
  </Frame>
</Motion>
```

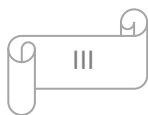
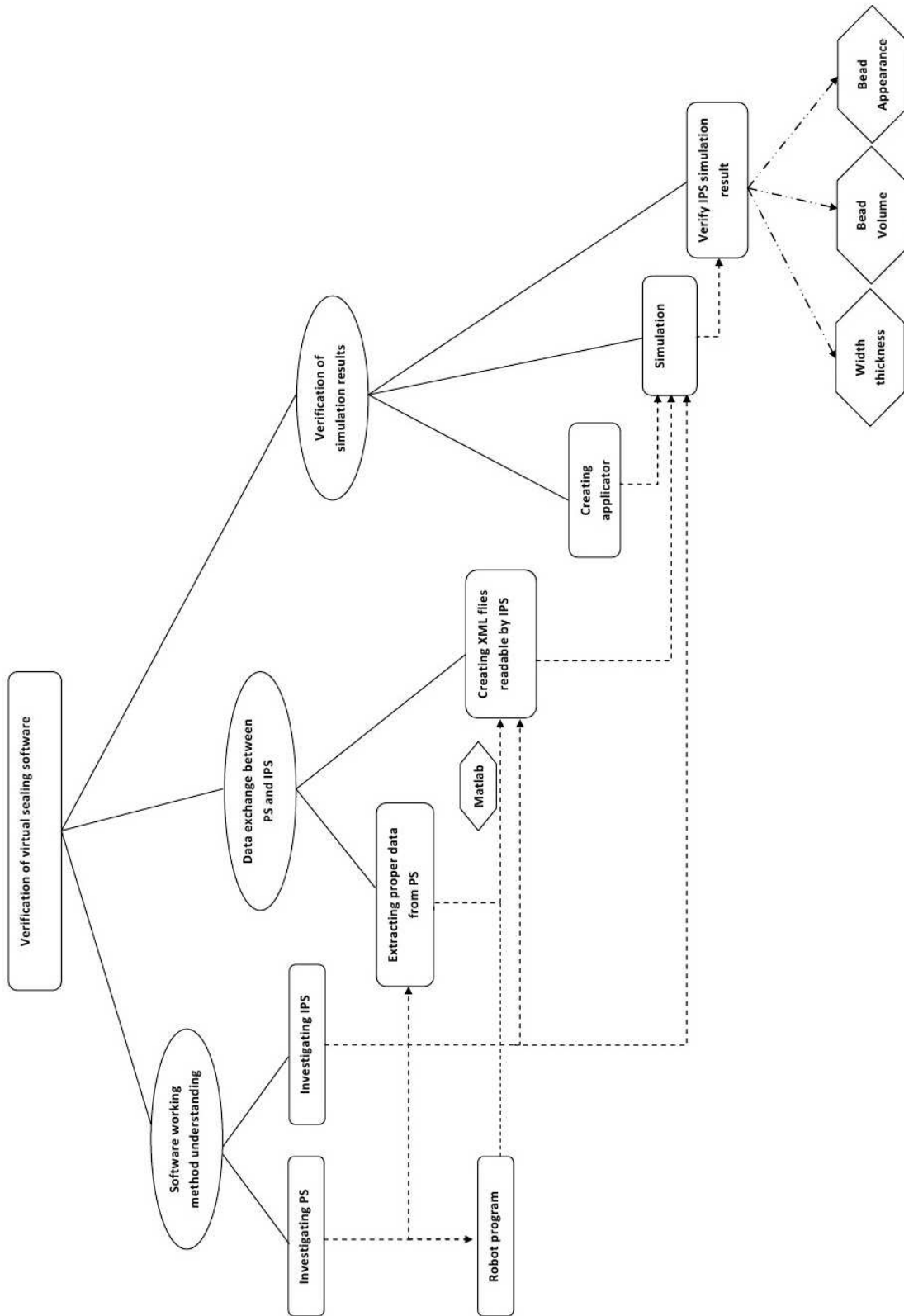


A.2 A portion of XML document for sealing applicator

```
-<Applicator model="My Favorite Model" class="sealing">
  -<Rheology id="ID_Rheology_1">
    <Density>1122.0</Density>
    <IsBingham>True</IsBingham>
    <Plastic_viscosity>2.16</Plastic_viscosity>
    <Yield_stress>260</Yield_stress>
  </Rheology>
  -<Brush id="B52">
    -<Bead type="flat">
      <Width>0.03</Width>
    </Bead>
    <Mass_rate>11.22e-3</Mass_rate>
    -<Injection_velocity>
      <X>0.0</X>
      <Y>0.0</Y>
      <Z>3.33</Z>
    </Injection_velocity>
    <Rheology id_ref="ID_Rheology_1"/>
  </Brush>
  -<Brush id="B55">
    -<Bead type="flat">
      <Width>0.01</Width>
    </Bead>
    <Mass_rate>13.464e-3</Mass_rate>
    -<Injection_velocity>
      <X>0.0</X>
      <Y>0.0</Y>
      <Z>4.0</Z>
    </Injection_velocity>
    <Rheology id_ref="ID_Rheology_1"/>
  </Brush>
  -<Brush id="Off">
    -<Bead type="flat">
      <Width>0.00</Width>
    </Bead>
    <Mass_rate>0.0e-3</Mass_rate>
    -<Injection_velocity>
      <X>0.0</X>
      <Y>0.0</Y>
      <Z>0.0</Z>
    </Injection_velocity>
    <Rheology id_ref="ID_Rheology_1"/>
  </Brush>
</Applicator>
```



Appendix B

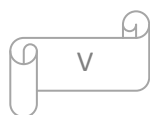


Appendix C

BEAD DATA USED TO CREATE ROBOT PROGRAM FOR ROBOTIC SEALING OF CARBOSDY COMPONENT

Bead	Speed	Flow(ml/s)	preset_ao	preset_off	preset_on
51	200	10	55	28	28
52	400	10	55	36	48
53	600	10	80	55	73
54	800	10	95	71	79
55	200	12	55	28	28
56	400	12	55	36	48
57	600	12	80	55	73
58	800	12	95	71	79
59	200	15	55	28	28
60	400	15	55	36	48
61	600	15	80	55	73
62	800	15	95	71	79
63	200	17	55	28	28
64	400	17	55	36	48
65	600	17	80	55	73
66	800	17	95	71	79
67	200	20	55	28	28
68	400	20	55	36	48
69	600	20	80	55	73
70	800	20	95	71	79
71	200	22.5	55	28	28
72	400	22.5	55	36	48
73	600	22.5	80	55	73

Bead	Speed	Flow(ml/s)	preset_ao	preset_off	preset_on
74	800	22.5	95	71	79
75	200	30	55	28	28
76	400	30	55	36	48
77	600	30	80	55	73
78	800	30	95	71	79



Appendix D

Visometric test step1

shear stress	shear rate	viscosity	time
Pa	1/s	Pa.s	s
428.4	0.9937	431.2	5.012
387.6	1.001	387.2	10.008
373.7	1.001	373.4	15.008
366.7	0.9993	367	20.008
364.2	0.9996	364.3	25.008
361.2	0.9982	361.9	30.012
360.4	0.9975	361.3	35.008
359.7	0.9974	360.6	40.008
359.9	0.9955	361.5	45.012
360.5	0.9976	361.4	50.008
360.3	0.9996	360.4	55.008
359.5	0.9988	359.9	60.012
359.7	0.999	360	65.016
359.3	0.995	361.1	70.012
359.9	0.9982	360.6	75.012
359.1	0.9939	361.3	80.012
359.6	0.9979	360.3	85.016
359.4	0.9996	359.6	90.012
360.1	0.9967	361.3	95.012
360.2	0.9997	360.3	100.01
358.9	0.9931	361.4	105.01
357.4	0.9957	358.9	110.01
355.1	0.9972	356.1	115.01
349.9	0.9964	351.2	120.01
343.1	0.988	347.3	125.01
335.1	0.9972	336	130.01
326.1	1	325.9	135.01
319.3	0.9943	321.2	140.01
315	0.9968	316	145.01
312.3	0.999	312.6	150.01

Visometric test step2

shear stress	shear rate	viscosity	time
Pa	1/s	Pa.s	s
367.6	4.998	73.54	5.012
348.3	4.995	69.74	10.012
346.1	5.005	69.16	15.016
345.9	4.992	69.3	20.016
346	5.017	68.96	25.012
344.8	4.98	69.23	30.012
344.2	4.994	68.91	35.012
343.6	5.01	68.58	40.028
343.1	5.003	68.57	45.056
342.4	4.991	68.6	50.056
341.7	4.99	68.48	55.028
340.8	5.004	68.1	60.012
339.7	4.99	68.07	65.012
338.4	5.003	67.63	70.064
337.2	4.989	67.59	75.064
336	4.999	67.22	80.056
334.9	4.994	67.07	85.024
333.9	5.002	66.75	90.012
333.1	5.01	66.48	95.012
332.2	4.996	66.49	100.02
331.5	5.008	66.19	105.06
330.8	4.981	66.4	110.06
330.3	4.987	66.24	115.07
330	4.997	66.05	120.06
329.9	5.003	65.93	125.06
329.6	5.005	65.86	130.01
329.7	5.001	65.94	135.02
329.6	4.992	66.03	140.01
329.7	5.002	65.92	145.06
329.7	4.995	66.02	150.06

Visometric test step3

shear stress	shear rate	viscosity	time
Pa	1/s	Pa.s	s
370.1	9.972	37.11	5.008
347.9	9.986	34.84	10.012
332.4	10	33.23	15.012
334.6	10	33.46	20.012
334.1	9.989	33.44	25.016
331.9	10.01	33.16	30.008
330.1	9.979	33.08	35.012
328.1	10	32.81	40.016
326.3	9.975	32.72	45.008
324.8	10.01	32.44	50.016
323.4	10.02	32.29	55.012
322.1	10.02	32.15	60.012
320.9	9.994	32.11	65.008
320.1	10.01	31.98	70.012
319.3	9.999	31.94	75.016
318.4	9.985	31.89	80.012
317.9	9.985	31.83	85.012
317.4	10	31.73	90.032
316.7	9.999	31.68	95.028
316.1	10	31.59	100.02
315	9.975	31.58	105.01
313.8	9.994	31.4	110.01
312.4	9.996	31.25	115.01
311.2	9.978	31.19	120.01
310.1	9.981	31.07	125.01
309.9	10.01	30.95	130.01
309	9.984	30.95	135.01
308.3	10	30.81	140.01
307.5	10.01	30.7	145.01
306.7	10	30.66	150.01

Visometric test step4

shear stress	shear rate	viscosity	time
Pa	1/s	Pa.s	s
297.6	30.02	9.914	5.012
297.2	30.01	9.901	10.016
298.8	30	9.958	15.012
295.5	30.01	9.846	20.012
299.6	30.02	9.979	25.016
295.6	30.01	9.848	30.012
294.4	30	9.813	35.012
297.8	30.02	9.921	40.012
293.2	29.99	9.775	45.016
296.4	30	9.881	50.012
294.9	30.03	9.82	55.012
291.5	30.01	9.713	60.012
294.9	30	9.828	65.012
291.5	30	9.718	70.012
293.3	29.99	9.782	75.012
293.6	30	9.787	80.012
289.7	29.99	9.662	85.012
293.3	30.01	9.774	90.012
290.6	30	9.686	95.016
290.3	30.01	9.674	100.01
292	30.01	9.73	105.01
287.5	30.01	9.58	110.02
290.4	30.01	9.678	115.02
290.1	30	9.67	120.01
287.1	30.01	9.568	125.01
289.7	30.01	9.653	130.02
285.4	30	9.515	135.01
287.4	30	9.582	140.01
286.3	30	9.543	145.02
284.7	30	9.488	150.01

Visometric test step5

shear stress	shear rate	viscosity	time
Pa	1/s	Pa.s	s
315.4	50.01	6.306	5.012
315.2	49.97	6.307	10.02
315.9	50.02	6.316	15.016
316.5	50.01	6.328	20.016
316.4	50	6.328	25.016
316.9	49.99	6.339	30.02
317	50	6.339	35.02
317.2	50	6.345	40.02
317.8	50.02	6.354	45.032
317.5	50	6.35	50.016
318	50.01	6.357	55.02
317.7	50.02	6.352	60.032
318.2	50.01	6.363	65.016
317.8	50.01	6.356	70.028
318.4	50	6.368	75.016
318.4	49.99	6.369	80.016
318.5	50.02	6.368	85.016
318.5	50.01	6.368	90.016
318.3	49.99	6.367	95.032
318.3	50	6.367	100.03
318	50.02	6.358	105.02
318.4	50.02	6.366	110.02
318.2	50.01	6.363	115.02
318.7	50.02	6.372	120.03
318.3	50.01	6.364	125.02
318.8	50.02	6.373	130.02
318.4	49.99	6.369	135.02
318.2	50.02	6.362	140.02
318.5	50.01	6.37	145.02
318.3	50.02	6.364	150.02

Visometric test step6

shear stress	shear rate	viscosity	time
Pa	1/s	Pa.s	s
401.2	100	4.01	5.028
402.4	100	4.023	10.04
403.7	99.99	4.038	15.032
405.2	100	4.052	20.036
405.8	99.98	4.059	25.04
407	100	4.068	30.04
407.3	100	4.071	35.032
408	100	4.079	40.032
408.4	100	4.082	45.036
408.8	100	4.088	50.028
409.3	100	4.092	55.032
410	100	4.099	60.032
410.5	99.97	4.106	65.032
410.2	100	4.101	70.032
411	100	4.109	75.04
410.9	100	4.108	80.032
411.7	100	4.115	85.04
411.5	100	4.114	90.044
412.3	100	4.122	95.028
412	100	4.118	100.03
412.9	99.99	4.129	105.04
412.8	100	4.127	110.04
413.5	100	4.134	115.04
413.2	100	4.131	120.02
413.7	100	4.137	125.04
414.2	100	4.14	130.04
414	100	4.139	135.04
415.1	100	4.15	140.04
414.6	100	4.145	145.04
415.4	100	4.152	150.03

Visometric test step7

shear stress	shear rate	viscosity	time
Pa	1/s	Pa.s	s
487.3	150	3.248	5.012
488	150.1	3.252	10.012
489.9	150	3.265	15.012
489.9	150.1	3.265	20.016
490.7	150	3.271	25.028
491	150	3.272	30.012
491.7	150.1	3.277	35.028
492.3	150	3.281	40.012
492.8	150	3.285	45.012
492.7	150	3.285	50.012
493.7	150.1	3.29	55.012
494	150	3.293	60.016
493.7	150.1	3.29	65.012
494.7	150	3.297	70.012
494.6	150	3.297	75.012
495.8	150	3.305	80.016
495.3	150.1	3.301	85.012
496.8	150	3.312	90.012
496.6	150	3.31	95.012
496.9	150.1	3.311	100.01
498	150	3.319	105.01
497.7	150.1	3.317	110.01
498	150.1	3.319	115.02
498	150.1	3.319	120.01
498.7	150.1	3.323	125.02
498.7	150	3.324	130.01
499.9	150.1	3.331	135.01
499.9	150	3.332	140.01
499.8	150	3.332	145.01
500.2	150.1	3.333	150.01

Visometric test step8

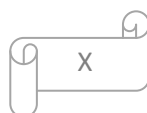
shear stress	shear rate	viscosity	time
Pa	1/s	Pa.s	s
566.2	200.1	2.83	5.004
567.2	200.1	2.835	10.004
568	200.1	2.839	15.004
568.3	200.1	2.84	20.004
569	200	2.845	25.004
569.4	200.1	2.846	30.004
570.1	200.1	2.85	35.004
570	200.1	2.849	40.008
571.1	200.1	2.854	45.004
571	200	2.855	50.004
571.4	200.1	2.856	55.004
571.5	200.1	2.856	60.004
571.8	200	2.858	65.004
572.1	200.1	2.86	70.004
573.1	200.1	2.865	75.004
573.1	200.1	2.865	80.004
573.3	200.1	2.866	85.02
573.5	200.1	2.866	90.008
574.2	200.1	2.87	95.004
574.1	200	2.87	100
574.5	200.1	2.872	105
574.5	200.1	2.871	110.02
575	200.1	2.874	115.01
574.9	200	2.874	120.02
575.8	200.1	2.878	125
576.3	200.1	2.88	130
576.7	200.1	2.882	135.01
576.9	200.1	2.884	140
577.1	200.1	2.884	145
576.7	200	2.884	150.01

Visometric test step9

shear stress	shear rate	viscosity	time
Pa	1/s	Pa.s	s
639.4	250.1	2.557	5.012
639.9	250	2.559	10.028
640.5	250.1	2.561	15.008
641.1	250.1	2.564	20.012
641.5	250.1	2.565	25.024
641.8	250.1	2.566	30.012
642.1	250.1	2.567	35.012
642.4	250.1	2.569	40.032
642.1	250.1	2.568	45.012
642.9	250.1	2.571	50.012
643.4	250.1	2.572	55.012
643.8	250.1	2.575	60.02
644.3	250.1	2.576	65.012
644.8	250.1	2.579	70.008
645.1	250.1	2.58	75.008
645.4	250	2.581	80.012
645.6	250.1	2.581	85.012
645.8	250.1	2.582	90.028
646	250.1	2.583	95.012
646.1	250.1	2.584	100.03
646.4	250.1	2.584	105.01
646.3	250	2.585	110.02
646.5	250.1	2.585	115.02
647.1	250.1	2.588	120.02
647.5	250.1	2.589	125.02
647.4	250.1	2.589	130.01
648.3	250.1	2.592	135.01
648	250	2.591	140.01
648.5	250.1	2.593	145.02
649	250.1	2.595	150.01

Visometric test step10

shear stress	shear rate	viscosity	time
Pa	1/s	Pa.s	s
864.6	450.1	1.921	5.016
865	450.2	1.922	10.032
864.5	450.2	1.92	15.032
865	450.1	1.922	20.032
865.8	450.1	1.924	25.036
866.2	450.2	1.924	30.032
866.5	450.2	1.925	35.032
865.7	450.1	1.923	40.032
866.4	450.1	1.925	45.036
866.3	450.2	1.924	50.032
867	450.1	1.926	55.016
865.4	450	1.923	60.02
866.9	450.2	1.926	65.04
866	450.1	1.924	70.048
866.6	450.2	1.925	75.056
866	450.2	1.924	80.048
866.1	450.1	1.924	85.016
866.9	450.2	1.926	90.016
866.3	450.2	1.925	95.016
866.3	450.1	1.925	100.02
866.8	450.2	1.925	105.03
866.5	450.2	1.925	110.02
866.1	450.1	1.924	115.03
866.6	450.2	1.925	120.02
866.8	450.2	1.926	125.02
866.2	450.2	1.924	130.05
867.4	450.1	1.927	135.04
867.1	450.1	1.926	140.03
867.3	450.2	1.927	145.04
866.8	450.1	1.926	150.03



Visometric test step11

shear stress	shear rate	viscosity	time
Pa	1/s	Pa.s	s
665	250.1	2.659	5.052
663.1	250.1	2.652	10.06
661.3	250	2.645	15.056
660.4	250.1	2.641	20.008
659.5	250.1	2.637	25.048
659.2	250	2.636	30.052
658.6	250.1	2.633	35.056
658.1	250.1	2.632	40.06
658.1	250.1	2.632	45.052
658	250.1	2.631	50.052
657.8	250.1	2.63	55.052
658	250.1	2.631	60.02
657.4	250	2.629	65.056
658.1	250.1	2.632	70.012
657.9	250.1	2.631	75.06
658.1	250	2.632	80.012
658.2	250.1	2.632	85.048
658.6	250.1	2.634	90.048
658.3	250.1	2.632	95.008
659	250.1	2.635	100.06
659	250.1	2.635	105.05
658.9	250.1	2.635	110.01
658.9	250.1	2.635	115.02
658.3	250	2.634	120.07
659.4	250.1	2.637	125.06
658.8	250	2.635	130.05
659.6	250.1	2.637	135.06
659.5	250	2.638	140.01
659.9	250	2.639	145.05
660.4	250.1	2.641	150.06

Visometric test step12

shear stress	shear rate	viscosity	time
Pa	1/s	Pa.s	s
603	200.1	3.014	5.012
602.1	200.1	3.009	10.012
602.2	200.1	3.01	15.008
601.7	200.1	3.007	20.012
602	200	3.01	25.016
601.9	200.1	3.008	30.008
602	200	3.009	35.008
601.7	200.1	3.007	40.012
602.2	200	3.01	45.008
601.8	200.1	3.008	50.016
601.7	200.1	3.008	55.012
601.6	200	3.009	60.012
602	200	3.01	65.028
601.7	200.1	3.007	70.012
602.4	200	3.011	75.012
602.3	200.1	3.01	80.008
602.7	200	3.013	85.008
602.4	200.1	3.011	90.008
602.7	200	3.013	95.008
602.2	200	3.011	100.02
602.9	200.1	3.013	105.02
602.1	200	3.01	110.01
602.9	200.1	3.013	115.01
603.2	200.1	3.015	120.01
603.6	200	3.018	125.01
603.4	200.1	3.016	130.01
603.5	200	3.017	135.02
603.4	200	3.017	140.03
604.1	200.1	3.019	145.01
604.2	200.1	3.02	150.01

Visometric test step13

shear stress	shear rate	viscosity	time
Pa	1/s	Pa.s	s
540.7	150	3.605	5.02
540.2	150.1	3.6	10.04
539.5	150	3.597	15.036
539.9	150.1	3.598	20.024
539.2	150	3.594	25.024
538.4	150.1	3.588	30.016
538.7	150	3.59	35.016
538.1	150	3.588	40.016
538	150	3.586	45.016
538	150	3.586	50.016
537.8	150	3.584	55.028
537.6	150.1	3.583	60.04
538.4	150	3.589	65.036
538.1	150.1	3.586	70.016
537.8	150.1	3.584	75.024
538.3	150	3.589	80.02
538.1	150	3.587	85.016
537.8	150.1	3.584	90.02
538.3	150	3.587	95.02
538.2	150	3.587	100.02
538.4	150	3.589	105.02
538.5	150.1	3.588	110.02
538.4	150	3.59	115.02
539	150.1	3.592	120.02
537.4	150.1	3.581	125.02
538.4	150	3.588	130.02
539.2	150.1	3.594	135.02
538.9	150	3.591	140.02
538.2	150	3.588	145.02
538.7	150	3.59	150.02

Visometric test step14

shear stress	shear rate	viscosity	time
Pa	1/s	Pa.s	s
469.6	100	4.695	5.016
468.7	100	4.685	10.016
467.9	100	4.677	15.016
467.2	99.97	4.673	20.012
466.6	100	4.666	25.016
466.4	100	4.663	30.016
466.2	100	4.66	35.024
465.8	100	4.657	40.012
464.8	100	4.646	45.012
465.7	100	4.657	50.012
465.1	99.98	4.652	55.016
465.1	100	4.65	60.02
464.5	100	4.643	65.016
464.8	100	4.646	70.012
464.4	100	4.643	75.012
464.3	100	4.642	80.016
464.3	100	4.641	85.016
464.2	100	4.64	90.012
464	100	4.639	95.012
464.1	100	4.639	100.02
463.9	100	4.638	105.02
464	100	4.639	110.01
464.1	100	4.639	115.02
463.9	100	4.638	120.02
464.2	100	4.64	125.03
463.8	99.98	4.639	130.02
463.9	100	4.638	135.02
463.9	100	4.639	140.02
463.8	99.99	4.638	145.02
464	100	4.638	150.02

Visometric test step15

shear stress	shear rate	viscosity	time
Pa	1/s	Pa.s	s
384.5	50.02	7.687	5.012
384.3	50.02	7.684	10.012
383.4	50.01	7.666	15.012
383.1	50.02	7.659	20.012
381.8	49.99	7.638	25.012
381.6	50.01	7.63	30.012
380.8	50.02	7.612	35.012
380	50.01	7.599	40.016
379.6	50.02	7.59	45.012
379.1	49.99	7.583	50.012
378.6	50.02	7.57	55.012
378.1	50	7.562	60.012
378	50.01	7.56	65.012
377.3	50.01	7.544	70.016
377	49.99	7.542	75.012
376.6	50.02	7.529	80.012
376.6	50.01	7.529	85.012
376	50.01	7.518	90.012
375.9	50.02	7.516	95.012
376.1	50.01	7.52	100.01
375.3	49.98	7.508	105.01
375.7	50.02	7.512	110.01
375.1	50.01	7.501	115.01
375.3	50.01	7.506	120.01
375.2	50.02	7.501	125.01
374.7	50.01	7.492	130.01
374.6	49.98	7.495	135.01
374.3	50.02	7.484	140.01
374.4	50.02	7.486	145.01
374	49.99	7.483	150.01

Visometric test step16

shear stress	shear rate	viscosity	time
Pa	1/s	Pa.s	s
340.6	30	11.36	5.024
341.3	29.97	11.39	10.028
342.6	29.98	11.43	15.064
338.7	29.98	11.3	20.024
341.9	29.99	11.4	25.024
340.6	30.01	11.35	30.024
339.5	30.01	11.32	35.064
340.5	29.99	11.35	40.024
338	30	11.27	45.024
339.2	29.99	11.31	50.024
339.4	29.99	11.31	55.04
336.9	29.99	11.23	60.024
340	30.01	11.33	65.024
335.9	29.99	11.2	70.024
337	29.99	11.24	75.064
338.9	30.01	11.29	80.028
335.6	30.01	11.18	85.072
337.5	29.99	11.26	90.028
335.5	30.02	11.18	95.068
335.2	30	11.18	100.02
337	30.01	11.23	105.06
334.2	30	11.14	110.02
336	30.01	11.2	115.03
335	30.01	11.16	120.02
333.8	30.01	11.12	125.03
337.3	30.03	11.23	130.04
333.9	30.02	11.12	135.02
334.3	30	11.14	140.06
334.8	29.99	11.17	145.02
332.9	30.01	11.09	150.02

Visometric test step17

shear stress	shear rate	viscosity	time
Pa	1/s	Pa.s	s
318.8	10.01	31.86	5.02
346.3	9.983	34.69	10.02
340.6	9.989	34.1	15.036
333.9	9.98	33.46	20.048
334.3	9.994	33.44	25.028
334.4	9.987	33.49	30.032
334.7	10.01	33.42	35.032
334.6	10.01	33.44	40.032
334.4	9.984	33.49	45.032
334.2	10.02	33.37	50.032
333.9	9.998	33.4	55.032
333.5	10.01	33.32	60.032
333.2	9.984	33.37	65.036
333.5	9.987	33.4	70.032
333.7	10.02	33.31	75.04
333.9	9.985	33.44	80.048
334.3	10.01	33.41	85.032
334.8	10.01	33.45	90.032
334.6	9.997	33.47	95.036
335.2	9.989	33.56	100.04
335.5	10.01	33.52	105.03
335.8	10.01	33.55	110.03
336	10.01	33.55	115.03
336.2	10	33.62	120.04
335.8	9.985	33.63	125.03
335.7	9.997	33.59	130.04
335.4	10.01	33.52	135.03
334.8	10.02	33.42	140.03
333.8	10.01	33.36	145.03
333.2	10	33.31	150.03

Visometric test step18

shear stress	shear rate	viscosity	time
Pa	1/s	Pa.s	s
319.4	4.995	63.95	5.024
319.7	5.003	63.9	10.04
312	4.997	62.43	15.052
313.1	4.987	62.79	20.028
313.6	5	62.71	25.036
313.7	5.013	62.58	30.036
313.8	5.008	62.66	35.036
313.5	5.004	62.64	40.036
313	4.981	62.84	45.02
312.7	5	62.54	50.036
312.2	5.006	62.37	55.056
311.9	5.011	62.24	60.02
311.6	4.999	62.34	65.02
311.5	4.989	62.43	70.036
310.9	4.982	62.42	75.036
310.6	4.997	62.16	80.036
310.1	4.988	62.18	85.036
309.8	4.981	62.19	90.036
309.6	5.027	61.59	95.04
309.9	4.996	62.03	100.04
310.1	4.981	62.26	105.04
310.4	5.011	61.93	110.04
310.8	4.992	62.25	115.04
311	4.998	62.22	120.05
311.2	4.992	62.34	125.04
311.3	5.007	62.17	130.05
311.3	5.001	62.25	135.02
311.2	5.008	62.13	140.04
311	4.997	62.23	145.04
310.8	4.997	62.2	150.04

Visometric test step19

shear stress	shear rate	viscosity	time
Pa	1/s	Pa.s	s
263.8	0.9972	264.6	5.016
272.8	0.9939	274.5	10.032
277.1	0.997	277.9	15.032
278.5	0.9984	278.9	20.032
280.3	1.004	279.2	25.032
280.7	0.9987	281	30.052
281.3	0.9951	282.7	35.032
282.2	0.9974	282.9	40.032
282.9	0.9973	283.7	45.032
284	0.9979	284.6	50.032
284.4	0.9983	284.9	55.032
284.2	0.9979	284.8	60.032
284.5	1.003	283.6	65.032
284.1	1.003	283.3	70.032
282.5	0.9974	283.2	75.032
283.6	1.001	283.2	80.036
281.7	0.9969	282.6	85.032
281.1	0.9976	281.8	90.032
279.6	0.9988	280	95.032
279.4	0.997	280.2	100.03
279.5	0.9997	279.6	105.05
279.9	1.001	279.6	110.03
279.9	1.001	279.7	115.04
280	1.002	279.5	120.03
279.1	1.003	278.2	125.04
279.1	1.001	278.7	130.05
278.4	1.001	278.2	135.03
277.8	1.003	276.9	140.04
276.8	0.9985	277.2	145.03
274.4	0.9987	274.8	150.03

Appendix E

DOE test result.

This DOE tests were done by VCC and Teamster Exports and the thesis team was not involved in it, but just received the result form them.

	Robotparameters			TEST 1				TEST 2					
	flow	speed	TCP	on 200 mm		on 300 mm		volume	on 200 mm		on 300 mm		volume
				width	thick	width	thick		width	thick	width	thick	
1	10	300	20	18.0	1.9	19.0	1.9	33.1	19.2	1.9	19.7	1.9	35.9
2	10	700	20	17.0	0.85	16.5	0.9		16.7	0.85	17.1	0.8	
3	20	500	35	29.5	1.1	30.2	1.2		29.9	1.2	30.4	1.2	
4	10	300	50	17.5	1.9	17.5	2.0	53.8	17.7	2.0	17.6	2.0	53.3
5	10	700	50	14.5	0.95	14.5	0.95		14.4	1.1	14.9	1.1	
6	20	500	35	30.7	1.1	31.0	1.1		30.7	1.2	31.0	1.2	
7	30	300	20	33.5	2.1	32.5	2.2	65.7	32.7	2.2	32.4	2.2	59.4
8	30	700	20	34.9	1.1	34.6	1.1		34.4	0.9	34.0	0.9	
9	20	500	35	31.5	1.1	31.9	1.1		31.2	1.2	32.5	1.1	
10	30	300	50	46.3	1.4	40.5	1.4	65.7	48.8	1.3	40.8	1.4	59.4
11	30	700	50	47.5	0.6	47.2	0.6		47.5	0.6	46.6	0.6	
12	20	500	35	34.7	1.1	34.5	1.1		35.2	1.0	35.3	1.0	
	ml/s	mm/s	mm	mm	mm	mm	mm	ml	mm	mm	mm	mm	ml

Appendix F

Results of width and thickness measurement for selected beads on V60

Bead Number	Reality(Measurement)			
	width _{mm}	Thickness _{mm}	average width _{mm}	average tickness _{mm}
Y352SB2511	30.00	2.80		
	33.00	2.60	31.00	2.20
	30.00	2.80		
Y352SB2609b	28.00	2.50		
	31.00	2.20	29.67	2.23
	30.00	2.00		
Y352SB6313d	29.00	1.70		
	29.00	1.60	30.00	1.63
	32.00	1.60		
Y352SB9307	32.00	1.50		
	32.00	1.80	32.33	1.60
	33.00	1.50		
Y352SB9602a	23.00	1.50		
	24.00	1.20	24.33	1.30
	26.00	1.20		
Y352SB6306	25.00	2.00		
	24.00	2.00	24.67	2.00
	25.00	2.00		
Y352SB6121	34.00	1.80		
	32.00	2.20	32.00	1.90
	30.00	1.70		
Y352SB9102	25.00	1.70		
	29.00	1.20	28.00	1.57
	30.00	1.80		
Y352SB1320	32.00	1.50		
	32.00	2.10	31.33	1.73
	30.00	1.60		
Y352SB2708	30.00	1.50		
	32.00	1.90	30.67	1.63
	30.00	1.50		
Y352SB2404b	30.00	1.80		
	30.00	1.80	31.33	1.20
	34.00	1.6		